CHARACTERIZATION OF MIXING AND SPREADING IN HETEROGENEOUS MEDIA

Gabriela Vanessa Zavala Sánchez

PhD Thesis

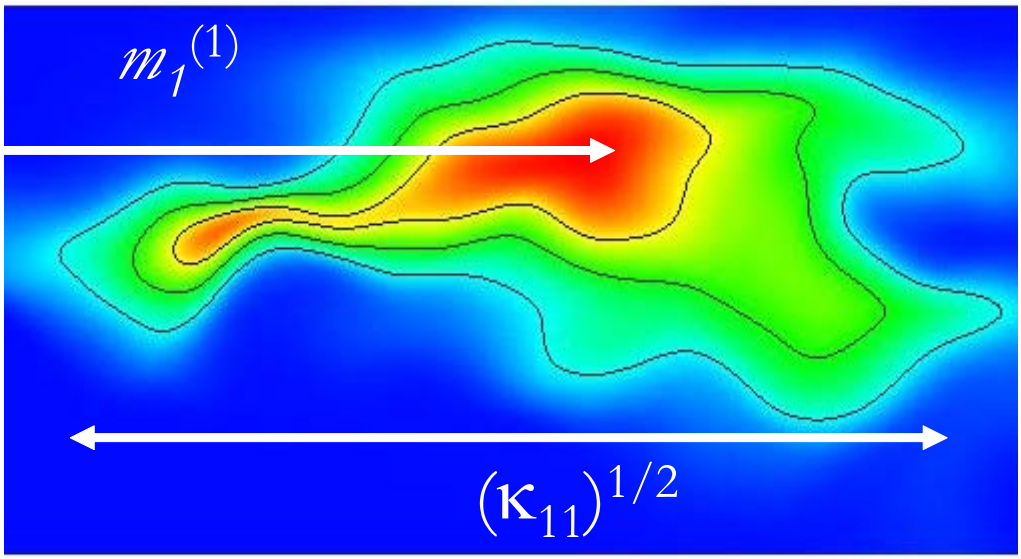

Supervisors:

Marco Dentz
Xavier Sánchez-Vila

Grup d'Hidrologia Subterrània
UNIVERSITAT POLITÈCNICA DE CATALUNYA

Julio 2008

CHARACTERIZATION OF MIXING AND SPREADING IN HETEROGENEOUS MEDIA

PhD Thesis

Department of Geotechnical Engineering and Geo-Sciences (ETCG)
Technical University of Catalonia, UPC

Gabriela Vanessa Zavala Sánchez

Julio 2008

Supervisors:

Marco Dentz
Xavier Sánchez-Vila

This thesis was funded by the the European Commission and the Departament d'Universitats, Recerca i Societat de la Informació de la Generalitat de Catalunya and by the UPC with a grant to finish the PhD thesis. It was developed in the framework of the ENRESA and the EU project IP FUNMIG (Contract No. 516514).

A mis padres Graciela y Jorge
A mi hermana Lo
A Tan
mi familia

Abstract

In this thesis we investigate solute transport through a heterogeneous aquifer. In contrast to the behavior observed in a homogeneous scenario, where mixing and spreading are identical, in a heterogeneous aquifer, mixing and spreading are different transport mechanisms which cannot be measured by a constant and common dispersion/diffusion coefficient.

One of the aim novelties of our work is the elaboration on the difference between mixing and spreading. We present concepts to characterize and quantify separately these phenomenas in terms of effective dispersion coefficients.

Spatial/chemical medium heterogeneities that lead to groundwater velocity variability, as well as temporal flow fluctuations, here are taken into account within a stochastic modeling approach. In this approach, an aquifer is seen as a typical realization of the ensemble of all possible realizations with the same statistical properties. In a single realization, the local effective dispersion coefficient is derived from the centered second moment of the spatial concentration distribution of a solute starting from a point-like injection. For an extended initial source, the global effective dispersion coefficient is defined as the weighted average over the local effective dispersion coefficient for the point-sources that constitute the extended source. The apparent dispersion coefficient, for an extended initial source, is defined as the

half rate of change of the width of a distribution. For early times, it reflects the purely advective spreading effect due to velocity variations within the extended distribution. For the ensemble of aquifer realizations, the effective and apparent dispersion coefficients are defined as ensemble averages over their realizations counterparts. We also define a local and global ensemble dispersion coefficients, which are derived from the second centered moment of the ensemble averaged concentration distribution. Both quantify an artificial effect due to center of mass fluctuations from realization to realization of the heterogeneous aquifers.

The defined effective measures allow us to systematically characterize and quantify mixing and spreading in two scenarios. A physically homogeneous, chemically heterogeneous medium subject to temporal flow fluctuations, and a stratified medium which can be seen as an idealized model of a geological formation. Tools like perturbation theory and axial moment equations are used to derive explicit analytic expressions for the effective dispersion coefficients. Numerical random-walk simulations are used to complement and verify the analytical solutions of the effective transport coefficients. We identify the mechanisms that induce mixing and spreading enhancement, and determine the spatial and time scales which control its temporal evolution.

Resumen

En esta tesis investigamos el transporte de solutos en acuíferos heterogéneos. Contrario al comportamiento observado en un escenario homogéneo, donde la mezcla y el spreading (ensanchamiento) son idénticos, en un acuífero heterogéneo, la mezcla y el spreading son mecanismos de transporte que no pueden ser medidos por un coeficiente de dispersión/difusión constante y único.

Una de las principales novedades de nuestro trabajo es el análisis sobre la diferencia entre la mezcla y el spreading. Presentamos conceptos para cuantificar separadamente estos fenómenos en términos de coeficientes efectivos de dispersión.

Las heterogeneidades espaciales/químicas que inducen variaciones en la velocidad del agua subterránea, asícomo las fluctuaciones temporales del flujo, son tomadas en cuenta aquí mediante un marco estocástico. Dentro de este marco, un acuífero es considerado como una realización típica del conjunto de todas las posibles realizaciones con las mismas características estadísticas. En una realización, el coeficiente local efectivo es derivado del segundo momento centrado de la distribución de concentración de un soluto que inicia desde un punto de inyección. Para una fuente inicial extendida, el coeficiente efectivo global es definido como el promedio ponderado sobre los coeficientes efectivos de dispersión de las fuentes puntuales que consti-

tuyen la fuente extendida. El coeficiente aparente de dispersión, para una fuente inicial extendida, es definido como la mitad de la taza de cambio del ancho de la distribución. Para tiempos cortos, refleja únicamente los efectos de spreading advectivo debido a las variaciones de la velocidad dentro de la distribución extendida. Para el conjunto de realizaciones de acuíferos, los coeficientes de dispersión efectivo y aparente son definidos como el promedio sobre el conjunto de coeficientes obtenido en cada realización. También definimos los coeficients del conjunto locales y globales, los cuales son derivados del segundo momento centrado del conjunto promediado de distribuciones de concentración. Éstos cuantifican un efecto artificial debido a las fluctuaciones de la posición del centro de masa de realización a realización de los acuíferos heterogéneos.

Las medidas efectivas definidas nos permiten cuantificar y caracterizar sistemáticamente la mezcla y el spreading en dos escenarios. Un medio físicamente homogéneo, químicamente heterogéneo sujeto a fluctuaciones temporales del flujo, y un medio estratificado que puede verse como un modelo idealizado de una formación geológica. Herramientas como la teoría de perturbaciones y ecuaciones de momentos axiales son usadas para derivar expresiones analíticas explícitas para los coeficientes efectivos de dispersión. Simulaciones numéricas "random-walk" son empleadas para complementar y verificar las soluciones analíticas de los coeficientes efectivos de transporte. Identificamos los mecanismos que inducen el ensanchamiento de la mezcla y el spreading, y determinamos las escalas espaciales y temporales que controlan su evolución temporal.

Agradecimientos

Gran parte de mi agradecimiento es para mi director Marco Dentz por su paciencia infinita al trabajar conmigo. Agradezco todos aquellos días en los que sólo he tenido que abrir una puerta para encontrarme con su disposición para ayudarme y guiarme. Realmente ha sido una experiencia inigualable y un orgullo trabajar con él. Toda mi admiración para el trabajo genial que realiza, y sobretodo mi admiración al entusiasmo que pone en él. Gracias Marco.

A mi codirector de tesis, Xavier Sánchez-Vila por su apoyo y guía constante durante estos años, muchas gracias. A Jesús Carrera por recibirme en el programa de Doctorado y brindarme la oportunidad de trabajar con él durante mi primer año, mi mas sincera gratitud y admiración. Gracias a todos los amigos y compañeros del Grupo de Hidrogeología del Departamento de Ingeniería del Terreno, a Tere a Silvia, por su amistad y ayuda, muchos de los buenos momentos en estos años los he pasado con ustedes. Gracias Luit por soportar todos los cambios de humor posibles, y por tu enorme amistad durante todos y cada uno de estos X años. A Geo y a Paolo, por los interminables viernes divertidos, todos hemos aprendido algo en ellos. Gracias por su amistad.

A mis padres por atender todas mis llamadas de auxilio desesperadas, por alentarme y calmarme cuando las cosas parecían ir muy mal, gracias por

permitir los asaltos bancarios que les he dado últimamente. A mi hermana Lo, por su compañía durante todos estos años, por su apoyo incondicional y su cariño enorme. Gracias Lo. A mis tías y a Marcela, gracias por su cariño eterno.

A Tan, ha sido difícil, parecía imposible pero lo hemos logrado, es hora de ir a casa. !Vuelvo a casa!. Gracias por estar siempre conmigo en todo este camino presencialmente o en la distancia. No lo hubiera podido hacer sin tí.

A mis amigos en México, gracias sobretodo por recibirme cada año con los brazos abiertos y darme ánimos constantemente, gracias por empujarme al avión en cada regreso a Barcelona. Rocío, amiga, gracias por no enloquecer demasiado. Cely, has estado día a día conmigo apoyándome y dándome ánimos, muchas gracias amiga. Ro, ha sido maravilloso contar contigo siempre. Memo, Gaby, Lalo, Toño, Alejandro, Marco, Ivette, Monty, Brenda, Manuel, Nereo, Clauz, Payo, Ivo, Ivón los he extrañado mucho, gracias por su apoyo.

Contents

Chapter 1

Introduction

The general aim of the present work is the study of solute transport in heterogeneous aquifers, especially its quantification in terms of effective transport parameters. The quantitative and qualitative understanding of transport in heterogeneous hydrogeochemical systems is of critical importance for transport modeling in natural groundwater systems, with applications to contamination problems and for the design of soil and aquifer remediation strategies.

Most hydrogeological models for solute transport assume that dispersion is Fickian, i.e., the dispersive mass flow rate is proportional to the concentration gradient. The combined mechanisms of advection and dispersion are represented by the advection-dispersion equation with constant coefficients.

However, in the groundwater context, an aquifer is constituted by an arrangement of different materials, whose hydraulic properties, such as the hydraulic conductivity, porosity and retardation coefficient, for example, are space dependent. The spatial variability of the hydraulic conductivity leads, via Darcy equation, to a spatially variable groundwater flow velocity. In addition to spatial fluctuations of the system parameters due to physical or chemical medium heterogeneities, groundwater velocity might also fluctuate

temporally on a range of scales. The interaction between these spatially and temporally velocity variations with the local dispersion, induces a scale dependence of the solute spreading and mixing behavior. This scale effect, which has been demonstrated by numerical (e.g.,[1]), laboratory experiments in column and tank experiments [2, 3, 4, 5], and field experiments [6, 7, 8], reveals the shortcomings of the traditional advection dispersion transport equation with constant coefficients.

Within a stochastic approach, a given aquifer is seen as a typical realization of an ensemble of all possible realizations with the same statistical properties. The systematic investigation of the impact of spatial/chemical heterogeneity and temporal flow fluctuations on the effective transport behavior can be addressed by two interrelated strategies, which can be called coefficients approach and dynamics approach. The large scale transport properties are derived from appropriately constructed averages over the ensemble of all medium realizations. The dynamics approach deals with the upscaling of the local scale transport equations in heterogeneous media, models such as Continuous Time Random Walk (CTRW), Multi Rate Mass Transfer (MRMT) and fractional dynamical systems (e.g., [9, 10, 11, 12, 13, 14]) represent transport models which describe the effective transport dynamics on a semi-phenomenological basis. The coefficients approach quantifies flow and transport in terms of effective transport coefficients such as effective dispersion coefficient, reaction rates and retardation coefficient, for example.

In this thesis we will focus on the coefficients approach to characterize mixing and spreading in heterogeneous media. Spatial or chemical heterogeneity and temporal fluctuations lead to an increase of solute mixing and spreading [15, 16, 17, 18, 19, 20] which can be characterized by large scale dispersion coefficients. The latter evolve with time or travel distance, which

has been frequently adressed in the literature e.g., [21, 22, 23, 24].

The full temporal evolution of the effective solute mixing and spreading in a physically and chemically heterogeneous medium has been studied in terms of effective and ensemble dispersion coefficients within a stochastic approach for a point like injection and extended sources [25, 26, 27]. The effective dispersion coefficient is given by the average of the dispersion in one realization and quantifies the properties of a typical realization. The ensemble dispersion coefficient which is derived from the concentration distribution of the averaged solute cloud quantifies an artificial spreading and mixing behavior due to sample to sample fluctuations of the center of mass from realization to realization. The conceptually difference between these coefficients is well known in the literature. Despite that, it is common to compute the mathematically simpler ensemble coefficient, since for large transport lengths or times, solutes have been dispersed over a such a large volume and the full heterogeneity spectrum is sampled, the effective and ensemble dispersion coefficients eventually reach a common asymptotic Fickian behavior. It must be taken into account that in most hydrological applications, the length/time scales (given by dispersion/diffusion over the heterogeneity large scale, when it exist) can be large. Then, the common macroscopic asymptotic values of the ensemble and effective dispersion coefficients does not provide a reliable measure of mixing and spreading at preasymptotic times. Hence, for preasymptotic times, the temporal evolution of the effective dispersion coefficient will characterize the actual mixing and spreading, while the ensemble dispersion coefficient overestimates the spreading and mixing behavior. Furthermore, in special cases as the unbounded stratified media model, where a strongly correlated disorder is present, the ensemble and effective dispersion coefficients behavior is anomalous for all times [21].

In the course of the transport coefficients investigation in heterogeneous media, we distinguish two main topics which deserve special attention and on which the development of the present thesis will be based.

First, we elaborate on the difference between spreading and mixing when studying transport in heterogeneous media and present concepts to quantify these phenomena in terms of transport coefficients. For transport in homogeneous media these two phenomena are identical and are measured by the unique diffusion/dispersion coefficient. For transport in heterogeneous media, however, solute spreading denotes the distortion and deformation of an initial plume due to the purely advective mechanism, for example. Solute mixing in contrast, denotes the mechanism which leads to actual dilution of a dissolved substance [28], for example. The interplay of heterogeneity-induced spreading and local mixing mechanisms can lead to macroscale mixing. The characterization of mixing is of importance for a series of applications such as, bioremediation, natural attenuation, mixing limited chemical reaction; that is, whenever the efficiency of a chemical or biological process depends on the mixing of the participating species.

Second, conduct an exhaustive and systematic investigation of the mixing and spreading mechanisms as on the characteristic spatial and time scales which control the spreading and mixing behavior in heterogeneous media, specially the transition from the non-Fickian to Fickian-type behavior. We study the interaction of chemical and spatial heterogeneities, local dispersion and temporal flow fluctuations and its role as an activation mechanisms of macroscopic mixing and spreading. To this end, we study two scenarios, a physically homogeneous, chemically heterogeneous infinite medium subject to temporal flow fluctuations, and then, a stratified medium as a simplest case of a physically heterogeneous medium.

In Chapter 2, we propose a generalization of the new measures for solute spreading and mixing for a single realization suggested by Dentz and Carrera [29], to transport in heterogeneous media within a stochastic approach. These measures are based on the local moments, i.e., first and second moments of the transport Green function. The transport Green function here denotes the solute distribution which evolves from a point-like injection in a reference time.

The description of the general solute flow and transport equations for the two scenarios under consideration, the stochastic approach and the methodology applied to derive the effective measures proposed, such as perturbation theory, axial moment equations, and numerical random walk simulations, are also introduced in Chapter 2.

Once we have defined the effective dispersion coefficients, we study in Chapter 3 the impact of the interaction of local dispersion, chemical heterogeneity and temporal flow fluctuations of the flow conditions on the effective mixing and spreading behavior of a sorbing solute. We focus on linear sorption reactions under instantaneous local equilibrium conditions. In a chemical heterogeneous medium, the local sorption properties are subject to spatial fluctuations, which can be characterized by a spatially varying retardation coefficient. The effective transport behavior in this practically relevant scenario is studied within a stochastic perturbative approach. Within this approach we derive compact analytical expressions for the temporal evolution of the longitudinal and transverse effective dispersion coefficients. Focusing on the contributions due to chemical heterogeneity and temporal fluctuations, we find enhanced transverse spreading characterized by a transverse effective dispersion coefficient that, in contrast to transport in steady flow fields, evolves to a disorder-induced macroscopic value (i.e., independent of local disper-

sion). At the same time, the asymptotic longitudinal dispersion coefficient can decrease. The simultaneous increase of the transverse and decrease of the longitudinal effective dispersion coefficients can be seen as a consequence of self-organization of the system. The compact expressions for the longitudinal and transverse effective dispersion coefficients presented in this Thesis can be used for the quantification of effective spreading and mixing in the context of the groundwater remediation based on hydraulic manipulation and for the effective modeling of reactive transport in heterogeneous media in general. This work has been published in ref. [30].

It turns out in Chapter 3 that temporal flow fluctuations lead to increased transverse solute mixing. This mechanism smoothes the transverse heterogeneity contrast and can lead to a decrease of longitudinal dispersion coefficient.

For transport in stratified media, *Matheron and de Marsily* [21] found an anomalous increase of the longitudinal dispersion coefficient with the square-root of time. *Clincy and Kinzelbach* [31] observed that the anomalous behavior is supressed in presence of a constant velocity component transverse to the stratification, i.e., in presence of a mechanism that induces the disorder sampling of the solute. In Chapter 4 we investigate specifically if the anomalous behavior of the effective spreading and mixing in unbounded stratified media persists when temporal flow fluctuations are added to the system. The effective dispersion coefficient obtained analytically indicates that temporal flow fluctuations do not enhance vertical solute mixing in unbounded stratified media.

Seeking for the mechanisms that lead to normal dispersion behavior, we considered modifications of the stratified geometry that enable the solute to sample the transverse heterogeneity contrast in a same effective way than by

diffusion. Thus we considered the so called Manhattan Grid model [32], that consist of the superposition of two field with perpendicular stratification, as well as a quasy-stratified flow [33].

In Chapter 5 we investigate solute mixing and spreading in a vertically bounded stratified random medium. Unlike for the infinite stratified medium, where a superdiffusive behavior of the apparent longitudinal dispersion coefficient is observed (e.g. [21]), here, at asymptotically long times, disorder-induced mixing and spreading is uniquely quantified by a constant "Taylor dispersion-type" coefficient [34]. This value is reached asymptotically after the time for complete vertical mixing is reached. We focus on preasymptotic times, for which solute transport is highly non-Fickian, and the transition from the preasymptotic to the asymptotic Fickian-type regime. We study initial position and source size memory effects in the effective spreading and mixing dynamics for single realizations and their quantification using stochastic averaging. The transition from finite to infinite media and its impact on the derived effective parameters is analyzed. The validity of the quantification of mixing and spreading by stochastic averages for a finite media is discussed. This chapter is based in paper [35] which has recently been accepted for publication.

In Chapter 6 the main conclusions of our work related to the characterization of mixing and spreading in heterogeneous media are provided.

Chapter 2

Basics

2.1 Introduction

We investigate solute transport through heterogeneous media models. Solute transport at the laboratory scale can be described by the advection dispersion equation, which establishes that the mass transport is fully controlled by two mechanisms. The advection mechanism, described by the Darcy equation, is associated to the solute movement due to the fluid flow, and the local dispersion mechanism, which is assumed to be Fickian.

However, at field scales, which are large compared to the laboratory scale, medium characteristics and driving forces, in general display large spatial and/or temporal variations. In the groundwater context, the hydraulic conductivity is a clear example of a heterogeneous parameter since its value fluctuates in orders of magnitude even in apparently homogeneous aquifers. This spatial variability of the hydraulic conductivity leads, via the Darcy equation, to a spatially variable groundwater flow velocity. In addition to spatial fluctuations of the system parameters due to physical or chemical medium heterogeneities, the groundwater flow velocity, in general also fluc-

tuates temporally on a range of scales. The interaction between these spatially and temporally flow velocity variations and local dispersion, induces a scale dependence of the solute spreading and mixing behavior. This scale effect, which has been observed in numerical and field experiments, must be taken into account when modeling effective solute transport in heterogeneous media.

The aim of the present work is to systematically characterize the impact of the physical or chemical medium heterogeneities as well as temporal flow fluctuations on solute transport behavior in terms of effective transport coefficients. These observables are described in section 2.6.

Here we present the general flow and solute transport equations for chemically/spatially heterogeneous media, in order to define the common terms and to set the framework for further argumentations. The stochastic framework and methodology are also addressed in this chapter. The presented concepts are then applied to a specific heterogeneous scenario for transport in horizontally stratified media.

2.2 Flow in Heterogeneous Media

The flow velocity $\mathbf{q}(\mathbf{x}, t)$ through a heterogeneous medium is given by the Darcy equation, [36],

$$\mathbf{q}(\mathbf{x}, t) = -K(\mathbf{x})\nabla h(\mathbf{x}, t) \tag{2.1}$$

where the hydraulic conductivity $K(\mathbf{x})$ is space dependent, and $h(\mathbf{x}, t)$ denotes the hydraulic head. Temporal flow fluctuations here are induced by temporal variability of the head boundary conditions. We disregard here inertia effects as the compressibility time scales are usually much smaller than the fluctuations scales [18, 37, 38]. Thus in the absence of sink and sources,

the divergence of $\mathbf{q}(\mathbf{x},t)$ is zero, i.e., $\nabla\cdot\mathbf{q}(\mathbf{x},t)=0$. The boundary conditions will be detailed in each specific application in the corresponding chapters.

2.3 Transport in Heterogeneous Media

The time evolution of a (mobile) solute in a heterogeneous porous media under spatially varying equilibrium sorption properties is given by a generalized advection-dispersion equation, (see e.g. [39, 40]),

$$R(\mathbf{x})\frac{\partial c_m(\mathbf{x},t)}{\partial t}+\mathbf{q}(\mathbf{x},t)\nabla c_m(\mathbf{x},t)-\nabla\cdot(\mathbf{D_o}\nabla c_m(\mathbf{x},t))=\rho(\mathbf{x})\delta(t), \quad (2.2)$$

where $c_m(\mathbf{x},t)$ is the spatial concentration of the mobile solute. The space dependent retardation coefficient $R(\mathbf{x})$ reflects spatial inhomogeneities in both the local porosity and the local chemical adsorption coefficient. The constant local dispersion tensor $\mathbf{D_o}$ is assumed to be diagonal, $D_{ij}=\delta_{ij}D_{ii}$ with $D_{11}=D_L$ and $D_{ii}=D_T$ for $i>1$.

Note that the total concentration distribution of the sorbing chemical is divided into a mobile fraction that is transported through the medium in the water flow, and a fraction that is adsorbed to the solid matrix,

$$c_{\mathrm{tot}}(\mathbf{x},t)=\phi(\mathbf{x})c_m(\mathbf{x},t)+[1-\phi(\mathbf{x})]\,c_{ad}(\mathbf{x},t), \quad (2.3)$$

where $c_{ad}(\mathbf{x},t)$ denotes the spatial distribution of the adsorbed concentration, and $\phi(\mathbf{x})$ denotes porosity.

The right hand side in (2.2) is the initial distribution of the solute at $t=0$,

$$c_m(\mathbf{x},t=0)=\rho(\mathbf{x}). \quad (2.4)$$

This implies for the mobile concentration $c_m(\mathbf{x},t=0)=R(\mathbf{x})^{-1}\rho(\mathbf{x})$. As boundary condition we assume,

$$\mathbf{n}\cdot\nabla c_m(\mathbf{x},t)|_{\mathbf{x}\in\partial\Omega^d}=0, \quad (2.5)$$

where $\partial\Omega^d$ are the boundaries of the transport domain Ω^d, and $\mathbf{n}$ is the outward pointing unit vector perpendicular to the domain boundaries.

According to the Duhamel principle, the concentration distribution $c_m(\mathbf{x}, t)$ can be written as,

$$c_m(\mathbf{x}, t) = \int_{\Omega^d} \mathrm{d}\mathbf{x}' \rho(\mathbf{x}) g(\mathbf{x}, t|\mathbf{x}'), \tag{2.6}$$

where the Green function $g(\mathbf{x}, t|\mathbf{x}')$ solves the advection dispersion equation (2.2) for a point like injection at $t = 0$, i.e. $\rho(\mathbf{x}) = \delta(\mathbf{x} - \mathbf{x}')$.

2.4 Stochastic Framework

A detailed description of flow and solute transport behavior in heterogeneous media requires a deterministic knowledge not only of the spatial distribution of the governing parameters at all scales, but also of the flow and transport processes which are relevant at such scales. However, in real scenarios we usually have a few values of hydraulic parameters at some particular locations and some indications about general trends. In order to deal with the lack of information, a stochastic approach [39, 40] has been used in groundwater hydrology as a tool to describe and quantify in a systematic manner the impact of spatial and temporal variabilities observed at small scales into an effective large scale flow and transport behavior, plus as a way to compute the uncertainty associated with a given prediction.

In a stochastic approach a given medium is seen as a typical realization of an ensemble of all media characterized by certain statistical properties. The large scale transport behavior is obtained by properly defined stochastic averages over the ensemble of random spatial/temporal fields.

In the stochastic framework considered in this thesis, the spatially fluc-

tuating retardation factor, $R(\mathbf{x})$ and the hydraulic conductivity $K(\mathbf{x})$ are modeled as stationary spatial random fields, while the temporal fluctuations of the flow boundary conditions that induce a fluctuating mean hydraulic gradient are modeled as a stationary temporal random process (e.g. [18, 20]).

Any random field may be decomposed into two components, a deterministic one, which could be its conditional mean value (either constant or spatially variable), and the random fluctuations around it. These random fluctuations are characterized by a correlation structure. In order to fully characterize a random field it would be necessary to assume that we know the multivariate probability density function.

We split the retardation factor into its mean value and fluctuations about it

$$R(\mathbf{x}) = \overline{R}\,[1 - \mu(\mathbf{x})]\,, \tag{2.7}$$

where $\overline{R}$ is the ensemble averaged retardation factor, $\mu(\mathbf{x})$ denotes the normalized fluctuation, whose ensemble average is zero by definition, $\overline{\mu(\mathbf{x})} = 0$. The correlation function of the normalized retardation fluctuations is given by,

$$\overline{\mu(\mathbf{x})\mu(\mathbf{x}')} = \sigma^2_{\mu\mu} C^{\mu\mu}(\mathbf{x} - \mathbf{x}'), \tag{2.8}$$

where the variance $\sigma^2_{\mu\mu} = \overline{\mu(\mathbf{x})^2}$. The correlation $C^{\mu\mu}(\mathbf{x})$ is assumed to decay exponentially fast for distances larger than the correlation length l_μ.

The mobile concentration and the flow velocity as well as the local dispersion coefficients are rescaled by mean retardation according to,

$$c(\mathbf{x}, t) = \overline{R} c_m(\mathbf{x}, t), \qquad \mathbf{D} = \frac{\mathbf{D}_0}{\overline{R}}, \qquad \mathbf{u}(\mathbf{x}, t) = \frac{\mathbf{q}(\mathbf{x}, t)}{\overline{R}}. \tag{2.9}$$

For quasi-steady flow conditions, i.e., instantaneous propagation of a temporal change in the flow boundary conditions, the normalized first-order solu-

tion of the flow problem (in the fluctuations of the log-hydraulic conductivity) can be decomposed as (e.g., [18, 20])

$$\mathbf{u}(\mathbf{x},t) = \mathbf{u}(t) - \mathbf{u}'(\mathbf{x},t). \tag{2.10}$$

The mean flow direction is aligned with the 1-direction of the coordinate system,

$$\langle\overline{\mathbf{u}(\mathbf{x},t)}\rangle = u\mathbf{e}_1 \tag{2.11}$$

with $\mathbf{e}_1$ the unit vector in 1-direction. The purely time-dependent part is given by

$$\mathbf{u}(t) = u\left[\mathbf{e}_1 - \boldsymbol{\upsilon}(t)\right] \tag{2.12}$$

with the normalized purely temporal velocity fluctuations $\boldsymbol{\upsilon}(t)$, whose mean is zero by definition,

$$\langle\boldsymbol{\upsilon}(t)\rangle = \langle\overline{\mathbf{u}'(\mathbf{x},t)}\rangle \equiv 0. \tag{2.13}$$

A brief discussion of the quality of the approximation of quasi-steady flow is given in [38]. The correlation functions of the normalized temporal velocity fluctuations $\boldsymbol{\upsilon}(t)$ are given by

$$\langle\upsilon_i(t)\upsilon_j(t')\rangle = \sigma_{vv}^2 C_{ij}^{vv}(t-t') \tag{2.14}$$

with the variance σ_{vv}^2 of the temporal fluctuations, which, for simplicity, is assumed to be equal in all directions. The correlations of the $\upsilon_i(t)$ are assumed to be short range, i.e., to decrease quickly for times larger than the correlation time τ.

Using the decomposition (2.10) in (2.2), we obtain our general working equation

$$\frac{\partial c(\mathbf{x},t)}{\partial t} + \mathbf{u}(t)\cdot\nabla c(\mathbf{x},t) - \nabla\mathbf{D}\nabla c(\mathbf{x},t) = \rho(\mathbf{x})\delta(t) + \mathbf{L}\{\mathbf{x},t\}c(\mathbf{x},t), \tag{2.15}$$

with $\mathbf{L}\{\cdot\}$ the perturbation transport operator that acts on $c(\mathbf{x}, t)$, here defined as,

$$\mathbf{L}\{\mathbf{x}, t\} = \mu(\mathbf{x})\frac{\partial}{\partial t} + \mathbf{u}'(\mathbf{x}, t)\nabla \tag{2.16}$$

2.5 Stratified Media Models

Here we detail the basics of horizontally stratified media models, which can be seen as an idealized case of heterogeneous media when considering the limiting case of infinite correlation length in the horizontal direction, the hydraulic conductivity varies only along the vertical.

2.5.1 Flow in Stratified Media

Flow through a stratified porous medium is characterized by the Darcy equation (2.1), which here can be written as follows,

$$\mathbf{u}(\mathbf{x}, t) = -K(\mathbf{y})\nabla h(\mathbf{x}, t), \tag{2.17}$$

where $\mathbf{x}$ is the position vector in Ω^d and $\mathbf{y} = (x_2, \ldots, x_d)^T$ is the position vector in the $(d-1)$-dimensional subdomain Ω, with $\Omega^d = \Omega \times \mathbf{R}$. The latter is perpendicular to the 1-direction of the coordinate system. The hydraulic conductivity is denoted by $K(\mathbf{y})$ and varies only in Ω, $h(\mathbf{x}, t)$ is the hydraulic head. Here we consider that the flow is driven by a temporally variable spatially constant head gradient $-\mathbf{J}(t)$. This boundary condition together with the incompressibility condition $\nabla \cdot \mathbf{u}(\mathbf{x}, t) = 0$ leads us to the following exact solution [41],

$$\mathbf{u}(\mathbf{x}, t) = K(\mathbf{y})\mathbf{J}(t), \tag{2.18}$$

i.e., flow varies only on the transverse direction as well.

The hydraulic conductivity $K(\mathbf{y})$ here is modeled as a stationary spatial random field. It can be decomposed into its (constant) mean value $\overline{K(\mathbf{y})} = \overline{K}$ and fluctuations about it,

$$K(\mathbf{y}) = \overline{K}\,[1 - k(\mathbf{y})]\,. \tag{2.19}$$

where $k(\mathbf{y})$ are the normalized conductivity fluctuations, whose mean is zero by definition. The overbar denotes the ensemble average. The translation-invariant autocorrelation function of $k(\mathbf{y})$ is given by,

$$\overline{k(\mathbf{y})k(\mathbf{y}')} \equiv \sigma_{kk}^2 C^{kk}(\mathbf{y} - \mathbf{y}'). \tag{2.20}$$

where the variance $\sigma_{kk}^2 = \overline{k(\mathbf{y})^2}$. In the following, the correlation function is assumed to be of short-range, i.e., to decay quickly on the correlation scale l.

For quasi-steady flow conditions, i.e., instantaneous propagation of a temporal change in the flow boundary conditions, the normalized first-order solution of the flow problem (in the fluctuations of the log-hydraulic conductivity) can be decomposed as (e.g., [18, 20])

$$\mathbf{u}(\mathbf{x}, t) = \mathbf{u}(t) - [\mathbf{u}'(\mathbf{y}) + \mathbf{u}'(\mathbf{y}, t)]\,. \tag{2.21}$$

where $\mathbf{u}$(t) is defined (2.12). The different contributions are given by,

$$\mathbf{u}'(\mathbf{y}) = u\, k(\mathbf{y}), \tag{2.22}$$

$$\mathbf{u}'(\mathbf{y}, t) = u\, k(\mathbf{y})\boldsymbol{\upsilon}(t). \tag{2.23}$$

2.5.2 Transport in Stratified Media

In stratified media, the advective-dispersive transport equation (2.2) of a conservative solute can be simplified as follows,

$$\frac{\partial c(\mathbf{x}, t)}{\partial t} + u(\mathbf{y}, t)\nabla c(\mathbf{x}, t) - \nabla \cdot (\mathbf{D_o}\nabla c(\mathbf{x}, t)) = 0. \tag{2.24}$$

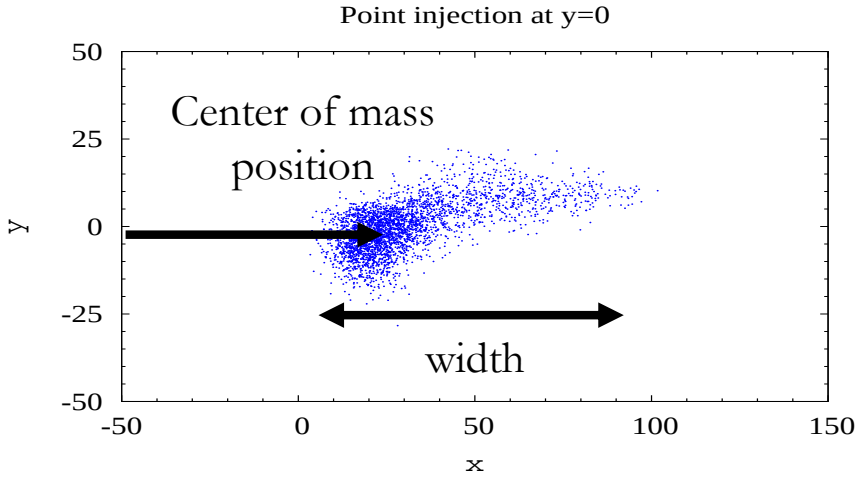

Figure 2.1: Center of mass position and width of a solute distribution evolving from a point-like injection in a heterogeneous medium.

The initial and boundary condition are defined in (2.4) and (2.5), respectively.

Using decomposition (2.21) and its correspondent contributions, in (2.24), we obtain,

$$\frac{\partial c(\mathbf{x},t)}{\partial t} + \mathbf{u}(t)\cdot\nabla c(\mathbf{x},t) - \nabla\cdot(\mathbf{D_o}\nabla c(\mathbf{x},t)) = \mathbf{L}\{\mathbf{y},t\}c(\mathbf{x},t), \qquad (2.25)$$

with the perturbation transport operator here defined as,

$$\mathbf{L}\{\mathbf{y},t\} = u\left[k(\mathbf{y}) + \upsilon_1(t)k(\mathbf{y})\right]\frac{\partial}{\partial x_1}. \qquad (2.26)$$

Note that the temporal flow fluctuations (2.12), are $\boldsymbol{\upsilon}(t) = [\upsilon_1(t), \upsilon_2(t), \ldots, \upsilon_d(t)]^T$.

2.6 Observables

Spreading and mixing can be quantified in terms of the evolution of the first and second centered moments of the solute distribution $c(\mathbf{x},t)$ (e.g., [28]).

The first moment represents the center of mass of the solute distribution while the second centered moment describes the dispersion of particles around its center of mass, see Figure 2.1. A Gaussian distribution is completely defined by its first and second moments. Solute distributions in heterogeneous media, however, are in general non-Gaussian. Depending on the focus of interest, different definitions for the centered moments and the quantities derived can apply. For risk assessment studies, for example, it may be sufficient to have a rough estimate of the possible extent of a contaminant plume. For reactive transport modeling, in contrast, it is important to have an accurate estimate on the actual spatial distribution of the reactant.

Recently, *Dentz and Carrera* [29] suggested and discussed effective transport formulations and dispersion measures (i) to study the mechanisms and processes that lead to solute spreading and ultimately enhanced mixing in stratified flows, (ii) to provide an upscaled transport framework that describes effective solute spreading and mixing at preasymptotic times.

These authors defined effective dispersion coefficients for a single medium realization in terms of local moments, i.e., moments of the transport Green function (solute distribution for a point-like injection) see (2.6), and applied the developed concepts to transport in the parabolic flow through a two-dimensional channel. Here, we generalize these concepts to transport in heterogeneous random media.

2.6.1 Local Moments

As defined in [29], the first and second local moments are defined in terms of the transport Green function $g(\mathbf{x},t|\mathbf{x}',t')$ (2.6), and are given by,

$$\mu_i^{(1)}(t|\mathbf{x}') = \int\limits_{\Omega^d} \mathrm{d}\mathbf{x} x_i g(\mathbf{x},t|\mathbf{x}',0), \tag{2.27}$$

$$\mu_{ij}^{(2)}(t|\mathbf{x}') = \int_{\Omega^d} \mathrm{d}\mathbf{x} x_i x_j g(\mathbf{x}, t|\mathbf{x}', 0), \tag{2.28}$$

The width of the distribution $g(\mathbf{x}, t|\mathbf{x}', 0)$ is given by the local second centered moment,

$$\kappa_{ij}^{e}(t|\mathbf{x}') = \mu_{ij}^{(2)}(t|\mathbf{x}') - \mu_{i}^{(1)}(t|\mathbf{x}')\mu_{j}^{(1)}(t|\mathbf{x}'). \tag{2.29}$$

2.6.2 Global Moments

The first and second moments of the concentration distribution $c(\mathbf{x}, t)$ given by (2.2) for the initial condition (2.4) are defined by,

$$m_{i}^{(1)}(t) = \int_{\Omega^d} \mathrm{d}\mathbf{x} \rho(\mathbf{x}) \mu_{i}^{(1)}(t|\mathbf{x}), \tag{2.30}$$

$$m_{ij}^{(2)}(t) = \int_{\Omega^d} \mathrm{d}\mathbf{x} \rho(\mathbf{x}) \mu_{ij}^{(2)}(t|\mathbf{x}), \tag{2.31}$$

From the global moments in (2.30) and (2.31), an apparent second centered moment of $c(\mathbf{x}, t)$ can be defined,

$$\kappa_{ij}^{a}(t) = m_{ij}^{(2)}(t) - m_{i}^{(1)}(t)m_{j}^{(1)}(t). \tag{2.32}$$

in analogy to (2.29).

2.6.3 Transport Coefficients. Single Realization

For a point-like injection, the temporal rate of change of the width of the solute distribution is quantified by the local effective dispersion coefficient (e.g., [29]),

$$D_{ij}^{e}(t|\mathbf{x}') = \frac{1}{2}\frac{\mathrm{d}}{\mathrm{dt}}\kappa_{ij}^{e}(t|\mathbf{x}'). \tag{2.33}$$

The local center of mass velocity is given by the time derivative of the first local moment,

$$\nu_i(t|\mathbf{x}') = \frac{\mathrm{d}}{\mathrm{dt}}\mu_i^{(1)}(t|\mathbf{x}'). \tag{2.34}$$

For an extended source distribution, the center of mass velocity is given by,

$$\nu_i(t) = \int\limits_{\Omega^d} \mathrm{d}\mathbf{x}'\rho(\mathbf{x}')\nu_i(t|\mathbf{x}') \tag{2.35}$$

according to (2.30). The global effective dispersion coefficient can be defined analogously by integration of (2.33) over the initial distribution as,

$$D_{ij}^e(t) = \int\limits_{\Omega^d} \mathrm{d}\mathbf{x}'\rho(\mathbf{x}')D_{ij}^e(t|\mathbf{x}'); \tag{2.36}$$

i.e the local effective dispersion coefficient measures the actual mixing produced in a solute cloud starting from a point like injection at $\mathbf{x}'$, while the the global effective dispersion coefficient, as a weighted average over the local effective dispersion coefficient, measures the average mixing within the initial plume and it not longer depends on the initial source location.

The rate of change of the apparent second centered moment in (2.32) defines the apparent dispersion coefficient,

$$D_{ij}^a(t) = \frac{1}{2}\frac{\mathrm{d}}{\mathrm{d}t}\kappa_{ij}^a(t). \tag{2.37}$$

As discussed in [29], for preasymptotic times, the apparent dispersion coefficient quantifies purely advective spreading of the solute due to velocity contrast within the initial plume. The global effective dispersion coefficient $D^e(t)$, in contrast, does not take into account such spreading effects as it is defined as the weighted sum over the local effective dispersion coefficients,

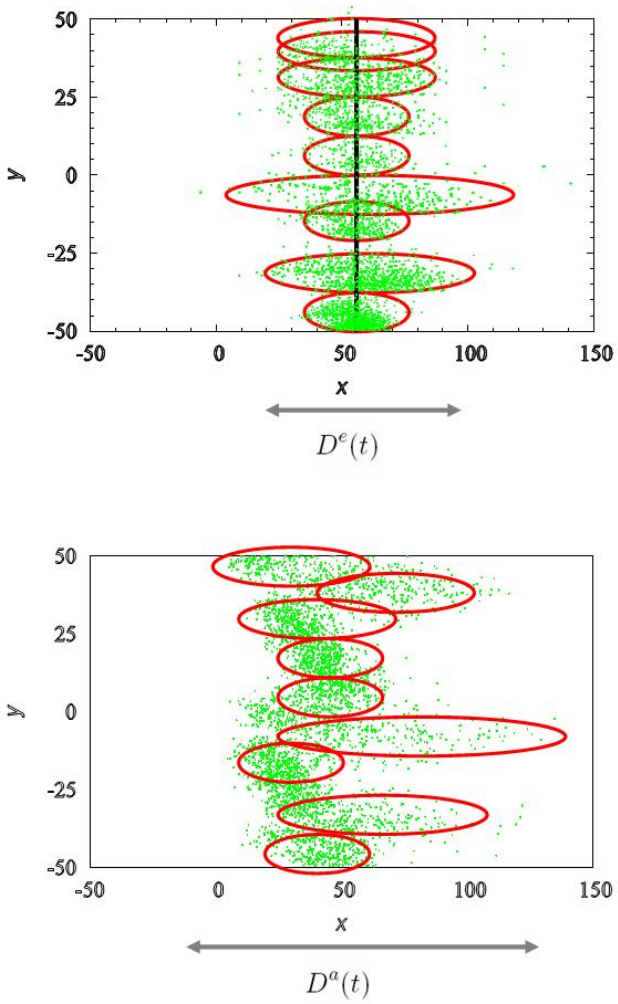

Figure 2.2: Solute distributions evolving from an extended source in one disorder realization to illustrate the conceptual difference between the local effective and apparent dispersion coefficient.

which measure solute dispersion originating from the point sources that constitute the initial plume.

Thus, advective spreading due to the velocity contrast inside the initial plume can be quantified by the difference between the apparent and the global effective dispersion coefficients,

$$D_{ij}^{a}(t) - D_{ij}^{e}(t) = \frac{1}{2}\frac{\mathrm{d}}{\mathrm{d}t}\int\limits_{\Omega^d} \mathrm{d}\mathbf{x}'\rho(\mathbf{x}')\mu_i^{(1)}(t|\mathbf{x}')\left[\mu_j^{(1)}(t|\mathbf{x}') - m_j^{(1)}(t)\right]. \quad (2.38)$$

The conceptual difference between these observables is illustrated in Figure 2.2.

Equation (2.38) describes the temporal rate of change of the mean squared deviation of the local from the global center of mass positions.

2.6.4 Transport Coefficients. Ensemble

As detailed in section 2.4, in a stochastic analysis, the physically or chemically heterogeneous aquifer is identified with one particular realization of an ensemble of aquifer realizations. As such, the effective transport coefficients can be expressed as averages over the ensemble of all possible realizations of the spatial and temporal random processes.

As pointed out in, e.g., [42] for average over spatial random process, and [20] for average over temporal random process, the definition of average dispersion coefficients is not unique and depends on the way the average is taken. This is analogous to the definition of the global effective and apparent dispersion coefficients described previously. The two quantities differ in the order, by which the "average" over the initial distribution is taken, see (2.36) and (2.37).

In a straightforward manner, we define the average center of mass velocity and local effective dispersion coefficients as the ensemble averages over (2.34)

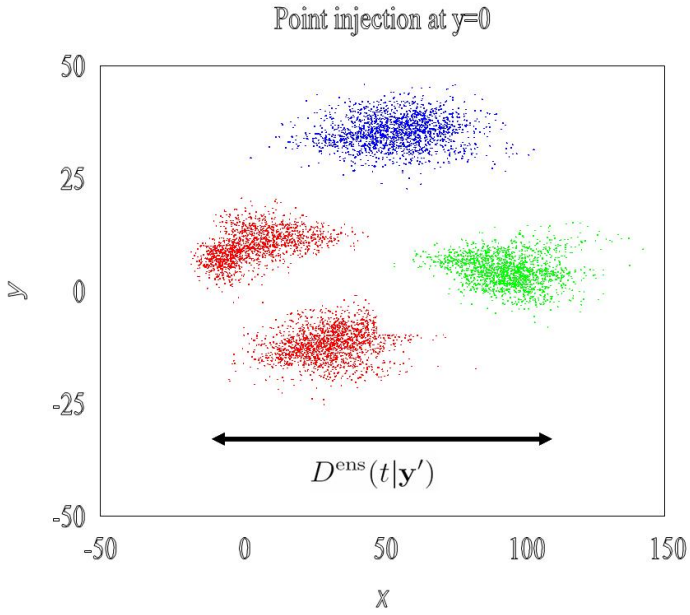

(a)

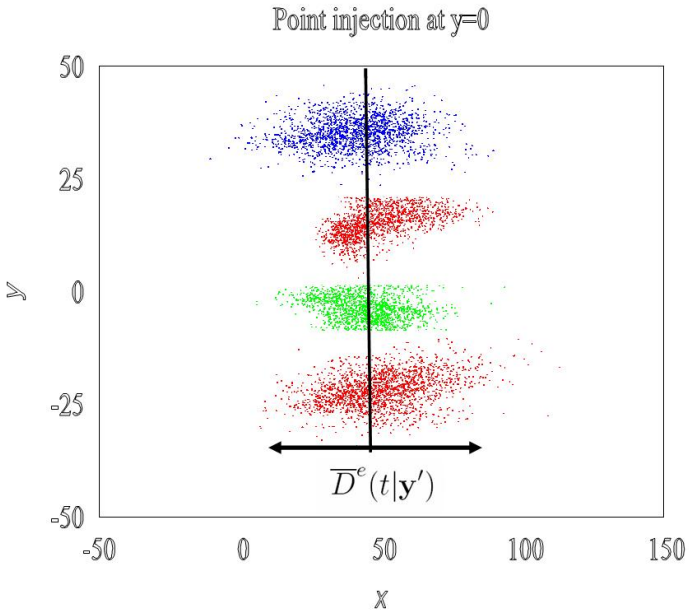

(b)

Figure 2.3: Solute distributions evolving from a point-like injection in different disorder realizations to illustrate the conceptual difference between the (a) ensemble and (b) averaged local effective dispersion coefficient.

and (2.33),

$$\overline{\nu}_i(t|\mathbf{x}') = \langle\overline{\nu_i(t|\mathbf{x}')}\rangle, \tag{2.39}$$

$$\overline{D}^{\mathrm{e}}_{ij}(t|\mathbf{x}') = \langle\overline{D^e_{ij}(t|\mathbf{x}')}\rangle. \tag{2.40}$$

For an extended solute distribution, the average global center of mass velocity and effective dispersion coefficient are given by,

$$\overline{v}_i(t) = \int\limits_{\Omega^d} \mathrm{d}\mathbf{x}'\rho(\mathbf{x}')\langle\overline{\nu}_i(t|\mathbf{x}')\rangle, \qquad \overline{D}^{\mathrm{e}}_{ij}(t) = \int\limits_{\Omega^d} \mathrm{d}\mathbf{x}'\rho(\mathbf{x}')\langle\overline{D}^{\mathrm{e}}_{ij}(t|\mathbf{x}')\rangle. \tag{2.41}$$

The average apparent dispersion coefficient is defined by the ensemble average over (2.37)

$$\overline{D}^a_{ij}(t) = \langle\overline{D^a_{ij}(t)}\rangle. \tag{2.42}$$

For early times, the apparent dispersion coefficient quantifies spreading due to the velocity contrast within the initial solute distribution, compare (2.38).

In addition, we will consider the so-called ensemble dispersion coefficient, which describes the temporal rate of change of the longitudinal width of the ensemble averaged Green function $\overline{g(\mathbf{x}, t|\mathbf{x}', t')}$,

$$D^{\mathrm{ens}}_{ij}(t|\mathbf{x}') = \frac{1}{2}\frac{\mathrm{d}}{\mathrm{d}t}\langle\overline{\mu^{(2)}_{ij}(t|\mathbf{x}')} - \overline{\mu^{(1)}_i(t|\mathbf{x}')\mu^{(1)}_j(t|\mathbf{x}')}\rangle. \tag{2.43}$$

The difference between the ensemble and average effective dispersion coefficients, is given by,

$$D^{\mathrm{ens}}(t|\mathbf{x}') - \overline{D}^{\mathrm{e}}(t|\mathbf{x}') = \frac{1}{2}\frac{\mathrm{d}}{\mathrm{d}t}\langle\overline{\mu^{(1)}_i(t|\mathbf{x}')\mu^{(1)}_j(t|\mathbf{x}')} - \overline{\mu^{(1)}_i(t|\mathbf{x}')}\ \ \overline{\mu^{(1)}_j(t|\mathbf{x}')}\rangle. \tag{2.44}$$

The conceptual difference is illustrated in Figure 2.3.

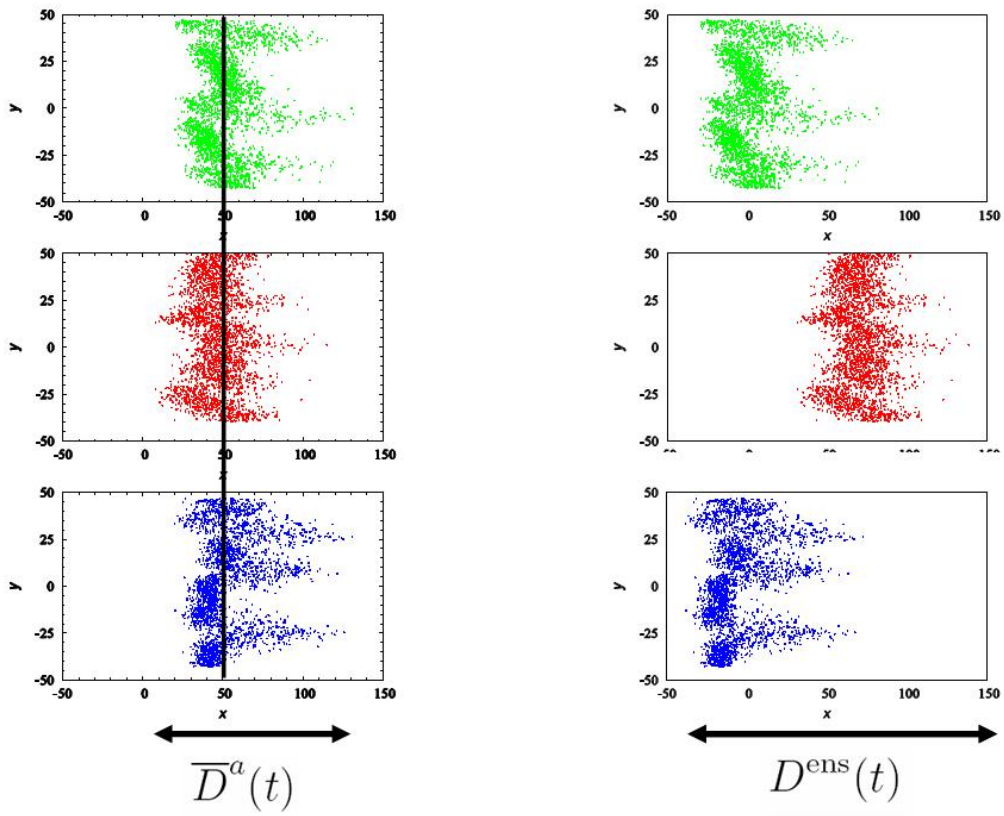

Figure 2.4: Solute distributions evolving from extended sources in different disorder realizations to illustrate the conceptual difference between the (a) averaged apparent and (b) global ensemble dispersion coefficient.

For an extended solute distribution, the ensemble dispersion coefficient is given by,

$$D_{ij}^{\text{ens}}(t) = \int_{\Omega^d} \mathrm{d}\mathbf{x}' \rho(\mathbf{x}') \langle D_{ij}^{\text{ens}}(t|\mathbf{x}') \rangle. \tag{2.45}$$

The difference between the ensemble and average apparent dispersion coefficients is given by,

$$D_{ij}^{\text{ens}}(t) - \overline{D}_{ij}^{a}(t) = \frac{1}{2}\frac{\mathrm{d}}{\mathrm{d}t} \int_{\Omega^d} \mathrm{d}\mathbf{x}' \rho(\mathbf{x}') \overline{\mu_i^{(1)}(t|\mathbf{x}') \left[m_j^{(1)}(t) - \mu_j^{(1)}(t|\mathbf{x}') \right]}. \tag{2.46}$$

The conceptual difference is illustrated in Figure 2.4

The ensemble and the average effective dispersion coefficients differ in the fluctuations of the center of mass from realization to realization. As outlined by *Dentz and Carrera*, [38], the difference between these coefficients quantifies an artificial dispersion effect caused by sample to sample fluctuations of the local center of mass position from realization to realization of the heterogeneous medium. This unphysical ensemble spreading mechanism is suppressed in the definition of the average effective dispersion coefficients in (2.41). The conceptual difference between these quantities has been extensively studied in the groundwater literature; i.e. [39, 43, 42, 44]; while the quantification of this difference was outlined by [25, 26].

Note that in the limit of an infinite medium, the dependence of the initial position is wiped out by the ensemble average, which leads to vertical homogenization and makes the average medium isotropic. This symmetry is broken for a finite medium so that even in average, the memory of the initial position is preserved in the behavior of the local effective and local ensemble dispersion coefficients.

2.7 Methodology

In order to obtain analytical expressions for the effective transport coefficients, the advection dispersion transport equation for the particular random flow field under consideration has to be solved to obtain the concentration distribution $c(\mathbf{x}, t)$, and then to calculate the correspondent spatial moments.

For arbitrary flow fields, the transport equation has no closed solution and tools like perturbation theory may be required. Perturbation theory has been extensively used in stochastic hydrology to solve flow and transport problems, (e.g.,[39, 40]). Temporal behavior of effective transport coefficients was analyzed by [27, 25] within a second order perturbation approach assuming small fluctuations of the heterogeneities. Note that in the literature it is usually referred to as a first order approach because after the ensemble average, the observables are of first order in the variances of the random fields. Transport in stratified media, however, can be solved exactly by axial moment equations; (e.g.,[29]). The general concepts of both techniques are described here, and in the following chapters, these techniques are applied to solve specific transport scenarios.

Numerical simulations were used in this thesis as a tool to complement and verify the analytical solutions of effective transport coefficients in stratified media models. Here we also describe the numerical random walk method employed.

2.7.1 Perturbation Theory

Since there is no closed form solution for the advection dispersion equation (2.15) for an arbitrary velocity field $\mathbf{u}(\mathbf{x}, t)$ considered, here we present the perturbation theory applied to systematically investigate the temporal be-

havior of the concentration distribution $c(\mathbf{x}, t)$.

For computational convenience we rewrite the equation (2.15) in terms of the Fourier transformed concentration $\tilde{c}(\mathbf{k}, t)$,

$$\frac{\partial \tilde{c}(\mathbf{k}, t)}{\partial t} - \mathrm{i}\,\mathbf{u}(t)\mathbf{k}\tilde{c}(\mathbf{k}, t) + \mathbf{k}\mathbf{D}\mathbf{k}\tilde{c}(\mathbf{k}, t) = \tilde{\rho}(\mathbf{k})\delta(t) + \int_{\mathbf{k}'} \tilde{\mathbf{L}}\{\mathbf{k}, \mathbf{k}', t\}\tilde{c}(\mathbf{k} - \mathbf{k}', t), \tag{2.47}$$

where the Fourier transformed variables are marked by a tilde. Note that the Fourier transform of $c(\mathbf{x}, t)$ and the back-transform are defined as,

$$\tilde{c}(\mathbf{k}, t) = \int \mathrm{d}x c(\mathbf{x}, t) \exp(\mathrm{i}\mathbf{k} \cdot \mathbf{x}), \tag{2.48}$$

$$c(\mathbf{x}, t) = \int_k \tilde{c}(\mathbf{k}, t) \exp(-\mathrm{i}\mathbf{k} \cdot \mathbf{x}), \tag{2.49}$$

where we used the short-hand notation,

$$\int_k \cdots = \int \frac{d^d k}{(2\pi)^d}. \tag{2.50}$$

The Fourier transformed perturbation operator $\tilde{\mathbf{L}}\{\mathbf{k}, \mathbf{k}', t\}$ in (2.47) is defined by,

$$\tilde{\mathbf{L}}\{\mathbf{k}, \mathbf{k}', t\} = \tilde{\mu}(\mathbf{k})\frac{\partial}{\partial t} - \mathrm{i}\mathbf{k}\tilde{\mathbf{u}}'(\mathbf{k}', t). \tag{2.51}$$

In order to solve the transport equation we rewrite equation (2.47) as an equivalent integral equation (see e.g. [20, 38]),

$$\tilde{c}(\mathbf{k}, t) = \tilde{c}_0(\mathbf{k}, t, 0)\tilde{\rho}(\mathbf{k}) + \int_{k'} \int_{-\infty}^{\infty} \mathrm{d}t' \tilde{c}_0(\mathbf{k}, t, t')\tilde{\mathbf{L}}\{\mathbf{k}, \mathbf{k}', t'\}\tilde{c}(\mathbf{k} - \mathbf{k}', t'). \tag{2.52}$$

The zeroth-order term $\tilde{c}_0(\mathbf{k}, t)$, is the known Fourier-transformed Green function of the unperturbed solution of the transport problem (2.47), for $\tilde{\mathbf{L}}\{\mathbf{k}, \mathbf{k}', t'\} = 0$, and point like injection (equivalent in Fourier space to $\tilde{\rho}(\mathbf{k}) = 1$).

The Fourier-transformed Green function $\tilde{c}_0(\mathbf{k},t,t')$ of the transport problem (2.15) for $\tilde{\mathbf{L}}\{\mathbf{k},\mathbf{k}',t'\}\equiv 0$ reads as,

$$\tilde{c}_0(\mathbf{k},t,t') = \exp\left[-\mathbf{k}\mathbf{D}\mathbf{k}(t-t') + \mathrm{i}\mathbf{k}\cdot\int_{t'}^{t}\mathrm{d}\tau\mathbf{u}(\tau)\right]\Theta(t-t') \qquad (2.53)$$

with $\Theta(t)$ the Heaviside step function.

Iterations of the integral expression (2.52) yields a perturbation expansion of $\tilde{c}(\mathbf{k},t)$ in terms of the perturbation operator $\tilde{\mathbf{L}}\{\mathbf{k},\mathbf{k}',t'\}$,

$$\begin{aligned}\tilde{c}(\mathbf{k},t) &= \tilde{c}_0(\mathbf{k},t,0)\tilde{\rho}(\mathbf{k}) + \int_{k'}\int_{-\infty}^{\infty}\mathrm{d}t'\tilde{c}_0(\mathbf{k},t,t')\tilde{\mathbf{L}}\{\mathbf{k},\mathbf{k}',t'\}\tilde{c}_0(\mathbf{k}-\mathbf{k}',t',0)\\ &+\int_{k'}\int_{-\infty}^{\infty}\mathrm{d}t'\int_{k''}\int_{-\infty}^{\infty}\mathrm{d}t''\tilde{c}_0(\mathbf{k},t,t')\tilde{\mathbf{L}}\{\mathbf{k},\mathbf{k}',t'\}\tilde{c}_0(\mathbf{k}-\mathbf{k}',t',t'')\\ &\times\tilde{\mathbf{L}}\{\mathbf{k}-\mathbf{k}',\mathbf{k}'',t''\}\tilde{c}_0(\mathbf{k}-\mathbf{k}'-\mathbf{k}'',t'',0)+\cdots\,. \qquad (2.54)\end{aligned}$$

This series expansion truncated after the second order of $\tilde{\mathbf{L}}$ constitutes the basis for our perturbation analysis of the transport coefficients.

Note that the Green function $\tilde{c}_0(\mathbf{k},t,t')$ depends on the temporal fluctuations $\boldsymbol{v}(t)$. To obtain consistent expressions for the transport coefficients, $\tilde{c}_0(\mathbf{k},t,t')$ will be expanded in powers of $\boldsymbol{v}(t)$ in the following,

$$\tilde{c}_0(\mathbf{k},t,t') = \widetilde{g}_0(\mathbf{k},t-t')\Big[1+u\mathrm{i}\mathbf{k}\cdot\int_{t'}^{t}\mathrm{d}t''\boldsymbol{v}(t'')+\ldots.\Big]\Theta(t-t') \qquad (2.55)$$

We defined here

$$\widetilde{g}_0(\mathbf{k},t) = \exp\left(-\mathbf{k}\mathbf{D}\mathbf{k}t + \mathrm{i}k_1ut\right), \qquad (2.56)$$

which is the Fourier transform of the solution of (2.15) for $\boldsymbol{v}(t)=\mathbf{u}'(\mathbf{x},t)\equiv 0$ and $\mu(\mathbf{x})=0$.

2.7.2 Axial Moment Equations

The advection dispersion equation for solute transport trough a stratified medium can be solved explicitly by the definition of axial moment equations. From the effective transport formulations and measures proposed by *Dentz and Carrera* [29], which we have discussed in this chapter in section 2.6.1, we rewrite the local moments as,

$$\mu_i^{(n)}(t|\mathbf{x}') = \int \mathrm{d}\mathbf{y} c_n(\mathbf{y}, t|\mathbf{x}'), \tag{2.57}$$

where we defined the local axial moments $c_n(\mathbf{y}, t|\mathbf{x}')$ by,

$$c_n(\mathbf{y}, t|\mathbf{x}') = \int_{-\infty}^{\infty} \mathrm{d}x_1 x_1^n g(\mathbf{x}, t|\mathbf{x}', 0). \tag{2.58}$$

with $i = 1, \ldots, d$. We remind here that the Green function $g(\mathbf{x}, t|\mathbf{x}', 0)$, is the solute distribution for a point like injection. The $c_0(\mathbf{y}, t|\mathbf{x}')$ is the vertical concentration profile integrated over the x_1-direction of a solute that evolves from a point injection at $\mathbf{x}'$ at time $t = 0$. The local axial center of mass at the vertical position $\mathbf{y}$ at time t is given by $c_1(\mathbf{y}, t|\mathbf{x}')$, while $c_2(\mathbf{y}, t|\mathbf{x}')$ is a measure for the width of the solute distribution at the vertical position $\mathbf{y}$ at time t.

Hence, by multiplication of the transport equation (2.25) with x_1^n and subsequent integration over x_1 we can obtain for $n = 0, 1, 2$ the following transport equations,(e.g., [29]),

$$\frac{\partial c_0(\mathbf{y}, t|\mathbf{y}')}{\partial t} + u\boldsymbol{v}_T(t) \cdot \nabla_{\mathbf{y}} c_0(\mathbf{y}, t|\mathbf{y}') - D_T \nabla_{\mathbf{y}}^2 c_0(\mathbf{y}, t|\mathbf{y}') = 0, \tag{2.59}$$

$$\frac{\partial c_1(\mathbf{y}, t|\mathbf{x}')}{\partial t} + u\boldsymbol{v}_T(t) \cdot \nabla_{\mathbf{y}} c_1(\mathbf{y}, t|\mathbf{y}') - D_T \nabla_{\mathbf{y}}^2 c_1(\mathbf{y}, t|\mathbf{x}') = u\boldsymbol{\Lambda}(\mathbf{y}, t) c_0(\mathbf{y}, t|\mathbf{y}'), \tag{2.60}$$

$$\frac{\partial c_2(\mathbf{y},t|\mathbf{x}')}{\partial t} + u\boldsymbol{\upsilon}_T(t)\cdot\nabla_{\mathbf{y}}c_2(\mathbf{y},t|\mathbf{y}') - D_T\nabla^2_{\mathbf{y}}c_2(\mathbf{y},t|\mathbf{x}') = 2u\boldsymbol{\Lambda}(\mathbf{y},t)c_1(\mathbf{y},t|\mathbf{x}') + 2D_L c_0(\mathbf{y},t|\mathbf{y}'), \tag{2.61}$$

where $\nabla_{\mathbf{y}}$ denotes the nabla operator in Ω. The $\boldsymbol{\upsilon}_T(t)$ are the temporal flow fluctuations transverse to the direction of the mean flow velocity, $\boldsymbol{\upsilon}_T(t) = [0, \upsilon_2(t), \ldots, \upsilon_d(t)]^T$. We defined the $\boldsymbol{\Lambda}(\mathbf{y},t)$ function as,

$$\boldsymbol{\Lambda}(\mathbf{y},t) = [1 - \upsilon_1(t) - k(\mathbf{y}) - \upsilon_1(t)k(\mathbf{y})] \tag{2.62}$$

The initial conditions are given by,

$$c_n(\mathbf{y},0|\mathbf{x}') = {x_1'}^n\delta(\mathbf{y}-\mathbf{y}'), \tag{2.63}$$

where $n = 0, 1, 2$. The boundary conditions are,

$$\mathbf{n}\cdot\nabla c_n(\mathbf{y},t|\mathbf{x}')|_{\mathbf{x}\in\partial\Omega^d} = 0. \tag{2.64}$$

where $\partial\Omega^d$ is the boundary of the transport domain Ω^d and $\mathbf{n}$ is the outward pointing unit vector perpendicular to the domain boundaries.

The initial and boundary conditions imply, (i) $c_0(\mathbf{y},t|\mathbf{x}') \equiv c_0(\mathbf{y},t|\mathbf{y}')$, and (ii),

$$\int_{\Omega} \mathrm{d}\mathbf{y} c_0(\mathbf{y},t|\mathbf{y}') = 1. \tag{2.65}$$

Applying Duhamel's principle in order to express $c_1(\mathbf{y},t|\mathbf{x}')$ and $c_2(\mathbf{y},t|\mathbf{x}')$ in terms of the auxiliary function $c_0(\mathbf{y},t|\mathbf{x}')$, we can write the expressions (2.60) and (2.61) as follows,

$$\begin{aligned} c_1(\mathbf{y},t|\mathbf{x}') &= (x_1' + ut)c_0(\mathbf{y},t|\mathbf{y}') \\ &\quad + u\int_0^t \mathrm{d}t' \int_{\Omega} \mathrm{d}\mathbf{y}'' c_0(\mathbf{y},t|\mathbf{y}'',t')\left[\boldsymbol{\Lambda}(\mathbf{y}'',t') - 1\right] c_0(\mathbf{y}'',t'|\mathbf{y}'), \end{aligned} \tag{2.66}$$

$$c_2(\mathbf{y},t|\mathbf{x}') = \left[x_1'^{\,2} + 2D_L t\right] c_0(\mathbf{y},t|\mathbf{y}') + 2u \int_0^t \mathrm{d}t' \int_\Omega \mathrm{d}\mathbf{y}'' c_0(\mathbf{y},t|\mathbf{y}'',t') \mathbf{\Lambda}(\mathbf{y}'',t') c_1(\mathbf{y}'',t'|\mathbf{x}'). \tag{2.67}$$

According to (2.57), we now obtain for the first and second local moments,

$$\mu_1^{(1)}(t|\mathbf{y}') = x_1' + u\,t + u \int_\Omega \mathrm{d}\mathbf{y}'' \int_0^t \mathrm{d}t' \left[\mathbf{\Lambda}(\mathbf{y}'',t') - 1\right] c_0(\mathbf{y}'',t'|\mathbf{y}'), \tag{2.68}$$

$$\begin{aligned}\mu_1^{(2)}(t|\mathbf{y}') &= (x_1' + u\,t)^2 + 2D_L t \\ &+ 2u(x_1' + u\,t) \int_\Omega \mathrm{d}\mathbf{y}'' \int_0^t \mathrm{d}t' \left[\mathbf{\Lambda}(\mathbf{y}'',t') - 1\right] c_0(\mathbf{y}'',t'|\mathbf{y}') \\ &+ 2u^2 \int_\Omega \mathrm{d}\mathbf{y}'' \int_\Omega \mathrm{d}\mathbf{y} \int_0^t \mathrm{d}t' \int_0^{t'} \mathrm{d}t'' \left[\mathbf{\Lambda}(\mathbf{y}'',t') - 1\right] \left[\mathbf{\Lambda}(\mathbf{y},t'') - 1\right] \\ &\times c_0(\mathbf{y}'',t'|\mathbf{y},t'') c_0(\mathbf{y},t''|\mathbf{y}').\end{aligned} \tag{2.69}$$

The first $m_T^{(1)}(t)$ and second $m_T^{(2)}(t)$ moments in the transverse directions are derived in Appendix C.

2.7.3 Numerical Random Walk simulations

Here we present the numerical random walk tool used to perform numerical simulations to investigate temporal behavior of the effective transport coefficients in stratified media models.

The numerical solution of the transport problem using random walk simulations are based on a Lagrangian transport framework, which in contrast to the Eulerian framework, describes the motion of solute particles. The solute particle movement is given by the divergence-free flow $\mathbf{u}(\mathbf{x})$, and a

stochastic force, $\xi(t)$, which models the erratic movement of a particle due to local dispersion. This is expresed by the following equation of motion [39],

$$\frac{\mathrm{d}}{\mathrm{d}t}\mathbf{x}(\mathbf{a},t) = \mathbf{u}\left(\mathbf{x}(\mathbf{a},t)\right) + \sqrt{2\mathbf{D}}\boldsymbol{\xi}(t), \tag{2.70}$$

where $\mathbf{x}(t)$ denotes the particle position at time t with initial position $\mathbf{x}(\mathbf{a}, t = 0) = \mathbf{a}$. The initial particle distribution is then given by $\rho(\mathbf{a})$; the $\boldsymbol{\xi}(t)$ is a Gaussian white noise random vector with zero mean correlation $\langle \xi(t)\xi(t')\rangle = \delta(t - t')$.

In discrete time, the equation of a solute particle is given by,

$$x^{(i,r)}(t + \Delta t|\mathbf{y}') = x^{(i,r)}(t) + \mathbf{u}\left(\mathbf{x}^{(i,r)}(t|\mathbf{x}')\right)\Delta t + \sqrt{2D_L\Delta t}\,\xi_N^{(i)} \tag{2.71}$$

$$\mathbf{y}^{(i,r)}(t + \Delta t|\mathbf{y}') = \mathbf{y}^{(i,r)}(t|\mathbf{y}') + \sqrt{2D_T\Delta t}\,\boldsymbol{\eta}_N^{(i)}, \tag{2.72}$$

where $\xi_N^{(i)}$ and $\boldsymbol{\eta}_N^{(i)}$ are mutually independent Gaussian random vectors with zero mean and unit variance; $x^{(i,r)}(t|\mathbf{y}')$ and $\mathbf{y}^{(i,r)}(t|\mathbf{y}')$ denote the particle trajectory starting from $\mathbf{x}(0)$ in the i-th noise and r-th disorder realization.

The random flow field $\mathbf{u}\left(\mathbf{x}^{(i,r)}(t|\mathbf{x}')\right)$ employed is described for each case in the followings chapters. We will also detail the medium dimensions, time discretization, number of realization, etc.

The local moments $\mu^{(n,r)}(t|\mathbf{x}')$ in the $r-$th disorder realization are derived from averages of the particle trajectories over all noise realizations as (e.g.,[29]),

$$\mu^{(n,r)}(t|\mathbf{x}') = \frac{1}{N}\sum_{i=1}^{N}\left[\mathbf{x}^{(i,r)}(t|\mathbf{x}')\right], \tag{2.73}$$

where N is the total number of noise realizations. The global moments in the $r-$th disorder realization then are obtained by summation of (2.73) over all initial positions as,

$$m^{(n,r)}(t) = \frac{1}{M} \sum_{j=1}^{M} \mu^{(n,r)}(t|\mathbf{y}'^{(j)}). \tag{2.74}$$

where M is the finite initial extent of the injection region, which is equivalent to averaging over various realizations.

Ensemble averages then are taken accordingly by summation of the respective observables over all realizations of the random conductivity field under consideration. Thus, the ensemble average is numerically approximated by,

$$\overline{\varphi\{k(\mathbf{y})\}} = \frac{1}{R} \sum_{r=1}^{R} \varphi\{k^{(r)}(\mathbf{y})\} \tag{2.75}$$

with $\varphi\{k(\mathbf{y})\}$ an arbitrary functional of the random conductivity field and R the total number of disorder realizations.

Chapter 3

Effective Dispersion in a Chemically Heterogeneous Medium under Temporally Fluctuating Flow Conditions

3.1 Introduction

Local scale physical and chemical medium heterogeneities lead to an effective large scale transport behavior that is qualitatively and quantitatively different from the one observed in homogeneous media. The interaction of spatial fluctuations of the system parameters and local scale transport processes leads in general to enhanced solute spreading and mixing.

The influence of spatially fluctuating physical and chemical system properties, such as hydraulic conductivity and sorption properties, for example, on solute transport has been studied extensively during the last two decades within the stochastic perturbative approach, e.g., [45, 46, 22, 24, 47, 48],

among others. The later studies disregard the effects of local dispersion or focus on the asymptotic long time behavior of solute transport. The full temporal evolution of effective solute spreading in a chemically and physically heterogeneous medium for finite local dispersion has been studied in terms of the time behavior of effective dispersion coefficients, see, e.g., [25, 26, 27]. The stochastic perturbative analysis yields an increase of the longitudinal effective dispersion coefficient to a macroscopic value as a result of physical and chemical medium heterogeneities, which is in agreement with experimental and numerical findings. The predicted asymptotic transverse dispersion coefficients, however, consistently underestimates numerical and experimental observations by at least one order of magnitude e.g., [3, 19, 4]. Recently, the scale dependence of macrodispersion and effective retardation factors for reactive chemicals has been studied in laboratory scale experiments [49] and critically compared to stochastic theories [50]. As been intimately connected with scale dependence, the temporal behavior of these effective parameters has been also investigated within a stochastic framework e.g., [51].

Transverse mixing is a critical process for geochemical processes in rivers [52], stream-aquifer interactions [53], saltwater intrusion [54, 55], and microbial reactions [56, 57]. The importance of transverse mixing for reactive transport modeling including precipitation (dissolution) reactions has recently been shown by [58]. Thus, the quantification of transverse mixing is of importance in a number of environmental problems such as soil and water bodies remediation.

In addition to spatial fluctuations of the system parameters due to physical and chemical medium heterogeneities, groundwater flow in general also fluctuates temporally on a range of scales including hyper annual climatic fluctuations, seasonal and irrigation cycles and daily barometric fluctuations,

for example. Such temporal flow fluctuations were first recognized as a source of enhanced solute spreading by [16]. Rehfeldt and Gelhar [18] presented a stochastic approach for the quantification of the impact of temporal flow fluctuations in a physically heterogeneous medium. Within such a stochastic framework, Kabala and Sposito [59] studied macrodispersion for reactive transport in a spatially heterogeneous medium. Solute spreading in a heterogeneous medium for periodic (deterministic) time fluctuations of the hydraulic gradient for purely advective transport (vanishing local dispersion) has been analyzed by, e.g., Zhang and Neuman [60] and Dagan et al [61]. Recently, Cirpka [62] studied the enhancement of transverse dispersion of kinetically sorbing compounds in spatially uniform flow field under sinusoidal (deterministic) temporal fluctuations and vanishing local dispersion.

A recent approach to characterize and quantify effective spreading and mixing in time-fluctuating flow through a physically heterogeneous medium is an analysis in terms of effective dispersion coefficients [20, 37, 38]. Effective dispersion coefficients characterize effective solute spreading and mixing in an heterogeneous environment [42, 25, 26]. For transport in time fluctuating spatial random flow fields, it was shown that the interaction between temporal fluctuations, local dispersion and spatial heterogeneity leads to macroscopic contributions to the longitudinal as well as, and more importantly, the transverse effective dispersion coefficients [20, 37, 38].

3.2 Basics

We investigate effective solute transport in a chemically heterogeneous infinite medium subject to temporal fluctuations of the flow conditions, the flow and transport model were introduced in section 2.2 and 2.3, respectively.

We focus on linear sorption reactions under instantaneous local equilibrium conditions, where the corresponding fluctuating retardation factor is modeled as a stationary random space function. The temporal variability of the flow is represented by a stationary temporal random process. The stochastic modeling approach is described in section 2.4.

Solute spreading is quantified by effective dispersion coefficients, which are derived from the ensemble average of the second centered moments of the normalized solute distribution in a single disorder realization. As we study here transport for a solute evolving from a point like injection at $t = 0$; i.e. $\rho(\mathbf{x}) = \delta(\mathbf{x})$, we will focus on transport coefficients derived from the first and second local moments defined in (2.27) and (2.28). Note that, as outlined in section 2.6.4, here the point observables do not depend on the injection position, as the memory is wiped out by the stochastic average. Thus, in the following we supress the injection position in the notation of the observables.

Using the first-order perturbation approach in the variances of the random fields described in 2.7.1, we derive explicit compact expressions for the time behavior of the disorder induced contributions to the effective dispersion coefficients.

3.3 Observables

As the simplest measures for the analysis of the evolution of the sorbing chemical, here we study the effective center of mass velocity, defined in (2.39), and effective dispersion coefficients in (2.40), of the (normalized) mobile solute fraction [25],

$$p(\mathbf{x}, t) = \frac{c_m(\mathbf{x}, t)}{\int \mathrm{d}^d y c_m(\mathbf{y}, t)}. \tag{3.1}$$

We refer here to the normalization of a distribution density which reads as,

$$\int \mathrm{d}^d x p(\mathbf{x}, t) = 1. \tag{3.2}$$

The effective dispersion coefficient for finite local dispersion has been analyzed by [25, 26, 27] for transport in a physical and chemically heterogeneous medium under steady flow conditions, and [20, 37, 38] for passive transport in temporally fluctuating flow. The relevance of effective dispersion coefficients for the quantification of solute mixing and thus for reactive transport modeling has been outlined by [28, 63, 64]. Thus, here we focus exclusively on the analysis of the effective transport velocity and dispersion coefficients.

Transport Coefficients

The effective transport velocity $\overline{v}_i^{\mathrm{e}}(t)$,(2.39), and the dispersion coefficients $\overline{D}_{ij}^{\mathrm{e}}(t)$, (2.40), can be expressed in terms of the Fourier transform of $p(\mathbf{x}, t)$, as (e.g., [25, 26])

$$\overline{v}_i^{\mathrm{e}}(t) = \frac{1}{\mathrm{i}} \frac{\mathrm{d}}{\mathrm{dt}} \frac{\partial}{\partial k_i} \langle \overline{\ln \widetilde{p}(\mathbf{k}, t)} \rangle \mid_{\mathbf{k}=\mathbf{0}} \tag{3.3}$$

$$\overline{D}_{ij}^{\mathrm{e}}(t) = -\frac{1}{2} \frac{\mathrm{d}}{\mathrm{dt}} \frac{\partial}{\partial k_i} \frac{\partial}{\partial k_j} \langle \overline{\ln \widetilde{p}(\mathbf{k}, t)} \rangle \mid_{\mathbf{k}=\mathbf{0}} \tag{3.4}$$

with the Fourier transform of $p(\mathbf{x}, t)$ given by

$$\widetilde{p}(\mathbf{k}, t) = \frac{\widetilde{c}(\mathbf{k}, t)}{\widetilde{c}(0, t)}, \tag{3.5}$$

where $\widetilde{c}(\mathbf{k}, t)$ is the second order perturbation expansion defined in (2.54).

Relations (3.3) and (3.4) can be readily verified by using the definition of the Fourier transform (2.49).

Inserting the series expansion (2.54) into (3.4) and expanding the resulting expression for small variances of the random fields the dispersion

coefficients decompose into,

$$\begin{aligned}\overline{D}^{\mathrm{e}}_{ij}(t) &= D_{ij} + \delta^{\mu\mu}\overline{D}^{\mathrm{e}}_{ij}(t) + \delta^{uu}\overline{D}^{\mathrm{e}}_{ij}(t) + \delta^{uv}\overline{D}^{\mathrm{e}}_{ij}(t) \\ &\quad + \delta^{u\mu}\overline{D}^{\mathrm{e}}_{ij}(t) + \delta^{\mu v}\overline{D}^{\mathrm{e}}_{ij}(t) \end{aligned} \tag{3.6}$$

and accordingly for the effective center of mass velocity (3.3). Note that strictly speaking for such an expansion to be valid, the variances of the random fields are required to be small.

The effective dispersion coefficients $\overline{D}^{\mathrm{e}}_{ij}(t)$ is given by the sum of the contributions due to (i) local dispersion D_{ij}, (ii) chemical heterogeneity $\delta^{\mu\mu}\overline{D}^{\mathrm{e}}_{ij}$ (see [25]), (iii) physical heterogeneity and temporal fluctuations of the flow conditions $\delta^{uu}\overline{D}^{\mathrm{e}}_{ij}$ and $\delta^{uv}\overline{D}^{\mathrm{e}}_{ij}$ (see, e.g., [26, 27, 20, 38], (iv) cross-correlations between physical and chemical heterogeneity $\delta^{u\mu}\overline{D}^{\mathrm{e}}_{ij}$ (see, e.g., [26] for the steady state case), and (v) the interaction between temporal fluctuations and chemical heterogeneity $\delta^{\mu v}\overline{D}^{\mathrm{e}}_{ij}$. In the following, we focus on a physically homogeneous, i.e., $\delta^{uu}\overline{D}^{\mathrm{e}}_{ij} = \delta^{uv}\overline{D}^{\mathrm{e}}_{ij} = \delta^{u\mu}\overline{D}^{\mathrm{e}}_{ij} = 0$, chemically heterogeneous medium.

This kind of simplified model might be appropriate to describe the transport of an organic solute in an aquifer, which is comparatively homogeneous with respect to the hydraulic conductivity, but exhibits a strongly varying organic carbon content which determines the retardation factor (i.e. [62]). We focus here on $\delta^{\mu v}\overline{D}^{\mathrm{e}}_{ij}$ and on its relative importance with respect to the contribution due to chemical heterogeneity only [25]. The $\delta^{\mu\mu}\overline{D}^{\mathrm{e}}_{ij} + \delta^{\mu v}\overline{D}^{\mathrm{e}}_{ij}$ quantify the total contributions to effective spreading for solute transport under fluctuating flow conditions in a chemically heterogeneous, physically homogeneous medium. Explicit expressions for $\delta^{\mu v}\overline{\nu}^{\mathrm{e}}_{i}$ and $\delta^{\mu v}\overline{D}^{\mathrm{e}}_{ij}$ are given in Appendix A.

3.3.1 Time Scales and the Validity of Effective Parameters

The temporal evolution of the effective dispersion coefficients is determined by three characteristic time scales, τ_u, τ_{D_i}, and τ_κ. The advection time scale τ_u measures the time for the solute to be advected over one longitudinal correlation length l_1,

$$\tau_u = \frac{l_1}{u}. \tag{3.7}$$

The dispersion time scales τ_{D_i} characterize the time for dispersive transport over one correlation length l_i,

$$\tau_{D_i} = \frac{l_i^2}{D_{ii}}. \tag{3.8}$$

The Kubo time scale τ_κ [38], measures the time for the local dispersive spreading over an effective length that is given by the correlation length l and the Kubo length $l_\kappa = u\tau$,

$$\tau_\kappa = (1+\kappa^2)\tau_{D_1} = (l^2 + l_\kappa^2)\tau_{D_1}. \tag{3.9}$$

We defined here the non-dimensional Kubo number, $\kappa = \tau/\tau_u = l_\kappa/l_1$, which compares the correlation time τ to the advection time scale τ_u, and equivalently the Kubo distance $l_\kappa = u\tau$ (which denotes the length over which the the solute is advected by the mean flow during one correlation time τ) to the correlation length in direction of the mean flow l_1.

The non-dimensional Peclet numbers $Pe_i = \tau_{D_i}/\tau_u$ compare the strength of advective and dispersive transport mechanism. In many hydrological applications transport is advection dominated, which implies large Peclet numbers, $Pe \gg 1$, or accordingly, small inverse Peclet numbers $\epsilon_i \equiv \tau_u/\tau_{Di} = D_{ii}l_1/(ul_i^2)$. In the following we will develop simple compact expressions for the effective dispersion coefficients under the assumption of small ϵ_i.

Note that for times smaller than the advection timescale, $t \leq \tau_u$, the solute has moved by mean advection over a distance shorter than the correlation length l_1 of the medium, and has spread by local dispersion over a distance which is much smaller than the corresponding correlation distance. On such short scales the medium looks quasi homogeneous and the solute does not "see" the heterogeneity of the medium. Thus, the spatial ensemble average and accordingly the effective parameters defined as ensemble averages, have only a limited formal meaning for $t \leq \tau_u$ as there can be large sample to sample fluctuations between the disorder realizations. Correspondingly, for times smaller than the correlation time τ (or equivalently, for transport distances smaller than the Kubo distance l_κ), the flow field appears to be quasi steady, and the temporal average has only a formal meaning.

Appendix A summarizes the somewhat lengthy calculations that lead to the expressions for the effective center of mass velocity and dispersion coefficients presented in the following. We employ an expansion for small inverse Peclet numbers $\epsilon_i \ll 1$ and time large compared to the advection time scale $t \gg \tau_u$ (e.g., [38]) in order to simplify the lengthy expressions given in Appendix A.

3.3.2 Effective Center of Mass Velocity

The leading contributions for small ϵ_i to the effective center of mass velocity, $\delta^{\mu\nu}\overline{\nu}_i^{\mathrm{e}}$, are given by (see Appendix A),

$$\delta^{\mu\nu}\overline{\nu}_i^{\mathrm{e}}(t) = u\sigma_{\mu\mu}^2\sigma_{\nu\nu}^2 \int_{k'} \widetilde{C}^{\mu\mu}(\mathbf{k}')\left[\delta_{i1}A(\mathbf{k}',t) + A_i(\mathbf{k}',t,0)\right]\exp\left(-\mathrm{i}uk_1't\right) + \ldots, \tag{3.10}$$

where the dots denote subleading contributions of the order of the inverse Peclet numbers. The auxiliary functions $A(\mathbf{k},t)$ and $A_i(\mathbf{k}',t,0)$ are defined by (A.18) and (A.19) in Appendix A. For short-range correlation functions, expression (3.10) decreases exponentially fast on the advection time scale τ_u.

3.3.3 Effective Dispersion Coefficients

As outlined in Appendix A, the leading behavior of $\delta^{\mu\nu}\overline{D}^{\mathrm{e}}_{ij}(t|\mathbf{x}')$ for small inverse Peclet numbers is given by,

$$\begin{aligned}\delta^{\mu\nu}\overline{D}^{\mathrm{e}}_{ij}(t) &= u^2\sigma^2_{\mu\mu}\sigma^2_{\nu\nu}\int\limits_{k'}\int\limits_{0}^{t}\mathrm{d}t'\widetilde{C}^{\mu\mu}(\mathbf{k}')\left[\delta_{i1}\delta_{j1}A(\mathbf{k}',t')\right.\\ &\quad\left.+\delta_{j1}A_i(\mathbf{k}',t',0)+\delta_{i1}A_j(\mathbf{k}',t',0)+C^{\nu\nu}_{ij}(t')\right]\\ &\quad\times\exp\left(-\mathrm{i}uk'_1t'\right)\left[1-\exp\left(-2k'^2_jl^2_jt/\tau_{D_j}\right)\right]. \qquad (3.11)\end{aligned}$$

3.4 Explicit Expressions for the Effective Dispersion Coefficients

We focus on a transport situation for which the temporal fluctuations are transverse to the direction of the mean flow velocity, $\boldsymbol{\upsilon}(t)=[0,\upsilon_2(t),\ldots,\upsilon_d(t)]^T$. In this case, (3.11) simplifies to,

$$\begin{aligned}\delta^{\mu\nu}\overline{D}^{\mathrm{e}}_{ij}(t) &= u^2\sigma^2_{\mu\mu}\sigma^2_{\nu\nu}\int\limits_{k'}\int\limits_{0}^{t}\mathrm{d}t'\widetilde{C}^{\mu\mu}(\mathbf{k}')\Big[\delta_{i1}\delta_{j1}A(k'_2,\ldots,k'_d,t')\\ &\quad\left.+C^{\nu\nu}_{ij}(t')p_ip_j\right]\exp\left(-\mathrm{i}uk'_1t'\right)\left[1-\exp\left(-2k'^2_jl^2_jt/\tau_{D_j}\right)\right],\end{aligned} \qquad (3.12)$$

where we defined $p_i = (1 - \delta_{i1})$. In the following, we study without loss of generality fluctuations in 2-direction, i.e.,

$$v_i(t) = \delta_{i2} v(t). \tag{3.13}$$

Using (3.13) in (2.14), the correlation matrix $C_{lm}^{\nu\nu}(t)$ reduces to,

$$C_{lm}^{\nu\nu}(t) = \delta_{l2}\delta_{m2} C^{\nu\nu}(t). \tag{3.14}$$

To derive explicit results, we need to specify the spatial and temporal correlation functions. The specific form of the spatial and temporal correlation functions $C^{\mu\mu}$ and $C^{\nu\nu}$, is to some extent arbitrary. A convenient choice made in the literature are Gauss-shaped functions. The temporal fluctuations of the flow field in (2.14) are assumed to be Gaussian correlated (e.g., [38]), i.e.,

$$C^{\nu\nu}(t) = \exp\Big[-\frac{t^2}{2\tau^2}\Big], \tag{3.15}$$

with τ the correlation time. In analogy to [25], we use a Gaussian shaped correlation function for the retardation field μ in (2.8), which in Fourier space reads as,

$$C^{\mu\mu}(\mathbf{k}) = (2\pi)^{\frac{d}{2}} \prod_{i=1}^{d} l_i \exp\Big[-\frac{1}{2}(k_i l_i)^2\Big]. \tag{3.16}$$

The length scales l_i are the correlation lengths of the retardation fields in direction i (with $i = 1....d$).

Inserting (3.14) with (3.15) and (3.16) into (3.12) and using (A.18) for $A(k_2', t')$, we obtain,

$$\begin{aligned}\delta^{\mu\nu}\overline{D}_{ij}^{\mathrm{e}}(t) = u l_1 \sigma_{\mu\mu}^2 \sigma_{\nu\nu}^2 \int_{k'} \int_0^{t/\tau_u} \mathrm{d}t' \Big[\delta_{i1}\frac{l_1^2}{l_2^2}\frac{{k_2'}^2}{2} \int_0^{t'} \mathrm{d}y \int_0^{t'} \mathrm{d}y' \exp\Big[-\frac{(y-y')^2}{2\kappa^2}\Big] \\ + \delta_{i2} \exp\left(-\frac{{t'}^2}{2\kappa^2}\right)\Big] \exp\left(-\mathrm{i}k_1' t'\right) \Big\{1 - \exp\left[-\frac{{k_j'}^2}{2}(1 + 4t/\tau_{D_j})\right]\Big\}.\end{aligned} \tag{3.17}$$

In the following we will restrict ourselves to isotropic disorder scenario, i.e., $l_1 = \cdots = l_d$. Then, for times large compared to the advection time scale τ_u, we obtain the following compact expressions for the effective dispersion coefficients,

$$\begin{aligned}\delta^{\mu\nu}\overline{D}^{\mathrm{e}}_{11}(t) &= \sqrt{\frac{\pi}{2}}\sigma^2_{\mu\mu}\sigma^2_{\nu\nu}ul\frac{\kappa^2}{a(\kappa)}\Big[a(\kappa)-1+\Big[(1+4t/\tau_\kappa)^{\frac{1}{2}}-a(\kappa)\Big] \\ &\quad \times(1+4t/\tau_{D_2})^{-\frac{3}{2}}\prod_{n=3}^{d}(1+4t/\tau_{D_n})^{-\frac{1}{2}}\Big] \qquad (3.18)\\ \delta^{\mu\nu}\overline{D}^{\mathrm{e}}_{22}(t) &= \sqrt{\frac{\pi}{2}}\sigma^2_{\mu\mu}\sigma^2_{\nu\nu}ula(\kappa)\Big[1-(1+4t/\tau_\kappa)^{-\frac{1}{2}}\prod_{n=2}^{d}(1+4t/\tau_{D_n})^{-\frac{1}{2}}\Big], \qquad (3.19)\end{aligned}$$

where we defined $a(\kappa) = \kappa/\sqrt{\kappa^2+1}$. Note that $\delta^{\mu\nu}\overline{D}^{\mathrm{e}}_{ii} \equiv 0$ for $i > 2$ for symmetry reasons. Furthermore, note that $\delta^{\mu\nu}\overline{D}^{\mathrm{e}}_{11} \leq 0$, however, $\delta^{\mu\mu}\overline{D}^{\mathrm{e}}_{11} + \delta^{\mu\nu}\overline{D}^{\mathrm{e}}_{11} \geq 0$, for small variances of the temporal flow fluctuations. For increasing $\sigma^2_{\nu\nu}$, this contribution can become negative, which, however, is a relic of the perturbation expansion in $\sigma^2_{\nu\nu}$, see Appendix A. Note that the expansions in the fluctuations in the random fields can lead to non-convergent series for some transient non-linear reactive transport problems [65]. For the linear reactive transport problem under consideration here, the non physical behavior of $\delta^{\mu\mu}\overline{D}^{\mathrm{e}}_{11} + \delta^{\mu\nu}\overline{D}^{\mathrm{e}}_{11} \leq 0$ is a relic of the perturbation expansion and not of the non-convergence.

For comparison we give here the explicit approximate expressions obtained by Attinger et al. [25] for $\delta^{\mu\mu}\overline{D}^{\mathrm{e}}_{ii}$, in d dimensions,

$$\begin{aligned}\delta^{\mu\mu}\overline{D}^{\mathrm{e}}_{11}(t) &= \sqrt{\frac{\pi}{2}}\sigma^2_{\mu\mu}ul\left[1-\prod_{n=2}^{d}\left(1+\frac{4t}{\tau_{D_n}}\right)^{-\frac{1}{2}}\right], \qquad (3.20)\\ \delta^{\mu\mu}\overline{D}^{\mathrm{e}}_{ii}(t) &= 0. \qquad (3.21)\end{aligned}$$

Note firstly, that the time evolution of $\delta^{\mu\mu}\overline{D}^{\mathrm{e}}_{11}$ depends only on the transverse

dispersion scale, and secondly that there is no macroscopic contribution to the transverse dispersion coefficient.

3.5 Effective Transport Behavior

It was shown by Attinger et al. [25] for transport under steady flow conditions that chemical medium heterogeneities change the behavior of the longitudinal dispersion coefficient in a quantitatively relevant way, whereas transverse solute spreading is only weakly influenced by the fluctuations of the retardation factor. As we saw at the end of the previous section, the effective transverse dispersion coefficient is in fact of the order of the local dispersion coefficient. For transport under a temporally fluctuating flow conditions, the behavior of transverse and longitudinal effective dispersion coefficients is different.

In the following, we investigate the asymptotic long time behavior and the temporal evolution of the effective dispersion coefficients in $d = 2$ dimensions. All results are normalized by $\sqrt{\frac{\pi}{2}}\sigma_{\mu\mu}^2\sigma_{\nu\nu}^2 ul$. The behavior in $d = 3$ dimensions is qualitatively similar.

3.5.1 Asymptotic Long Time Behavior

We study here the asymptotic behavior of the contributions to the effective dispersion coefficients for isotropic local dispersion, $D_{11} = D_{22} = D$, as a function of the Kubo number κ. We define for the following,

$$\lim_{t\to\infty} \delta^{\mu\nu}\overline{D}_{11}^{\mathrm{e}}(t) = \delta^{\mu\nu}D_{11}^{\infty}(\kappa), \tag{3.22}$$

$$\lim_{t\to\infty} \delta^{\mu\nu}\overline{D}_{22}^{\mathrm{e}}(t) = \delta^{\mu\nu}D_{22}^{\infty}(\kappa). \tag{3.23}$$

Figure 3.1 illustrates the asymptotic behavior of $\delta^{\mu\nu}D_{22}^{\infty}(\kappa)$ and $\delta^{\mu\nu}D_{11}^{\infty}(\kappa)$.

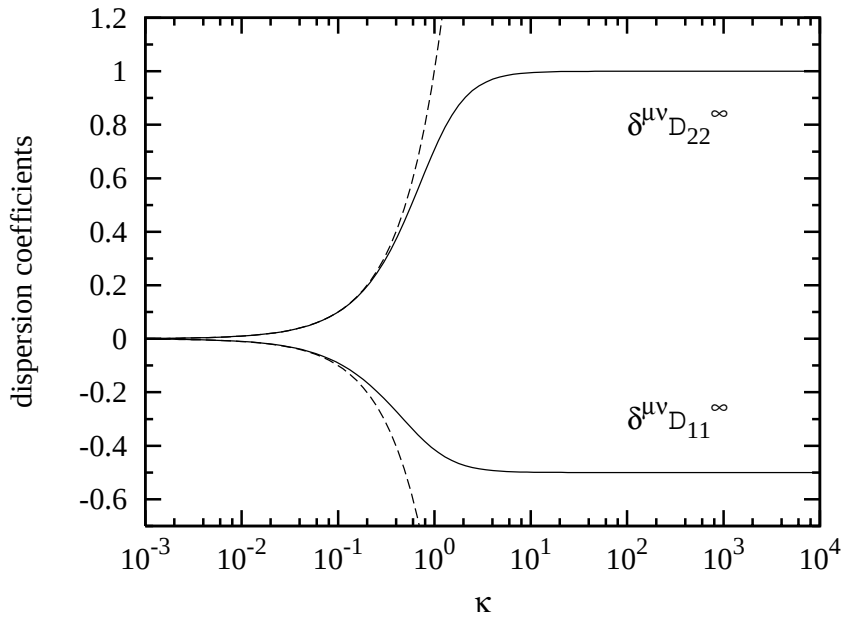

Figure 3.1: Asymptotic behavior of the contributions to the effective dispersion coefficients due to chemical heterogeneity and temporal fluctuations in solid lines. The dashed lines describe the behavior of $\delta^{\mu\nu} D_{22}^{\infty}$ and $\delta^{\mu\nu} D_{11}^{\infty}$ according to (3.24) and (3.25), respectively.

Both contributions to the longitudinal and transverse effective dispersion coefficients tend to zero in the limit $\kappa \to 0$. In this limit, the correlation time τ is much smaller than the advection time τ_u, or equivalently, the Kubo length is much smaller than the correlation length, $l_\kappa \ll l$. Thus, during a many temporal fluctuations cycle the medium look quasi homogeneous to the transported solute and, as shown by Dentz and Carrera [20], there are no contributions to effective solute spreading due to temporal velocity fluctuations in homogeneous media.

For $10^{-1} < \kappa < 1$, $\delta^{\mu\nu} D_{22}^{\infty}(\kappa)$ increases linearly,

$$\delta^{\mu\nu} D_{22}^{\infty}(\kappa) = \sqrt{\frac{\pi}{2}} \sigma_{\mu\mu}^2 \sigma_{\nu\nu}^2 u l \kappa. \tag{3.24}$$

In this regime, the Kubo length is of the order of the spatial correlation length, $l_\kappa \lesssim l$, i.e., the solute samples actually the spatial heterogeneity after many correlation times, which leads to enhanced spreading in transverse direction.

$\delta^{\mu\nu} D_{11}^{\infty}(\kappa)$, in contrast, decreases linearly in the same κ-interval,

$$\delta^{\mu\nu} D_{11}^{\infty}(\kappa) = -\frac{1}{2} \sqrt{\frac{\pi}{2}} \sigma_{\mu\mu}^2 \sigma_{\nu\nu}^2 u l \kappa. \tag{3.25}$$

The asymptotic values of $\delta^{\mu\nu} D_{22}^{\infty}(\kappa)$, and $\delta^{\mu\nu} D_{11}^{\infty}(\kappa)$, are reached for $\kappa \gg 1$.

Note that, in contrast to transport under steady flow conditions, where the disorder-induced contribution to effective transverse dispersion is of the order of local dispersion, here $\delta^{\mu\nu} D_{22}^{\infty}$ is macroscopic and dependent on the Kubo number κ. At the same time, the longitudinal dispersion coefficient decreases as $\delta^{\mu\nu} D_{11}^{\infty}$ is negative as shown in Figure 3.1. The simultaneous increase of the transverse and decrease of the longitudinal effective dispersion coefficients is a consequence of self-organization of the system. Increased transverse spreading smooths out the concentration contrast along direction normal to the mean flow, which in turn leads to a decrease of longitudinal

effective spreading. A similar mechanism is observed for the Taylor problem of transport in linear flow [34]. There, solute dispersion is enhanced as a consequence of the fact that the solute samples the transverse velocity contrast in the direction vertical to the mean flow, the resulting concentration contrast is smoothed out by transverse dispersion. Thus, an increase of the transverse dispersion leads to a decrease of the Taylor dispersion coefficient.

3.5.2 Time behavior

We study the time evolution of the contributions to the effective dispersion coefficient using the explicit expressions (3.18) and (3.19) for the longitudinal and transverse dispersion coefficients, respectively. We investigate different scenarios in order to study the different mechanisms which affect the behavior of the effective dispersion coefficients. At first we investigate an isotropic scenario for small and large Kubo numbers. Secondly, we investigate an anisotropic local dispersion scenario varying the longitudinal local dispersion coefficient.

Isotropic scenario

For the isotropic scenario, the inverse Peclet numbers ϵ_i and the dispersion time scales τ_{D_i} reduce to $\epsilon_i = \epsilon$ and $\tau_{D_i} = \tau_D$ for $i = 1, \ldots, d$.

Figures 3.2a and 3.2b illustrate the time evolution of the contributions $\delta^{\mu\nu}\overline{D}^{\mathrm{e}}_{22}$ to the transverse and $\delta^{\mu\nu}\overline{D}^{\mathrm{e}}_{11}$ to the longitudinal effective dispersion coefficients in $d = 2$ for $\kappa = 10^{-1}$ and $\kappa = 10$. The dispersion time scale is $\tau_D = 10^3\tau_u$, i.e., the advection and dispersion time scales τ_u and τ_D are clearly separated.

For large values of κ, corresponding to $\tau_\kappa \gg \tau_D$, the Kubo scale τ_κ together with τ_u and τ_D, separates three different time regimes: (i) the interme-

diate time regime $\tau_u \ll t \ll \tau_D$, (ii) the Kubo time regime $\tau_D \ll t \ll \tau_\kappa$, and (iii) the long-time regime $t \gg \tau_\kappa$. The Kubo scale sets a relevant asymptotic time scale. Note that the solute has to be spread by local dispersion over at least one correlation length of the medium to "see" the chemical heterogeneity and it has to be spread over at least one Kubo length l_κ to notice the influence of temporal flow fluctuations. Note that for small κ, $\tau_\kappa \approx \tau_D$, see definition (3.9), i.e., the Kubo scale is of importance for large Kubo numbers only. In order to illustrate this feature, we choose $\kappa = 10^{-1}$ and $\kappa = 10$.

(i) Intermediate time regime $\tau_u \ll t \ll \tau_D$

In this time regime, spatial heterogeneity is being activated as a macroscopic spreading mechanism and we observe a cross-over from local dispersive spreading and mixing to macroscopic heterogeneity induced effective dispersion. The contribution to the effective transverse dispersion coefficient, $\delta^{\mu\nu}\overline{D}^{\mathrm{e}}_{22}$, both for $\kappa = 10^{-1}$ and $\kappa = 10$ evolve linearly with time,

$$\delta^{\mu\nu}\overline{D}^{\mathrm{e}}_{22}(t) = \sqrt{2\pi}\sigma^2_{\mu\mu}\sigma^2_{\mu\nu}ula(\kappa)\frac{(\kappa^2+2)}{(\kappa^2+1)}\frac{t}{\tau_D} + \ldots, \tag{3.26}$$

where the dots denote subleading contributions. Contrary to the behavior observed under steady flow conditions, where transverse spreading is mainly given by local dispersion, here the transverse dispersion coefficient grows from the (microscopic) local scale dispersion coefficient to a macroscopic value. As shown in Figure 3.2b, the contribution to the longitudinal coefficient decreases linearly according to,

$$\delta^{\mu\nu}\overline{D}^{\mathrm{e}}_{11}(t) = -\sqrt{2\pi}\sigma^2_{\mu\mu}\sigma^2_{\mu\nu}ula(\kappa)\Big[2 + 3\kappa(\kappa - \sqrt{\kappa^2+1})\Big]\frac{t}{\tau_D} + \ldots, \tag{3.27}$$

towards a negative macroscopic value and thus, longitudinal effective dispersion decreases as discussed in Section 3.5.1.

(ii) Kubo time regime $\tau_D \ll t \ll \tau_\kappa$

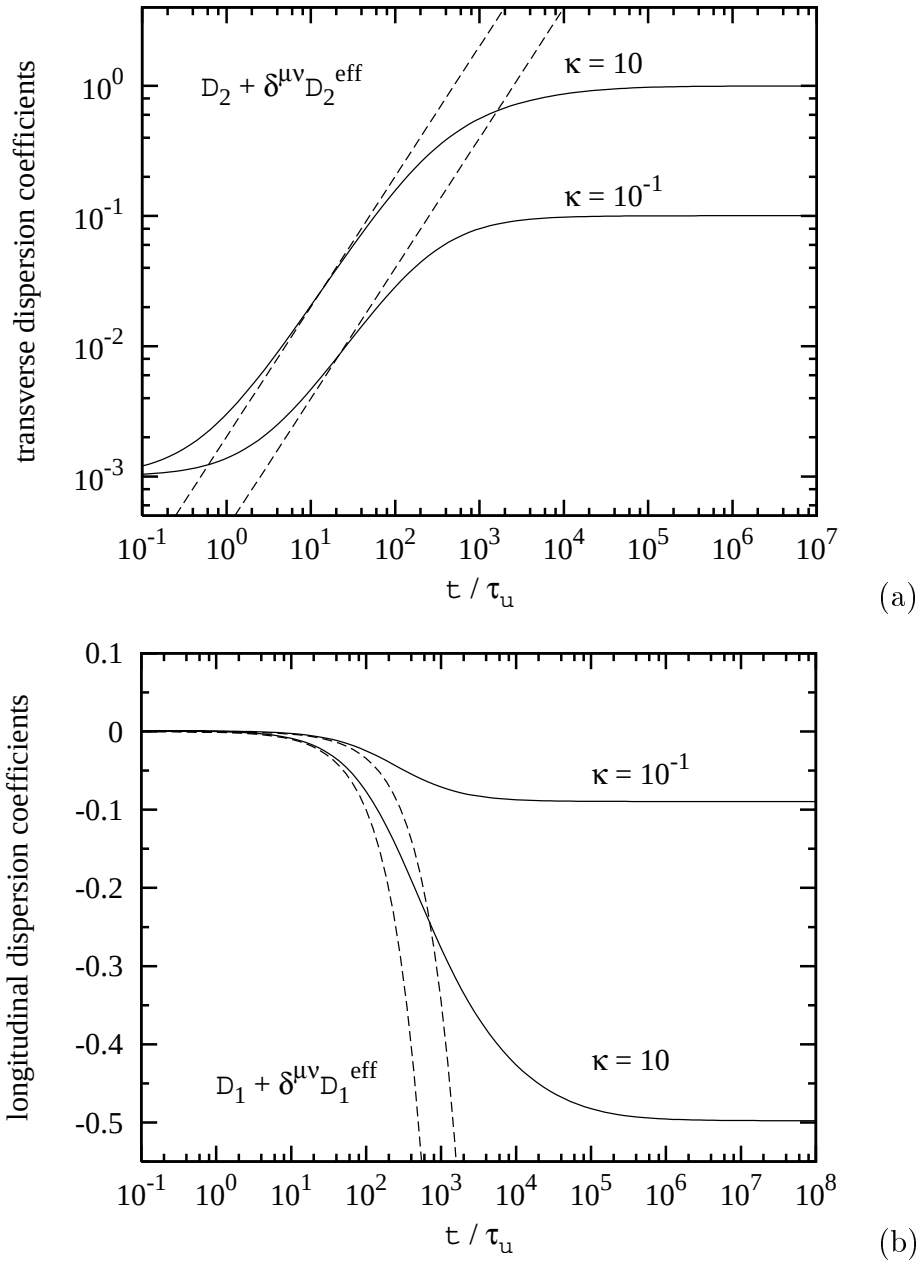

Figure 3.2: Time behavior of the contributions to the (a) transverse effective dispersion coefficients, (b) longitudinal effective dispersion coefficients, in $d = 2$ for $\tau_D = 10^3 \tau_u$, $\epsilon = 10^{-3}, t \gg \tau_u, \kappa = 10^{-1}$ and $\kappa = 10$. The dashed lines in (a) and (b) describe the behavior of $\delta^{\mu\nu}\overline{D}^{e}_{22}$ and $\delta^{\mu\nu}\overline{D}^{e}_{11}$ according to (3.26) and (3.27), respectively.

For $\kappa = 10$, $\delta^{\mu\nu}\overline{D}^{\mathrm{e}}_{22}$, see Figure 3.2a, evolves approximately according to $t^{-1/2}$, which is identical to the behavior observed for the longitudinal component under steady state conditions [25]. For $\kappa = 10^{-1}$, i.e., $\tau_\kappa \approx \tau_D$ and the Kubo and long time regimes coincide. The contribution $\delta^{\mu\nu}\overline{D}^{\mathrm{e}}_{22}$ evolves as t^{-1} towards its asymptotic macroscopic value. The difference in the behaviors for $\kappa = 10^{-1}$ and 10 can be well observed in Figure 3.2a. For $\kappa = 10^{-1}$ the evolution of the $\delta^{\mu\nu}\overline{D}^{\mathrm{e}}_{22}$ is faster than for $\kappa = 10$. Note that for times, $\tau_D \ll t \ll \tau_\kappa$, the solute has spread out over a distance larger than the correlation length l, hence, the solute has sampled a representative part of the chemical heterogeneity. However, for large Kubo numbers, the Kubo length is much larger than the correlation length, $l_\kappa \gg l$, i.e., the solute has been transported over more than one correlation length without noticing the temporal variability of the flow. Thus spreading is dominated by the interaction of local dispersion and chemical heterogeneities, and the behavior of $\delta^{\mu\nu}\overline{D}^{\mathrm{e}}_{22}$ is similar to the one observed for the longitudinal dispersion coefficient under steady flow conditions as in this time regime, $v(t)$ is approximately constant, i.e., there is an approximately constant transverse velocity component. For $\kappa = 10^{-1}$, the solute has spread by local dispersion over distances larger than both, the correlation length and the Kubo length. Thus, both spatial heterogeneity as well as temporal flow fluctuations are activated as macroscopic spreading mechanisms. For this reason $\delta^{\mu\nu}\overline{D}^{\mathrm{e}}_{22}$ evolves faster for $\kappa = 10^{-1}$ than for $\kappa = 10$. The same behavior can be observed in Figure 3.2 for $\delta^{\mu\nu}\overline{D}^{\mathrm{e}}_{11}$, which decreases faster for $\kappa = 10^{-1}$ than for $\kappa = 10$ for the reasons given above.

(iii) Long time regime $t \gg \tau_\kappa$

As pointed out above, for $\kappa = 10^{-1}$, the Kubo and long time regimes coincide. For $\kappa = 10$, the long time regime is set by the Kubo scale, see

Figures 3.2a and 3.2b. As pointed out above, only when the solute has been spread out over distances which are larger than both the correlation and the Kubo lengths, the interaction between chemical heterogeneity and temporal fluctuations are activated as macroscopic spreading mechanisms. As discussed above for $\kappa = 10^{-1}$, here both $\delta^{\mu\nu}\overline{D}^{\mathrm{e}}_{22}$ and $\delta^{\mu\nu}\overline{D}^{\mathrm{e}}_{11}$ evolve towards their respective asymptotic values according to t^{-1}, i.e., faster than the contribution $\delta^{\mu\mu}\overline{D}^{\mathrm{e}}_{11}$ in the absence of temporal flow fluctuations.

Anisotropic scenario

Here we study the temporal behavior of the effective dispersion coefficients for anisotropic local dispersion and isotropic disorder correlation.

Figures 3.3a and b illustrate the time behavior of $\delta^{\mu\nu}\overline{D}^{\mathrm{e}}_{22}$ and $\delta^{\mu\nu}\overline{D}^{\mathrm{e}}_{11}$ for a fixed $\epsilon_1 = 10^{-1}$ and varying ϵ_2 of $\epsilon_2 = 10^{-7}, 10^{-6}, 10^{-5}$ and $\epsilon_2 = 10^{-4}$, in $d = 2$, for $\kappa = 1$. The temporal behavior of $\delta^{\mu\nu}\overline{D}^{\mathrm{e}}_{22}$ is plotted only for the cases $\epsilon_2 = 10^{-7}$ and $\epsilon_2 = 10^{-4}$. For the values in between, the curves are quite similar.

For the isotropic scenario discussed in the previous Section 3.5.2, $\tau_\kappa \geq \tau_D$ and the asymptotic long time regime was defined by the Kubo time scale τ_κ. For the anisotropic scenario under consideration here, the Kubo scale is smaller than the transverse dispersion time scale, $\tau_\kappa \ll \tau_{D_2}$. Thus, τ_{D_2} defines the relevant asymptotic time scale. These two time scales, along with the advection scale, define three time regimes which characterize the interaction of local dispersion, spatial heterogeneity and temporal fluctuations: (i) the Kubo time regime $\tau_u \ll t \ll \tau_\kappa$, (ii) the intermediate time regime $\tau_\kappa \ll t \ll \tau_{D_2}$, and (iii) the long-time regime $t \gg \tau_{D_2}$.

(i) Kubo time regime $\tau_u \ll t \ll \tau_\kappa$.

In this time regime, the solute has been transported by advection over

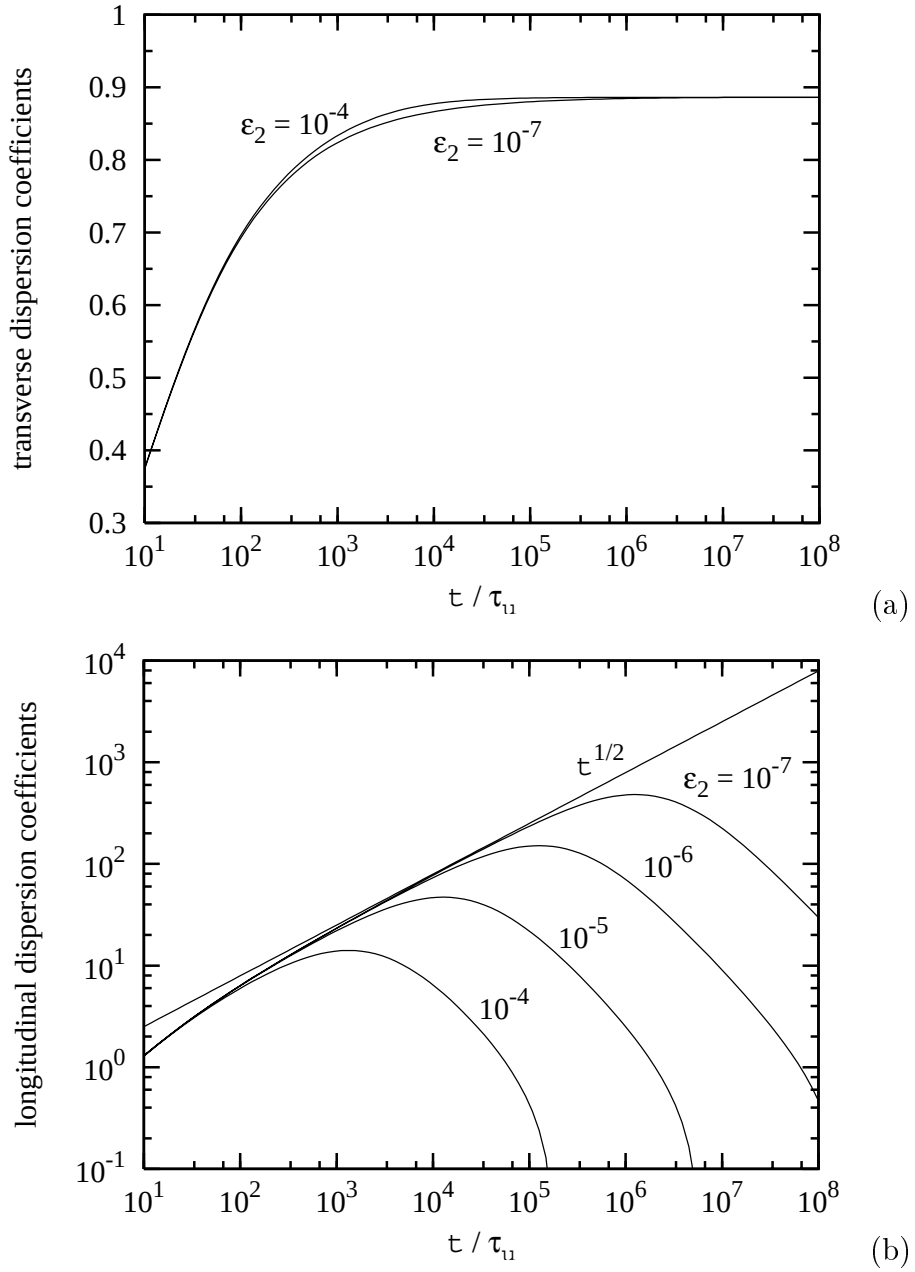

Figure 3.3: Time behavior of (a) $\delta^{\mu\nu}\overline{D}^{\mathrm{e}}_{22}(t)$, and (b) $\delta^{\mu\nu}\overline{D}^{\mathrm{e}}_{11}$ (both scaled by $\sqrt{\frac{\pi}{2}}\sigma^2_{\mu\mu}\sigma^2_{\nu\nu}ul$) in $d = 2$ for $\kappa = 1$ and a fixed $\epsilon_1 = 10^{-1}$; ϵ_2 varies between 10^{-7} and 10^{-4}.

a distance larger than the correlation length l of the chemically heterogeneous medium. Solute has not been spread by local dispersion over distances larger than both the correlation length l and the Kubo length l_κ. In this regime, temporal fluctuations and spatial heterogeneity are activated as relevant macroscopic spreading mechanism and we observe a cross-over from microscopic local dispersion to macroscopic disorder-induced spreading and mixing. The $\delta^{\mu\nu}\overline{D}^{\mathrm{e}}_{22}$ and $\delta^{\mu\nu}D^{\mathrm{eff}}_{11}$, see Figures 3.3a and 3.3b, evolve linearly with time, as observed in the isotropic scenario.

(ii) Intermediate time regime $\tau_\kappa \ll t \ll \tau_{D_2}$.

Here, the solute has spread by longitudinal local dispersion over the Kubo length l_κ. In transverse direction, however, the solute has not yet sampled one spatial correlation length of the medium by transverse local dispersion.

The evolution of $\delta^{\mu\nu}\overline{D}^{\mathrm{e}}_{22}$ for $\epsilon = 10^{-4}$ is different from the one observed for $\epsilon_2 = 10^{-7}$. For $\epsilon_2 = 10^{-4}$, $\delta^{\mu\nu}\overline{D}^{\mathrm{e}}_{22}$ evolves faster towards its asymptotic long time value as transverse local dispersive mixing is more efficient.

The evolution of $\delta^{\mu\nu}\overline{D}^{\mathrm{e}}_{11}$ depends strongly on the value ϵ_2. In this time regime, $\delta^{\mu\nu}\overline{D}^{\mathrm{e}}_{11}$ evolves as $t^{1/2}$ towards a maximum, which it assumes for times of about $10^{-1}\tau_{D_2}$. For steady flow conditions, transport would be quasi unidimensional in this regime, as local transverse dispersion is subleading. In the presence of transverse flow fluctuations, however, there is vertical mass exchange. The transverse heterogeneity contrasts encountered by the solute leads then to the anomalous $t^{1/2}$ growth of $\delta^{\mu\nu}\overline{D}^{\mathrm{e}}_{11}$. Note that local transverse dispersion, which smoothes out these vertical contrasts, is subleading. The anomalous diffusive behavior found here is similar to the one observed in stratified flow (e.g., [21, 31]). The mechanisms are similar, but slightly different. While in the case of the stratified medium, local transverse dispersion is the vertical solute spreading and mixing mechanisms that leads, in inter-

action with the vertical velocity contrast, to the characteristic $t^{1/2}$ growth of the longitudinal effective dispersion coefficient, here transverse flow fluctuations cause vertical mass exchange. These mechanisms, local dispersion and transverse flow fluctuations, are different.

(iii) Long time regime $t \gg \tau_{D_2}$.

Here, the solute has spread over a correlation length of the medium by transverse local dispersion. Thus, spatial heterogeneity has been activated as a macroscopic spreading mechanism. The $\delta^{\mu\nu}\overline{D}^{\mathrm{e}}_{22}$ converges towards its macroscopic asymptotic long time value. As a consequence of the increase in transverse effective dispersion, which leads to a smoothing out of the vertical heterogeneity contrast, $\delta^{\mu\nu}\overline{D}^{\mathrm{e}}_{11}$, decreases towards its asymptotic long time value. The transverse dispersion time scale τ_{D_2} is a cut-off time scale for the anomalous diffusive behavior observed in the previous time regime.

3.6 Summary

Here we investigated the effective transport of a reactive solute through a chemically heterogeneous medium. We focused on spatially fluctuating equilibrium sorption properties, which were characterized by a random retardation factor. The flow velocity was fluctuating in time with fluctuations transverse to the mean flow direction. The effective transport behavior was studied in a stochastic modeling framework. Chemical heterogeneity and temporal flow fluctuations were modeled by mean of correlated spatial and temporal random fields, respectively.

We studied effective dispersion coefficients, which were defined by the ensemble averages of the corresponding quantities in a single realization. Using a first-order perturbation approach in the variances of the random

processes we derived explicit compact expressions for the time behavior of the transverse and longitudinal effective dispersion coefficients, which allow for a detailed study of the time evolution of effective solute spreading and mixing.

The effective dispersion coefficients were given as the sum of the contributions due to (i) local dispersion, (ii) the interaction of local dispersion and chemical heterogeneity, (iii) the interaction of local dispersion physical heterogeneity and temporal flow fluctuations, (iv) the interaction of local dispersion and cross-correlations between physical and chemical heterogeneity, and (v) the interaction between local dispersion, temporal fluctuations and chemical heterogeneity. We focused on a physically homogeneous, chemically heterogeneous medium, hence, we studied the latter contribution.

The time behavior of the effective dispersion coefficients were dominated by the following time scales: (i) the advection time scale $\tau_u = l/u$, (ii) the dispersion time scale $\tau_{D_2} = l/D_{22}$, which gives the activation time scale for chemical heterogeneities as a relevant macroscopic spreading mechanism, and (iii) the Kubo time scale $\tau_\kappa = (l^2 + l_\kappa^2)/D_{11}$ which measures the time for the local dispersive spreading over a distance larger than both the correlation length l and the Kubo length, $l_\kappa = u\tau$. Only after the time τ_κ, the interaction between chemical heterogeneities and temporal flow fluctuations is activated as a macroscopic spreading mechanism. As a consequence of temporal flow fluctuations, transverse effective dispersion evolves towards a macroscopic asymptotic value, which is in sharp contrast to the corresponding results for steady flow conditions, where no macroscopic contribution to transverse effective dispersion has been found. We observe an interesting phenomenon of self organization as the longitudinal effective dispersion decreases at the same time as transverse dispersion increases. The increase in transverse effective

dispersion, i.e., an increase of transverse spreading and mixing, leads to an increased smoothing of the transverse heterogeneity contrast, which in turn leads to a decrease of longitudinal effective dispersion.

We consider two scenarios for a point-like initial condition in $d = 2$ spatial dimensions, (i) a completely isotropic scenario characterized by isotropic local dispersion and disorder correlation and (ii) one characterized by an isotropic correlation structure and anisotropic local dispersion.

In the first case, the time scales are ordered according to $\tau_u \ll \tau_D \ll \tau_\kappa$, which defines three time regimes given by (i) the intermediate time regime $\tau_u \ll t \ll \tau_D$, (ii) the Kubo time regime $\tau_D \ll t \ll \tau_\kappa$ and (iii) the long time regime $t \gg \tau_\kappa$. In the first time regime, the solute has not been spread by local dispersion over one correlation length of the medium. As the solute spreads, effective solute dispersion crosses over from local dispersion to macroscopic disorder induced spreading, which is characterized by a linear cross-over of the effective dispersion coefficients. In the Kubo regime, temporal fluctuations have not yet been activated as a macroscopic spreading mechanisms as the solute has not yet covered a distance of the order of the Kubo distance. The asymptotic time scale is set by the Kubo time. For time large compared to τ_κ the effective coefficients approach their macroscopic long time values.

The second scenario is characterized by a different order of scales given by $\tau_u \ll \tau_\kappa \ll \tau_{D_2}$, which implies three time regimes: (i) the Kubo time regime $\tau_u \ll t \ll \tau_\kappa$, (ii) the intermediate time regime $\tau_\kappa \ll t \ll \tau_{D_2}$ and (iii) the long time regime $t \gg \tau_{D_2}$. In the Kubo regime spatial heterogeneity and temporal fluctuations are activated and the effective coefficient cross-over to macroscopic heterogeneity induced values, which are approached in the intermediate regime due to the interaction of temporal fluctuations and

the longitudinal heterogeneity contrast, and faster in the asymptotic regime, where the transverse heterogeneity contrast is activated by local transverse dispersion. We observe anomalous diffusive behavior for the longitudinal effective dispersion coefficient in the intermediate regime, where it evolves as $t^{1/2}$. Transverse solute spreading is due to the vertical flow fluctuations as local transverse dispersion is subleading in this time regime. Thus, concentration contrast that the solute experiences by transverse flow fluctuations causes the anomalous diffusive behavior, which is cut-off as soon as transverse dispersion kicks in and smoothes these contrasts at asymptotic time $t \gg \tau_{D_2}$.

The studied effective dispersion behavior and the analysis of the different micro and macroscopic spreading mechanisms and the interaction between them sheds new light on the understanding of effective transport processes in heterogeneous media. Particularly, the observed enhancement of transverse dispersion due to temporal flow fluctuations can have important practical implications for the assessment of groundwater remediation based in hydraulic manipulation, for example, as well as for the assessment and prediction of the migration of reactive contaminants in the context of performance assessment in nuclear waste management, for example. The developed compact and simple expressions for the effective dispersion coefficients can be easily used for the quantification of effective solute spreading and mixing in such applications.

Chapter 4

Superdiffusion in Stratified Unbounded Media Models

4.1 Introduction

Transport in stratified media has been frequently studied in the groundwater literature as a model for transport in geological media. Natural sandy aquifers often exhibit geological and geostatistical stratification characterized by a much larger horizontal than vertical correlation length (see, e.g., [66] and literature therein).

A mathematically simple layered model can be assumed in the idealized limiting case of infinity correlation length in the horizontal direction. In this model, called perfectly stratified, the hydraulic conductivity depends only on the vertical direction. Transport in perfectly stratified media has been frequently studied in the groundgwater literature. *Matheron and de Marsily* [21] studied transport in a perfectly stratified infinite medium as an idealized aquifer model. They observed superdiffusive solute spreading quantified by an anomalous increase of the longitudinal dispersion coefficient

with the square root of time.

Following [21], transport in an infinite perfectly stratified random medium has been investigated extensively (e.g., [67, 68, 69, 70, 71, 72, 31, 41]) using stochastic modeling as a systematic means to quantify the impact of spatial heterogeneity on large scale transport. The latter has been studied in terms of the average solute distribution density and its moments, its spatial and temporal moments as well as in terms of (apparent) longitudinal dispersion coefficients.

The anomalous dispersion behavior such as the one observed in stratified media, called super-diffusive, has been also studied in the physics literature (e.g. [73, 74, 75]) as the simplest case where long-range correlations lead to anomalous diffusion.

Local transverse dispersion is the vertical solute spreading and mixing mechanisms that leads, in interaction with the vertical velocity contrast, to the characteristic $t^{1/2}$ growth of the longitudinal effective dispersion coefficient in a perfectly random medium. Unlike for the case for wich head gradient is aligned with the direction of stratification, in a more general case when there is a constant velocity component in the direction perpendicular to the stratification, the longitudinal effective dispersion coefficients reach a aonstant asymptotic long time value [21, 31].

In this chapter we investigate the temporal behavior of effective mixing and spreading in stratified media models in terms of effective dispersion coefficients for different flow regimes in order to evaluate if the non-Fickian behavior of these coefficients persist. In all cases described in the following we do not assume a constant vertical velocity component.

In section 4.2 we derive analytical expressions for the effective and ensemble dispersion coefficients and study effective mixing and spreading behavior

under transverse temporal flow fluctuations of the flow conditions in a infinite stratified random medium. Then, under steady state flow conditions, in section 4.3 we investigate two spatially varying flow fields, a Manhattan Grid distribution, and a nearly stratified flow.

4.2 Parallel Random Flow with Transverse Temporal Flow fluctuations

In section 3.5.2, we analyzed the temporal effective dispersion coefficients behavior when considering a chemically heterogeneous media subject to randomly temporal fluctuations of the flow conditions. A superdiffusive behavior of the longitudinal effective dispersion coefficient was observed during a certain time regime whenever transverse local dispersion is much smaller than the longitudinal. As discussed, transverse temporal flow fluctuations lead to enhanced leads to mass exchange even tough transverse local dispersion is subleading. When transverse local dispersion is activated as a spreading mechanism, the longitudinal effective dispersion coefficient decreases to its asymptotic long time Fickian behavior.

The mechanism which leads to non-Fickian behavior in the random retardation described in 3.5.2, and the mechanisms leading to anomalous dispersion in stratified media are similar. The interaction of temporal flow fluctuations and medium heterogeneities can modify the superdiffusive behavior under certain conditions. Hence, we study here the impact of transverse temporal flow fluctuations for spreading and mixing in a unbounded stratified random medium.

Weeks and Sposito [76] modeled passive solute mixing in a perfectly stratified aquifer during both steady and unsteady groundwater flows. They

showed that under unsteady flow conditions the solute plume boundaries become highly irregular. Irregularity of plume boundaries can be used as a measure of mixing, which is a very significant process for transport of reactive species, since chemical and biological reactions are driven by mixing at the local scale. A recent study on enhanced mixing and spreading due to chaotic advection (in which fluid pathlines completely fill the spatial domain) is presented in [77]. The effects of this unsteady flow in chemical activity and reactions has been investigated experimentally by [78, 79].

In this chapter we quantify effective mixing and spreading of a solute transported through a infinite stratified medium under temporally fluctuating flow conditions in terms of effective transport coefficients. We study the influence of the interaction between the layer to layer permeability variations, local dispersion, and the temporal transverse fluctuations of the flow velocity as a transverse mixing mechanisms, especially its influence over the super-diffusive behavior of the stratified random media model addressed by [21, 31].

4.2.1 Basics

We study flow and transport of a conservative solute in the nonsteady, nonuniform flow in the stratified media model addressed in section 2.5. In this scenario, the flow and transport are given by (2.18) and (2.24), respectively. As initial condition, we consider a point-like injection, i.e. in (2.4) $\rho(\mathbf{x}) = \delta(\mathbf{x} - \mathbf{x}')$. The d-dimensional flow and transport domain, here is assumed infinite. We assume vanishing concentration at the boundaries at infinity.

Medium heterogeneities and temporal flow fluctuations are taken into account using the stochastic approach described in 2.5.1.

As we are interested in the effective solute mixing and spreading of a solute starting from a point like injection the effective transport parameters can be derived from the first and second local moments defined in (2.27) and (2.28) respectively. Since we study an infinite medium, the dependence of the initial plume position is wiped out by the ensemble averaging. Thus, in the following we supress the injection position in the notation of the observables.

Using the axial moment equations established in section 2.7.2 the transport problem can be solved. The first (2.68), and second (2.69), local moments in x_1-direction are then obtained. Once we have the expressions of the first and second local moments, the effective transport parameters can be derived after performing the ensemble average over the spatial and temporal random processes.

4.2.2 Transport Coefficients

The observables of interest are the center of mass velocity $\overline{\nu_i}(t)$ (2.39), the local effective $\overline{D}^e_{ij}(t)$ (2.40), and the ensemble dispersion coefficients $D^{\text{ens}}_{ij}(t)$ (2.43), which are defined as averages of the single realization coefficients over all realizations of the ensemble of stratified media.

Effective Center of Mass Velocity

For the center of mass velocity in the longitudinal direction we obtain after inserting (2.68) in (2.34) and taking the ensemble average over all realizations of the stratified media and over the temporal random process as described in (2.39),

$$\overline{\nu}_1(t) = u, \tag{4.1}$$

from which we can see that there is no disorder-induced contribution to the effective center of mass velocity. For the transverse direction, we obtain $\overline{\nu}_T(t) = 0$, see Appendix C.

Effective Dispersion Coefficients

For the ensemble and effective local dispersion coefficients the behavior is different. Inserting the first (2.68), and second (2.69), local moments in (2.43) and (2.40), we derived the following expressions,

$$D_{11}^{\mathrm{ens}}(t) = D_L + u^2 \int_\Omega \mathrm{d}\mathbf{y}'' \int_\Omega \mathrm{d}\mathbf{y} \int_0^t \mathrm{d}t' c_{0_1}(\mathbf{y}'', t|\mathbf{y}, t') c_{0_1}(\mathbf{y}, t'|0)$$
$$\times \left[\sigma_{kk}^2 C^{kk}(\mathbf{y} - \mathbf{y}'') + \sigma_{vv}^2 C_{11}^{vv}(t - t') + \sigma_{kk}^2 \sigma_{vv}^2 C^{kk}(\mathbf{y} - \mathbf{y}'') C_{11}^{vv}(t - t')\right], \tag{4.2}$$

$$\overline{D}_{11}^{e}(t) = D^{\mathrm{ens}}(t) - u^2 \int_\Omega \mathrm{d}\mathbf{y} \int_\Omega \mathrm{d}\mathbf{y}'' c_{0_1}(\mathbf{y}'', t|0) \int_0^t \mathrm{d}t' c_{0_1}(\mathbf{y}, t'|0)$$
$$\times \left[\sigma_{kk}^2 C^{kk}(\mathbf{y} - \mathbf{y}'') + \sigma_{vv}^2 C_{11}^{vv}(t - t') + \sigma_{kk}^2 \sigma_{vv}^2 C^{kk}(\mathbf{y} - \mathbf{y}'') C_{11}^{vv}(t - t')\right], \tag{4.3}$$

while the ensemble and the effective local dispersion coefficients in the transverse direction remain of the order of local transverse dispersion, $D_T^{\mathrm{ens}}(t) = \overline{D}_T^{\mathrm{e}}(t) = D_T$, see Appendix C.

4.2.3 Analytical Solutions for the Local Dispersion Coefficients

In the following we derive analytical solutions for the local dispersion coefficients for a $d = 2$ dimensional medium focusing on transport governed by temporal fluctuations transverse to the direction of the mean flow velocity,

$\boldsymbol{v}(t) = [0, v_2(t)]^T$. In this case, (5.26) and (5.27) reduce to,

$$\begin{aligned} D_{11}^{\text{ens}}(t) &= D_L + u^2\sigma_{kk}^2 \int_\Omega \mathrm{d}\mathbf{y}'' \int_\Omega \mathrm{d}\mathbf{y} C^{kk}(\mathbf{y}-\mathbf{y}'') \\ &\quad \times \int_0^t \mathrm{d}t' c_0(\mathbf{y}'', t|\mathbf{y}, t') c_0(\mathbf{y}, t'|0) \qquad (4.4) \\ \overline{D}_{11}^{e}(t) &= D^{\text{ens}}(t) - u^2\sigma_{kk}^2 \int_\Omega \mathrm{d}\mathbf{y}'' \int_\Omega \mathrm{d}\mathbf{y} C^{kk}(\mathbf{y}-\mathbf{y}'') \\ &\quad \times c_0(\mathbf{y}'', t|0) \int_0^t \mathrm{d}t' c_0(\mathbf{y}, t'|0) \qquad (4.5) \end{aligned}$$

The Green function $c_0(\mathbf{y}, t|0, t')$, can be determined for a $d = 2$ dimensional model medium considering the initial condition (2.63) and vanishing concentration at the boundaries at infinity,

$$c_0(\mathbf{y}, t|0, t') = \frac{1}{\sqrt{4\pi D_T(t-t')}} \exp\left(-\frac{\left(y - u\int_{t'}^{t} \mathrm{d}t'' v_2(t'') \right)^2}{4D_T(t-t')} \right). \qquad (4.6)$$

To derive explicit results of the local effective and ensemble dispersion coefficients we need to specify the spatial C^{kk}. The spatial conductivity fluctuations (and thus velocity fluctuations), are assumed to decay exponentially fast on the correlation scale l. On an observation scale L that is much larger than the correlation scale, $L \gg l$, conductivity correlation can be approximated as a δ- correlated random field.

Hence the spatial correlation function in (2.20) here reads as,

$$C^{kk}(y - y') = l\,\delta(y - y'). \qquad (4.7)$$

This approximation is discussed in more detail in section 5.2.4

Inserting the correlation function (3.15), and the Green function (4.6) into (4.4) and (4.5), we obtain in Fourier space,

$$D_{11}^{\mathrm{ens}}(t) = D_L - \int_{k'} \int_0^t \mathrm{d}t' \Big\langle \exp\left(-k'^2 D_T t' - \mathrm{i}u\, k' \int_0^{t'} \mathrm{d}t'' v_2(t'') \right) \Big\rangle, \tag{4.8}$$

$$\overline{D}_{11}^{\mathrm{e}}(t) = D_{11}^{\mathrm{ens}}(t) - \int_{k'} \int_0^t \mathrm{d}t' \exp\left(-k'^2 D_T (2t - t') - \mathrm{i}u\, k' \int_0^{t'} \mathrm{d}t'' v_2(t'') \right) \Big\rangle. \tag{4.9}$$

Averaging equations (4.8) and (4.9) over the Gaussian random field $v_2(t)$, see Appendix B, we obtain the following results,

$$\begin{aligned} D_{11}^{\mathrm{ens}}(t) &= D_L + \frac{1}{\sqrt{\pi}} u^2 \sigma_{kk}^2\, l \\ &\quad \times \int_0^t \mathrm{d}t' \frac{1}{\sqrt{4\, D_T\, t' + 2\, u^2 \sigma_{vv}^2 \int_0^{t'} \mathrm{d}t'' \int_0^{t'} \mathrm{d}t''' C_{22}^{vv}(t'' - t''')}} \end{aligned} \tag{4.10}$$

$$\begin{aligned} \overline{D}_{11}^{\mathrm{e}}(t) &= D_{11}^{\mathrm{ens}}(t) - \frac{1}{\sqrt{\pi}} u^2 \sigma_{kk}^2\, l \\ &\quad \times \int_0^t \mathrm{d}t' \frac{1}{\sqrt{4\, D_T\, (2t - t') + 2\, u^2 \sigma_{vv}^2 \int_0^{t'} \mathrm{d}t'' \int_0^{t'} \mathrm{d}t''' C_{22}^{vv}(t'' - t''')}}, \end{aligned} \tag{4.11}$$

The temporal fluctuations of the flow field C^{vv} are assumed to be Gaussian correlated as in Chapter 3, see equation (3.15).

The integral equations for the local ensemble (4.10), and local effective (4.11), longitudinal dispersion coefficients are solved numerically in the following.

4.2.4 Effective Transport Behavior

The non-Fickian temporal behavior of the longitudinal effective dispersion coefficients in unbounded stratified media models has been addressed by *Matheron and de Marsily* [21] for transport in steady flow conditions. They showed that when the velocity flow is strictly parallel to the stratification, the superdiffusive behavior persist at all times. They also demonstrated that if a transverse flow component is added to the system, even if this component is small, the interaction of the transverse local dispersion and the constant flow component activates a mixing mechanism which leads at asymptotically large times, to a Fickian behavior of the dispersion coefficients. Furthermore, the effective dispersion coefficients in the transverse direction remains of the order of the local dispersion.

Here we study the impact of a temporally fluctuating flow component transverse to the direction of stratification.

As in steady flow conditions, there is no disorder-induced contribution to the effective and ensemble dispersion coefficients in the direction perpendicular to the stratification. Both remain of the order of the local dispersion.

Fig.4.1 shows the temporal evolution of $D_{11}^{\mathrm{ens}}(t)$ and $\overline{D}_{11}^{\mathrm{e}}(t)$ for different correlation times τ. The superdiffusive behavior of the ensemble and effective dispersion coefficients persist, however they are smaller than their counterparts in steady state conditions. For a constant velocity component transverse to stratification, the dispersion coefficients assume constant asymptotic value as addressed in [31].

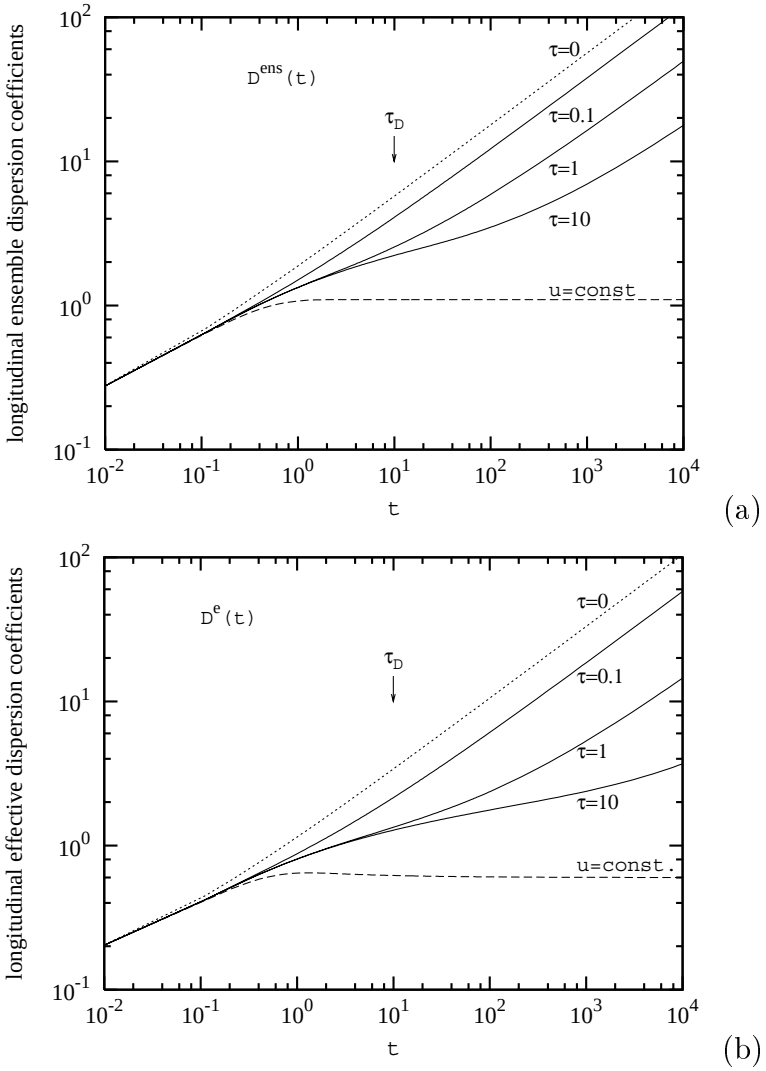

Figure 4.1: Temporal behavior of the longitudinal (a) ensemble $D_{11}^{\mathrm{ens}}(t)$, and (b) effective $\overline{D}_{11}^{\mathrm{e}}(t)$ dispersion coefficients in an unbounded stratified medium under temporal fluctuating flow conditions for different correlation times τ according to (4.10) and (4.11), respectively. The dashed lines correspond to the temporal behavior of the dispersion coefficient for a constant velocity in the transverse direction. The dotted lines show the behavior of dispersion coefficients in stratified media under steady flow conditions.

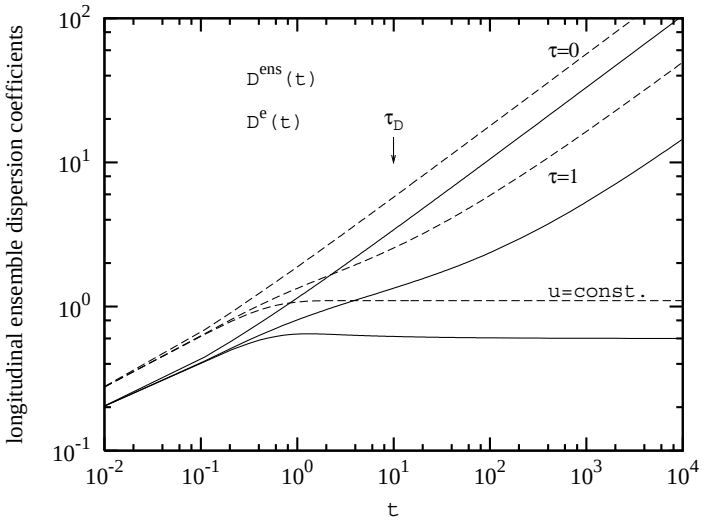

Figure 4.2: Nonconvergent behavior of $D_{11}^{\mathrm{ens}}(t)$ in dashed lines, and $\overline{D}_{11}^{\mathrm{e}}(t)$ in solid lines in a unbounded stratified medium under temporal fluctuating flow conditions for $\tau = 0$, $\tau = 1$ and $u = const.$

The relevant scale for the activation of the interaction between local transverse dispersion and transverse velocity contrast as a spreading mechanisms is the dispersion time scale $\tau_D = l^2/D_T$. At short times, $t < \tau_D$, we observe that transverse mass transport due to the temporal flow fluctuations leads to a slower increase of the dispersion coefficients. However, for times of the order or larger than τ_D, the interaction of transverse temporal flow fluctuations and local transverse dispersion do not cause transverse mixing that is strong enough to smooth the transport velocity contrast sampled by the solute. Thus the conductivity contrast is still the dominant macroscopic spreading mechanism which leads to the Non-Fickian behavior of the effective dispersion coefficients at large times.

As in the absence of temporal fluctuations, here the ensemble and effective dispersion coefficients do not converge at asymptotic time, see Figure 4.2.

This indicates that the sample to sample fluctuations of the center of mass position from realization to realization persist.

4.3 Parallel Random Flow with Short Range Spatially Correlated Flow Fluctuations

The complete temporal evolution of the effective and ensemble dispersion coefficients in physically heterogeneous media has been analyzed in the past [15, 16, 17, 18, 19, 26].

In heterogeneous media, the interaction of local dispersion and short range correlated spatial disorder causes the effective and ensemble dispersion to evolve towards a common asymptotic long time value. Here we investigate if short range spatially correlated flow perturbations affects the superdiffusive transport behavior observed in an unbounded stratified medium.

In the following we study effective mixing and spreading in a $d = 2$ dimensional medium by systematic numerical random walk simulations. We consider an infinite stratified arrangement subjected to incompressible random flow perturbations associated to the path structure assumed. We study first a Manhattan Grid structure and then, a nearly stratified flow model. Both models are described in the following.

4.3.1 Manhattan Grid

Like random walk/Brownian motion, the Manhattan Grid is a mobility synthetic model developed for ad-hoc network simulations [32]. The structure, based on the regular arrangement of the streets of Manhattan, New York, forces movements to be along vertical or horizontal directions, it can be see

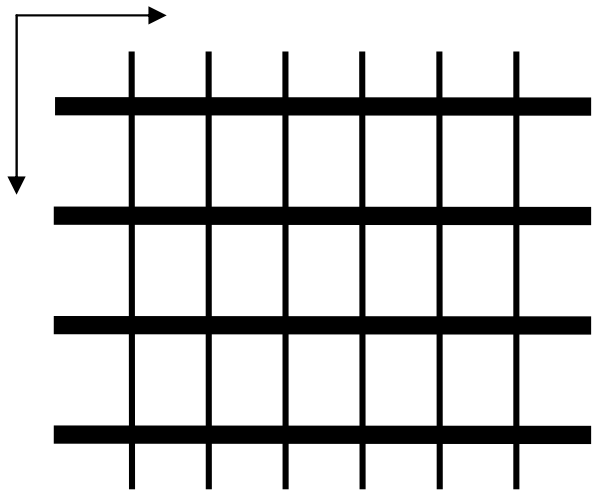

Figure 4.3: Deterministic Regular Manhattan Grid Structure.

as a doubly stratified structure. A deterministic regular Manhattan Grid structure is illustrated in Figure 4.3.

Basics

Flow through a Manhattan Grid model here is characterized by,

$$\mathbf{u}(\mathbf{x}) = u\,(y)\,\mathbf{e}_1 + v\,(x)\,\mathbf{e}_2, \tag{4.12}$$

i.e., the flow velocity is constant within a stratum but varies from layer to layer in each direction of the double stratification. The unit vectors in 1 and 2−directions are denoted by $\mathbf{e_1}$ and $\mathbf{e_2}$ respectively.

The advective dispersive transport equation is given by (2.2). In the following we consider conservative solute transport under steady state flow conditions. The initial condition defined in (2.4), here is chosen to be a point-like injection, we assume vanishing concentration at infinity as a boundary condition.

The layer to layer velocity variations in each direction can be taken into account by a generalization of the stochastic approach described in section 2.5.1 for a simple stratified medium. In the $d = 2$ dimensional medium under consideration here, the flow problem in (4.12), can be decomposed as follows,

$$\mathbf{u}(\mathbf{x}) = [u - u'(y)]\,\mathbf{e}_1 - v'(x)\mathbf{e}_2, \tag{4.13}$$

with u the constant mean flow velocity aligned with the 1-direction of the medium, $u'(y)$ and $v'(x)$ are the zero mean fluctuations in each direction of the double stratification.

In order to derive the local effective (2.40) and ensemble (2.43) dispersion coefficients the transport equation in (2.2) must be solved for the initial and boundary conditions defined. Contrary to the transport in a simple stratified medium, here, the transport problem can not be solved explicitly by local axial equations, and tools like perturbation theory may be required. However, in the following we focus on a systematic numerical investigation of the temporal behavior of the effective transport coefficients using a random-walk method described in Section 2.7.3.

Numerical Simulations

The flow field fluctuations in (4.13) are generated by Gaussian random fields based on the superposition of random cosine modes, see e.g.[80, 81],

$$u(y)' = \sigma_{uu}\sqrt{\frac{2}{N}}\sum_{j=1}^{N}\cos\left(k_2^{(j)}\cdot y + \varphi^{(j)}\right)\mathbf{e}_1, \tag{4.14}$$

and,

$$v(x)' = \sigma_{vv}\sqrt{\frac{2}{N}}\sum_{j=1}^{N}\cos\left(k_1^{(j)}\cdot x + \varphi^{(j)}\right)\mathbf{e}_2, \tag{4.15}$$

where the vectors $k_i^{(j)}$ for $i = 1, 2$ are derived from a Gaussian distribution with zero mean, unit variance and width l_i^2. The random phase φ^j is equally distributed in the interval $[0, 2\pi]$. For an infinite number of modes $N \to \infty$, $u'(y)$ and $v'(x)$ have the statistical characteristics of a Gaussian distribution. The flow fluctuations generated by this method have a Gaussian correlation as demonstrated in [80, 81].

Transport through a Manhattan Grid model characterized by the flow field (4.13), with the Gaussian correlated flow fluctuations given by (4.14) and (4.15) is then solved by the random-walk method described in section 2.7.3. The local moments in (2.73) here are computed over a $N = 10000$ noise realizations. The ensemble average are then taken over $R = 500$ disorder realizations.

Effective Transport Behavior

Here we analyze the temporal behavior of the effective and ensemble dispersion coefficients in a Manhattan Grid Model obtained by numerical random-walk simulations. The temporal behavior of the effective mixing and spreading is compared with the perfectly stratified medium results [31].

As shown in Figure 4.4, in the double stratified media under consideration here, the superdiffusive behavior of the effective and ensemble dispersion coefficients in the longitudinal direction, i.e., in the direction of the mean stratification, persists. The short range Gaussian correlation of the flow fluctuations in the 2−direction does not activate a transverse mixing mechanism that leads to a transition to a Fickian behavior of the effective dispersion coefficients. The solute never sees the full heterogeneity spectrum in the transverse direction.

A more interesting behavior is observed for the transverse dispersion co-

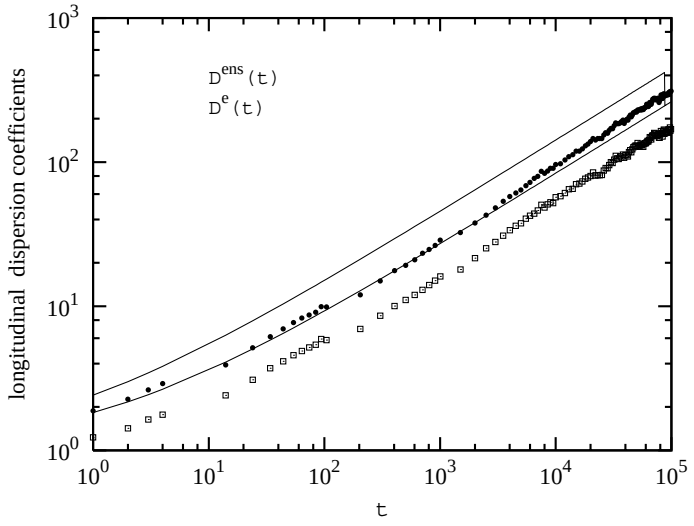

Figure 4.4: Comparison between the effective and ensemble dispersion coefficients behavior in a Manhattan Grid Model in dots, and a perfectly stratified medium in solid lines.

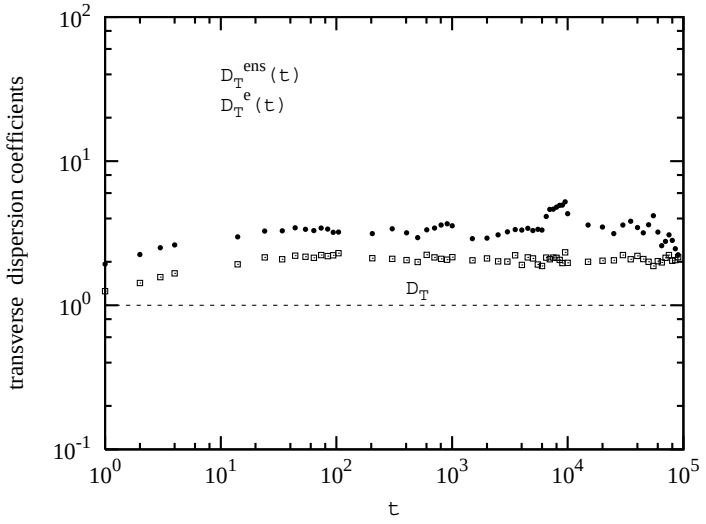

Figure 4.5: Comparison between the effective and ensemble dispersion coefficients behavior in a Manhattan Grid Model in dots, and a perfectly stratified medium in dashed lines.

efficients. In contrast to the perfectly stratified media, where both transverse ensemble and effective dispersion coefficients remain of the order of the local dispersion, here $D_T^{\text{ens}}(t)$ and $\overline{D}_T^{\text{e}}(t)$ evolve towards a constant value larger than the local dispersion. However, the increase in the transverse dispersion is not enough to re-organize the system and to modify the non-Fickian behavior of the longitudinal mixing and spreading as observed in Chapter 3.

Furthermore, note that the nonconvergence behavior observed for the effective and ensemble longitudinal dispersion coefficients in perfectly stratified media, here is also observed for the transverse effective and ensemble dispersion coefficients. Here, however, they assume (different) constant asymptotic long time values.

4.3.2 Nearly Stratified Flows

We analyze here a more realistic model which can be applied to geological formations. The flow through a layer with constant velocity is perturbed by incompressible flow that varies in all directions.

Basics

The random velocity field in the $d = 2$ nearly stratified medium under consideration here has the following structure, [33],

$$\mathbf{u}(\mathbf{x}) = u(y)\mathbf{e}_1 + \mathbf{v}(x, y)\mathbf{e}_2 \tag{4.16}$$

where $u(y)$ has the statistical properties of a perfectly stratified medium. The flow perturbation $\mathbf{v}(x, y)$ is divergence free, $\nabla \cdot \mathbf{v}(x, y) = 0$, and has zero mean. Its correlation is Gaussian.

The transport equation in this setup is again given by (2.2). Here we focus on steady flow conditions and assume as initial condition a conservative

solute that is instantaneously injected in a point.

Applying the stochastic approach described in section 2.5.1 for a perfectly stratified medium, and generalizing it to the scenario under consideration here, the flow field in (4.16) can be decomposed as follows,

$$\mathbf{u}(\mathbf{x}) = u\left[1 - u'(y)\right]\mathbf{e}_1 + \mathbf{v}(x,y)\mathbf{e}_2 \tag{4.17}$$

with u the mean flow velocity aligned with the 1 direction, $u'(y)$ the stratified flow fluctuation, i.e., the flow fluctuation that determines the stratified structure.

In the following we focus on a systematic numerical investigation of the temporal behavior of the local effective (2.40) and ensemble (2.43) dispersion coefficients using the random-walk method described in 2.7.3.

Numerical Simulations

Following the method for the generation of the Gaussian velocity field based on the superposition of randomly chosen cosines modes [80, 81], described briefly above for the Manhattan Grid model, here the flow field is obtained as follows,

$$\begin{aligned}
\mathbf{u}(\mathbf{x}) \;=\; & \Big[u - \sigma_{uu}\frac{2}{\sqrt{N}}\sum_{j=1}^{N}\cos\left(k_2^{(j)}\cdot y + \varphi^{(j)}\right) \\
& + \sigma_{uu}\frac{2}{\sqrt{N}}\sum_{j=1}^{N} p_1\left(\mathbf{k}^{(j)}\right)\cos\left(k_1^{(j)}\cdot x + k_2^{(j)}\cdot y + \varphi^{(i)}\right)\Big]\mathbf{e}_1 \\
& + \sigma_{vv}\frac{2}{\sqrt{N}}\sum_{j=1}^{N} p_2\left(\mathbf{k}^{(j)}\right)\cos\left(k_1^{(j)}\cdot x + k_2^{(j)}\cdot y + \varphi^{(j)}\right)\mathbf{e}_2,
\end{aligned} \tag{4.18}$$

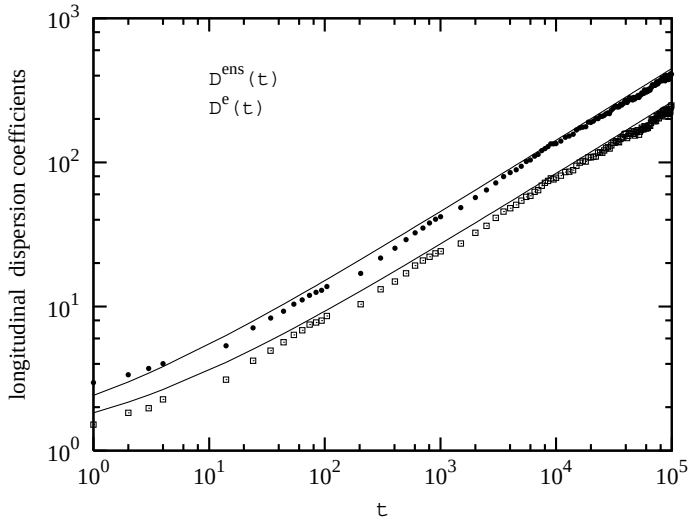

Figure 4.6: Comparison between the effective and ensemble dispersion coefficients behavior in a nearly stratified model in dots, and a perfectly stratified medium in solid lines.

with $k^{(j)}$ and $\varphi^{(j)}$ as described before for the Manhattan Grid model. The $p_i\left(\mathbf{k}^{(j)}\right)$ are a consequence of the solenoidality of the flow and read [15],

$$p_i\left(k_i\right) = \left(\delta_{i1} - \frac{k_1 k_i}{k^2}\right). \tag{4.19}$$

For the nearly stratified model the local moments in (2.73) here are computed over a $N = 10000$ noise realizations. The ensemble average is then taken over $R = 500$ disorder realizations.

Effective Transport Behavior

Here we present our numerical results of the local effective and ensemble dispersion coefficients for a nearly stratified model.

The longitudinal effective and ensemble dispersion coefficients illustrated in dots in Figure 4.6, evolve superdiffusively. Its behavior is practically the

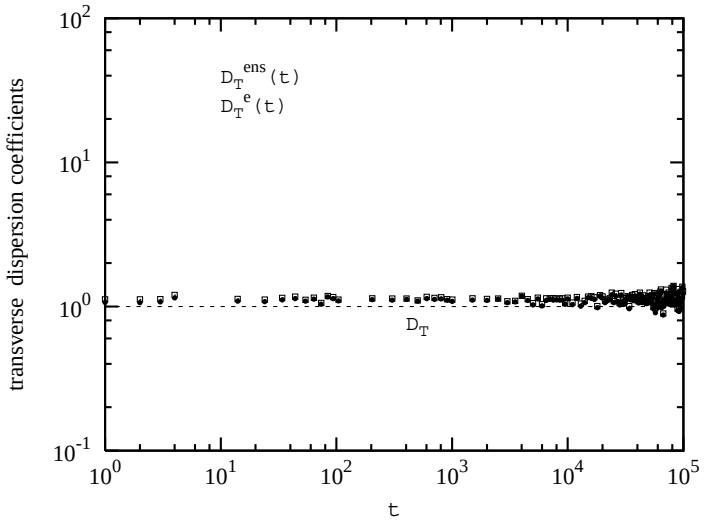

Figure 4.7: Comparison between the effective and ensemble dispersion coefficients behavior in a Nearly Stratified Model in dots, and a perfectly stratified medium in dashed lines.

same as for the perfectly stratified media, illustrated in the figure in solid lines. The stratification in the longitudinal direction is still the dominant spreading mechanisms that leads to the non-Fickian behavior of the dispersion coefficients. Even in the presence of short-range flow correlations in both directions, the anomalous behavior is not modified. This has been concluded also in [33] from an approximated analytical study.

Furthermore, as for the stratified medium, here the transverse dispersion coefficients remains of the order of the local dispersion coefficients, there is not disorder-induced contribution, see Figure 4.7.

4.4 Summary

We investigated the impact of spatial and temporal flow fluctuations on the anomalous behavior of local effective and ensemble dispersion coefficients for a conservative solute starting from a point-like injection in unbounded stratified models. We focus on $d = 2$ dimensional models.

The superdiffusive behavior of the apparent dispersion coefficient was studied for a perfectly stratified medium by [21], where a constant mean velocity aligned with the stratification was assumed. They showed that the non-Fickian behavior disappears when a constant velocity component in the transverse direction to the stratification is considered. This constant transverse velocity activates a mixing mechanism that allows the solute to sample the entire physical heterogeneity in the transverse direction.

Spatial and temporal flow fluctuations lead to an increase of mixing and spreading, which can be quantified by the increase of the dispersion coefficients [16, 17, 18, 15, 20]. Here we investigated if the interaction of spatial and temporal flow fluctuations modify the anomalous behavior observed in the strongly correlated model.

In section 4.2 transverse temporal flow fluctuations were added to the stratified medium model studied by [21]. Within a stochastic modeling approach, we derived analytic expressions for the local effective and ensemble coefficients. For this scenario the spatial velocity fluctuations were assumed delta-correlated.

We observe that the superdiffusive behavior of the longitudinal effective dispersion coefficients remains at large times, while the dispersion coefficients in the transverse direction remains of the order of the local transverse dispersion. The interaction of transverse temporal flow fluctuations and the layer to layer permeability variations does not activate an efficient mixing mecha-

nism which leads to the solute sampling the vertical heterogeneity. Advective spreading in the direction parallel to the stratification is still the dominant mechanism.

The influence of short-range Gaussian correlated incompressible flow perturbations was investigated in section 4.3.2. We studied two models, a Manhattan Grid structure and a nearly stratified model. In both cases we assumed a constant mean velocity aligned with the 1-direction. We used a superposition of randomly chosen cosines to generate the Gaussian correlated flow fluctuations. Transport was solved by numerical random-walk simulations and local moments were obtained.

The Manhattan Grid is a mobility synthetic model which here was used to simulate a double stratified medium, i.e., stratified in both directions. The non-Fickian mixing and spreading behavior persists. However, in contrast to the behavior in a perfectly stratified medium, here the transverse dispersion coefficients evolve to a constant value larger than the local transverse dispersion.

The nearly stratified model can be seen as a more realistic scenario. The stratified flow component seems to dominate transport and leads to a mixing and spreading behavior similar to the one observed in perfectly stratified media. The stratification together with the absence of an efficient transverse mixing mechanisms leads to anomalous dispersive transport behavior.

Chapter 5

Mixing and Spreading in a Bounded Stratified Medium

5.1 Introduction

Following the deterministic work of Marle et al. [82], Matheron and de Marsily [21] studied this perfectly stratified medium as an idealized aquifer model. They found that the apparent longitudinal dispersion coefficient grows superdiffusively with the square root of time and used this result to demonstrate that transport in porous media is not always diffusive. Transport in an infinite perfectly stratified random medium has been investigated extensively (e.g., [67, 68, 69, 70, 71, 72, 31, 41]) using stochastic modeling as a systematic means to quantify the impact of spatial heterogeneity on large scale transport. The latter has been studied in terms of the average solute distribution density and its moments, its spatial and temporal moments as well as in terms of (apparent) longitudinal dispersion coefficients.

The superdiffusive growth of the apparent longitudinal dispersion coefficient is caused by strong spatial correlation as quantified by the La-

grangian velocity correlation (e.g., [83, 84]). These aspects of transport in stratified flows have been extensively studied in the physics literature (e.g., [73, 74, 75, 85]). As seen in the previous chapter, this anomalous behavior is not modified neither by transverse temporal flow fluctuations, nor by spatially flow fluctuations, the long-range correlation is still the dominant spreading mechanism that in the absence of an efficient transverse mixing mechanisms leads to the anomalous behavior of the effective transport parameters.

In contrast to the unbounded stratified medium, for which transport is superdiffusive for all times, for a vertically (i.e., transverse to the direction of stratification) bounded medium, transport becomes eventually Gaussian and can be completely characterized by a constant macrodispersion or "Taylor dispersion-type" coefficient. Several authors have addressed the issue of enhanced dispersion and effective transport dynamics for bounded stratified random media and shear flows in general (e.g., [66, 86, 87, 88, 89]). Taylor [34] was the first to quantify enhanced solute dispersion in the parabolic (stratified) Hagen-Poiseuille flow through a tube by the well known Taylor dispersion coefficient,

$$D^* \propto \frac{a^2 U^2}{D_T}, \tag{5.1}$$

where a is a measure for the vertical extent of the flow domain, U the averaged flow velocity and D_T the transverse local dispersion coefficient, i.e. the transverse component of the (constant) dispersion tensor at local scale. The Taylor dispersion coefficient (5.1) reflects the mechanism that leads to enhanced spreading and mixing in stratified flows, namely, the solute's sampling of the vertical velocity contrast (U^2) by local transverse dispersion (D_T). The process is controlled by the dispersion time scale τ_D,

$$\tau_D = \frac{a^2}{D_T}, \tag{5.2}$$

which measures the time for the solute to sample the whole vertical velocity contrast. For times large compared to the dispersion time scale, $t \gg \tau_D$, the Taylor dispersion coefficient D^* quantifies both large scale spreading and mixing as well as the evolution of the solute concentration. In hydrological applications, however, this dispersion time scale can be large and the constant Taylor or macrodispersion coefficient does not provide a measure of mixing and spreading. At preasymptotic times, i.e., for times smaller than τ_D, solute spreading and mixing is controlled by local transverse dispersion, which activates the vertical velocity contrast as a macroscopic spreading and mixing mechanisms. As outlined in [28], transverse dispersion mixes the solute vertically, the velocity contrast experienced by the solute through vertical mixing stretches the plume and increases the plume surface (spreading). Transverse dispersion then again leads to vertical mass exchange between the solute layers and smoothes concentration contrasts out (mixing).

Here, we investigate solute mixing and spreading in a vertically bounded stratified random medium using a stochastic modeling approach in terms of the effective dispersion coefficients described in 2.6. Unlike for the infinite stratified medium, where a superdiffusive behavior of the apparent longitudinal dispersion coefficient is observed (e.g. [21]), here, at asymptotically long times disorder-induced mixing and spreading is uniquely quantified by a constant "Taylor dispersion" coefficient which is reached in asymptotic regime characterized by the time for complete vertical mixing. We study initial position and source size memory effects in the effective spreading and mixing dynamics for single realizations and their quantification using stochastic averaging. The transition from finite to infinite media and its impact on the derived effective parameters is analyzed. The validity of the quantification of mixing and spreading by stochastic averages for a finite media is discussed.

5.2 Basics

We study transport of a conservative solute in a confined horizontally stratified medium. The d-dimensional steady flow and transport domain denoted by Ω^d, which were defined in sections 2.5.1 and 2.5.2, here is assumed to be of infinite extension at least in the 1-direction and finite only in one of the transverse directions.

5.2.1 Flow and Transport in Bounded Stratified Media

Flow through a stratified porous medium is characterized by the Darcy equation, (2.17), in the scenario under consideration here, the flow is driven by a constant head gradient $\mathbf{J}$, which is aligned with the direction of stratification, $\mathbf{J} = -J\mathbf{e}_1$, where $\mathbf{e}_1$ is the unit vector in 1-direction. Together with the incompressibility condition $\nabla \cdot \mathbf{u}(\mathbf{x}) = 0$, this boundary condition leads to the exact solution (e.g., [41]),

$$\mathbf{u}(\mathbf{x}) = u(\mathbf{y})\mathbf{e}_1 = K(\mathbf{y})J\mathbf{e}_1. \tag{5.3}$$

Advective-dispersive transport of a conservative solute in the stratified flow field is given by (2.24). Note that in the following we focus on steady flow conditions. As defined in (2.4), we assumed as initial condition an instantaneous solute injection at $t = 0$. Here, we study transport of a solute evolving from a point-like injection and from an extended source perpendicular to stratification. Both initial conditions will be described in the following. The boundary conditions for $c(\mathbf{x}, t)$ in a bounded stratified medium are,

$$\lim_{x_1 \to \pm\infty} c(\mathbf{x}, t) = 0, \qquad \mathbf{n} \cdot \nabla c(\mathbf{x}, t)|_{\mathbf{x} \in \partial\Omega^d} = 0, \tag{5.4}$$

where $\partial\Omega^d$ is the boundary of the transport domain Ω^d, and $\mathbf{n}$ is the outward pointing unit vector perpendicular to the domain boundaries.

5.2.2 Stochastic Model

We use a stochastic modeling approach to account for the impact of spatial heterogeneity on the effective large scale transport behavior. In this approach, described in section 2.5.1, a given medium is seen as a typical realization of an ensemble of aquifers.

In the media model under consideration here, the spatial random field fluctuations $k(\mathbf{y})$ can be characterized by its $2n$-point joint distribution density $P_n(\{k(\mathbf{y}_i)\}_{i=-n}^{n})$. In Section 5.2.4 we specify these statistical characteristics and introduce the $d = 2$ dimensional model medium for the numerical random walk simulations.

In the following, we use the stochastic approach as a systematic tool to quantify the heterogeneity impact on large scale mixing and spreading. Note that the correlation function for the confined medium is not translation invariant. It is given by,

$$\overline{k(\mathbf{y})k(\mathbf{y}')} = \sigma^2 C_\Omega(\mathbf{y} - \mathbf{y}'|\mathbf{y}'), \tag{5.5}$$

with $\mathbf{y}, \mathbf{y}' \in \Omega$. The $C_\Omega(\boldsymbol{\xi}|\mathbf{y}')$ is given by,

$$C_\Omega(\boldsymbol{\xi}|\mathbf{y}') = C(\boldsymbol{\xi}) \tag{5.6}$$

for $\mathbf{y}' + \boldsymbol{\xi} \in \Omega$ and zero elsewhere.

5.2.3 Dimensionless Form of the Transport Equation

The observation length λ, and the flow velocity $\overline{u}$, define the advection time scale τ_u,

$$\tau_u = \frac{\lambda}{\overline{u}}, \tag{5.7}$$

which denotes the mean transport time over the distance λ along the direction of stratification by mean advection.

We define now non-dimensional time and distance by,

$$t = \hat{t}\tau_u, \qquad \mathbf{x} = \hat{\mathbf{x}}\lambda, \tag{5.8}$$

respectively. Thus the working transport equation, defined in (2.25), can be rewritten for steady flow conditions in non-dimensional terms as,

$$\frac{\partial \hat{c}(\hat{\mathbf{x}},\hat{t})}{\partial \hat{t}} + \frac{\partial \hat{c}(\hat{\mathbf{x}},\hat{t})}{\partial \hat{x}_1} - \hat{\nabla}\hat{\mathbf{D}}\hat{\nabla}\hat{c}(\hat{\mathbf{x}},\hat{t}) = \hat{\mathbf{L}}\{\hat{\mathbf{y}},\hat{t}\}\hat{c}(\hat{\mathbf{x}},\hat{t}), \tag{5.9}$$

with the perturbation transport operator here defined as,

$$\hat{\mathbf{L}}\{\hat{\mathbf{y}},\hat{t}\} = \hat{k}(\hat{\mathbf{y}})\frac{\partial}{\partial \hat{x}_1}. \tag{5.10}$$

Note that $\hat{\nabla}$ denotes the nabla operator in dimensionless coordinates. The non-dimensional solute concentration, dispersion tensor and conductivity fluctuations are defined by,

$$c(\mathbf{x},t) = \lambda^d \hat{c}(\mathbf{x}'\lambda, t'\tau_u), \qquad \mathbf{D} = \hat{\mathbf{D}}\overline{u}\lambda, \qquad k(\mathbf{y}) = \hat{k}(\hat{\mathbf{y}}\lambda). \tag{5.11}$$

The initial and boundary conditions (2.4) and (5.4) are non-dimensionalized accordingly. The non-dimensional correlation length is given by $\hat{l} = l/\lambda$.

Equation (5.9) constitutes our working equation in the following. For convenience, we drop the hats, which indicate non-dimensional quantities, in the following.

5.2.4 Model Medium

The $k(\mathbf{y})$ fluctuates on the correlation scale l. We consider here an aquifer scenario, for which the lateral halfwidth a of the domain is much larger than the correlation scale l. Thus, the conductivities in the different strata can be

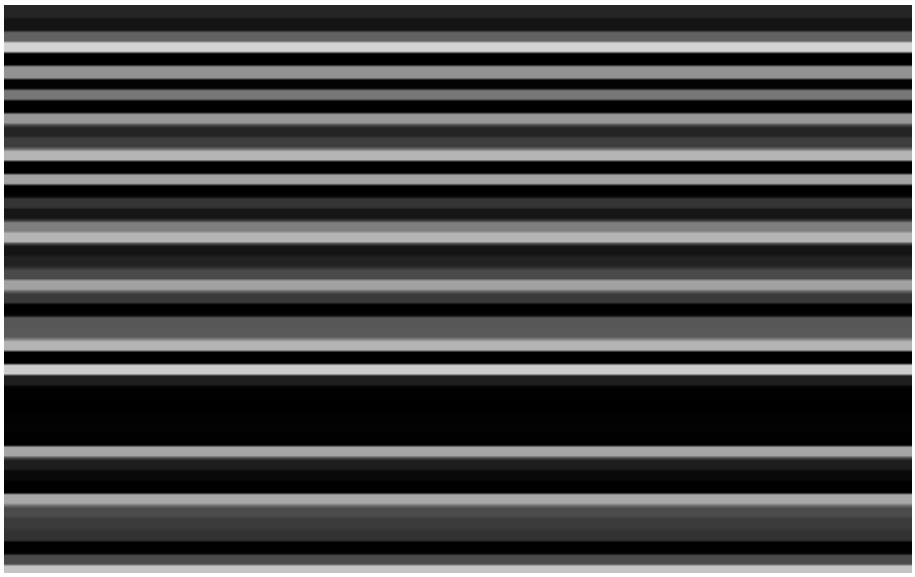

Figure 5.1: One realization of a confined stratified medium with 100 strata. Hydraulic conductivity is lognormally distributed; different greyscales denote different values of hydraulic conductivity.

considered uncorrelated. On this scale the $2n$-point joint distribution of the conductivity fluctuation $k(\mathbf{y})$ is given by (e.g., [90]),

$$P_n\left(\{k'(\mathbf{y}_i)\}_{i=-n}^{n}\right) = \exp\left\{-\ln P_1\left[k'(\mathbf{y}_i)\right]\right\}, \tag{5.12}$$

where $P_1(k')$ is the single variable distribution. We consider a $d = 2$ dimensional model medium. The medium under consideration consists of strata of the constant thickness l, see Figure 5.1. Thus, one particular realization of $k(y)$ is given by,

$$k(y) = \sum_{n=-a/l}^{a/l} k_n \Theta\left[y + b - nl\right]\left\{1 - \Theta\left[y + b - (n+1)l\right]\right\}, \tag{5.13}$$

where the k_n are distributed according to $P_1(k)$, b is uniformly distributed in the interval $[-l, l]$, with $\Theta\left[y + b\right]$ the Heaviside step function defined in [91];

the position vector is $\mathbf{x} = (x, y)^T$. Using representation (5.13) of the conductivity fluctuations, we obtain for the two point correlation function (2.20) (see Appendix D),

$$C(y - y') = l \left\{ \frac{1}{2l} \left[1 - \frac{|y - y'|}{l} \right] \right\} \tag{5.14}$$

for $|y - y'| < l$ and 0 elsewhere. This correlation function is translation invariant everywhere in the medium except for positions in the strata at the domain boundaries. If the width l of the strata is small, this can be disregarded. Thus in the following, we consider the limit $l \ll 1$, i.e., the observation scale is much larger than the correlation scale. In this limit, the expression in the curly brackets in (5.14) can be identified with the delta distribution so that the correlation function reads as,

$$C(y - y') = l\delta(y - y'). \tag{5.15}$$

In this limit boundary effects on the correlation function can be disregarded.

Nevertheless, note that the confined stratified medium under consideration here has only a finite number of strata. As such, spatial averages are not necessarily identical to the ensemble averages and are random functions by themselves due to the finiteness of the sample. This can be illustrated for the spatial mean of $k(\mathbf{y})$ for the confined stratified medium,

$$\langle k(y) \rangle = \frac{1}{2a} \int_{-a}^{a} \mathrm{d}\mathbf{y} k(\mathbf{y}) \tag{5.16}$$

where the angular brackets denote the vertical average. The fluctuations of the spatial average about the ensemble mean value is quantified by the variance of the spatial average $\langle k(y) \rangle$,

$$\overline{\langle k(y) \rangle^2} = \frac{\sigma_{uu}^2 l}{2a}. \tag{5.17}$$

where we used representation (5.13) for $k(y)$. As expected the variance decreases with increasing vertical extent of the medium.

The conductivity field $K(y)$ here is lognormally distributed so that the k_n in (5.13) are given by,

$$k_n = 1 - \exp\left(f_n - \frac{\sigma_{\mathrm{ff}}^2}{2}\right), \tag{5.18}$$

where the f_n are normally distributed random variables with zero mean and variance σ_{ff}^2.

5.3 Transport Coefficients

The lateral solute transport under consideration here, is completely determined by lateral local dispersion and no affected by spatial heterogeneity. This can be easily seen by projection of transport in the stratified medium onto plane perpendicular to the direction of stratification by integration of (5.9) over x_1, as seen in section 2.7.2 in the methodology of axial moment equations used here to the transport coefficients development. Thus, in the following we focus on transport along the direction of stratification.

Dentz and Carrera [29] suggest and discuss several measures for solute spreading and mixing based on the first and second moments of the transport Green function $g(\mathbf{x}, t|\mathbf{x}', t')$ (2.6), which solves the advection dispersion equation for a point like injection. The measures and the generalization of them for transport within a stochastic modeling approach were introduced in section 2.6. The dispersion concepts for single realizations and the ensemble of realizations of the stratified medium are summarized in table 1, where the corresponding equation numbers are also listed.

Table 5.1: Dispersion concepts

Single Realization	Eq.	Ensemble Average	Eq.	Concept
$D^a(t)$	(2.37)	$\overline{D}^a(t)$	(2.42)	apparent dispersion
$D^e(t\|\mathbf{x}')$	(2.33)	$\overline{D}^e(t\|\mathbf{x}')$	(2.40)	local effective dispersion
$D^e(t)$	(2.36)	$\overline{D}^e(t)$	(2.41)	global effective dispersion
D_L, D_T	(2.24)	N/A	-	local dispersion
D^*	(5.1)	$\overline{D}^*$	(5.29)	Taylor dispersion
N/A	-	$D^{\text{ens}}(t\|\mathbf{x}')$	(2.43)	local ensemble dispersion
N/A	-	$D^{\text{ens}}(t)$	(2.45)	global ensemble dispersion

Transport Coefficients: Single Realization

As stated in section 2.7.2 the advection dispersion equation for solute transport trough a stratified medium can be solved explicitly by the definition of axial moments equations. Having found expressions for the first (2.68), and second (2.69), local moments in the x_1-direction, we can write down the expressions for the local center of mass velocity and effective dispersion coefficients. They are given by,

$$\nu(t|\mathbf{x}') = 1 - \int_\Omega \mathrm{d}\mathbf{y}'' k(\mathbf{y}'') c_0(\mathbf{y}'', t|\mathbf{y}') \tag{5.19}$$

$$\begin{aligned} D^e(t|\mathbf{x}') = {} & D_L + \int_\Omega \mathrm{d}\mathbf{y}'' \int_\Omega \mathrm{d}\mathbf{y} \int_0^t \mathrm{d}t' k(\mathbf{y}'') k(\mathbf{y}) \times \\ & \left[c_0(\mathbf{y}'', t - t'|\mathbf{y}) - c_0(\mathbf{y}'', t|\mathbf{y}')\right] c_0(\mathbf{y}, t'|\mathbf{y}'). \end{aligned} \tag{5.20}$$

The global center of mass velocity and effective dispersion coefficient are obtained by integration of (5.19) and (5.20) over the initial distribution.

The apparent dispersion coefficient is given by,

$$D^a(t) = D_L + \int_\Omega \mathrm{d}\mathbf{y}'' \int_\Omega \mathrm{d}\mathbf{y} \int_0^t \mathrm{d}t' k(\mathbf{y}'')k(\mathbf{y}) \times \\ \int_\Omega \mathrm{d}\mathbf{y}' \rho(\mathbf{y}') \left[c_0(\mathbf{y}'', t - t'|\mathbf{y}) - \int_\Omega \mathrm{d}\mathbf{y}''' \rho(\mathbf{y}''') c_0(\mathbf{y}'', t|\mathbf{y}''') \right] c_0(\mathbf{y}, t'|\mathbf{y}'). \tag{5.21}$$

As detailed in [29], the center of mass fluctuations within the initial extended source given by the difference between $D^a(t)$ and $D^{\mathrm{e}}(t)$, see (2.38), tends to zero for $t \to \infty$, hence,

$$\lim_{t\to\infty} D^{\mathrm{e}}(t) = \lim_{t\to\infty} D^a(t), \tag{5.22}$$

i.e., in the limit $t \to \infty$ the effective and apparent dispersion coefficients converge to same asymptotic Taylor dispersion-type coefficient, which is independent of the initial plume,

$$D^* = D_L + \frac{1}{D_T V_\Omega} \int_\Omega \mathrm{d}\mathbf{y} \int_\Omega \mathrm{d}\mathbf{y}' k(\mathbf{y}) k(\mathbf{y}') \varphi(\mathbf{y}|\mathbf{y}'). \tag{5.23}$$

The $\varphi(\mathbf{y}|\mathbf{y}')$ solves the steady state diffusion equation,

$$\frac{1}{V_\Omega} - \nabla^2_{\mathbf{y}} \varphi(\mathbf{y}|\mathbf{y}') = \delta(\mathbf{y} - \mathbf{y}'), \tag{5.24}$$

for Neumann boundary conditions.

Transport Coefficients: Ensemble

By performing the ensemble average over (5.19), we straightforwardly obtain for the center of mass velocity,

$$\overline{\nu}(t|\mathbf{x}') = 1, \tag{5.25}$$

i.e., there is no disorder-induced contribution to the ensemble averaged center of mass velocity. This is different for the average dispersion coefficients.

Inserting (2.68) and (2.69) for the local moments in (2.43) and (2.40) for the ensemble and effective dispersion coefficients, we obtain,

$$\begin{aligned} D^{\text{ens}}(t|\mathbf{y}') &= D_L + \sigma^2 \int_\Omega \mathrm{d}\mathbf{y}'' \int_\Omega \mathrm{d}\mathbf{y} \int_0^t \mathrm{d}t' C(\mathbf{y}-\mathbf{y}'') \times \\ &\quad c_0(\mathbf{y}'', t-t'|\mathbf{y}) c_0(\mathbf{y}, t'|\mathbf{y}'). \qquad (5.26) \\ \overline{D}^e(t|\mathbf{y}') &= D^{\text{ens}}(t|\mathbf{y}') - \sigma^2 \int_\Omega \mathrm{d}\mathbf{y} \int_\Omega \mathrm{d}\mathbf{y}'' C(\mathbf{y}-\mathbf{y}'') \\ &\quad \times c_0(\mathbf{y}'', t|\mathbf{y}') \int_0^t \mathrm{d}t' c_0(\mathbf{y}, t'|\mathbf{y}'), \qquad (5.27) \end{aligned}$$

The corresponding expressions for extended initial plumes are obtained by integration over the source distribution according to (2.41) and (2.45).

For the average apparent dispersion coefficient (2.42), we obtain,

$$\begin{aligned} \overline{D}^a(t) = D^{\text{ens}}(t) - \sigma^2 \int_\Omega \mathrm{d}\mathbf{y}'' \int_\Omega \mathrm{d}\mathbf{y} C(\mathbf{y}-\mathbf{y}'') \times \\ \int_\Omega \mathrm{d}\mathbf{y}''' \rho(\mathbf{y}''') c_0(\mathbf{y}'', t|\mathbf{y}''') \int_0^t \mathrm{d}t' \int_\Omega \mathrm{d}\mathbf{y}' \rho(\mathbf{y}') c_0(\mathbf{y}, t'|\mathbf{y}'). \qquad (5.28) \end{aligned}$$

The average asymptotic Taylor dispersion-type coefficient is given by,

$$\overline{D}^* = D_L + \frac{\sigma^2}{D_T V_\Omega} \int_\Omega \mathrm{d}\mathbf{y} \int_\Omega \mathrm{d}\mathbf{y}' C(\mathbf{y}-\mathbf{y}') \varphi(\mathbf{y}|\mathbf{y}'), \qquad (5.29)$$

the $\varphi(\mathbf{y}|\mathbf{y}')$ solves the steady state diffusion equation,

$$\frac{1}{V_\Omega} - \nabla^2_{\mathbf{y}} \varphi(\mathbf{y}|\mathbf{y}') = \delta(\mathbf{y}-\mathbf{y}'), \qquad (5.30)$$

for Neumann boundary conditions.

5.3.1 Explicit Analytical Solutions for $d = 2$ Dimensions

Having defined the $d = 2$ dimensional model medium in Section 5.2.4, and in particular the conductivity correlation function (5.15), we can explicitly evaluate the expressions for the average dispersion coefficients. We consider two initial conditions; point-like injection at the position $(0, y')^T$, i.e.,

$$\rho(\mathbf{x}) = \delta(x)\delta(y - y'), \tag{5.31}$$

and a line source that extends over the whole medium cross-section at $x = 0$,

$$\rho(\mathbf{x}) = \frac{1}{2a}\delta(x). \tag{5.32}$$

The position vector in the following is given by $\mathbf{x} = (x, y)^T$.

The explicit solution of the effective and the ensemble dispersion coefficients depends on the form of the Green function $c_0(y, t|y')$, which solves the diffusion problem (2.59) for the initial and boundary conditions defined in (2.63) and (2.64). It is given by [29],

$$\begin{aligned} c_0(y, t|y') &= \frac{1}{2a} + \frac{1}{a}\sum_{n=1}^{\infty} \exp\left(-\frac{(n\pi)^2}{4}\frac{t}{\tau_D}\right) \\ &\quad \times \cos\left[\frac{n\pi(y + a)}{2a}\right] \cos\left[\frac{n\pi(y' + a)}{2a}\right]. \end{aligned} \tag{5.33}$$

The dispersion time scale τ_D in (5.33), measures the time for transport by local dispersion over the medium cross section,

$$\tau_D = \frac{a^2}{D_T}, \tag{5.34}$$

where D_T is the transverse local dispersion coefficient.

Inserting the spatial correlation function (5.15) and Green function (5.33) into the general expressions (5.26) and (5.27), we obtain for the ensemble and

average effective dispersion coefficients,

$$D^{\text{ens}}(t|y') = D_L + \frac{\sigma^2 l}{2a}t + \frac{2\sigma^2 l}{a}\tau_D \sum_{n=1}^{\infty} \frac{1}{(n\pi)^2} \times \left[1 - \exp\left(-\frac{(n\pi)^2}{4}\frac{t}{\tau_D}\right)\right] + \frac{2}{3a}\sigma^2 l \tau_D \sum_{m} \frac{(-1)^m}{(m\pi)^2} \times \left[\exp\left(-\frac{(m\pi)^2}{4}\frac{t}{\tau_D}\right) - \exp\left(-(m\pi)^2\frac{t}{\tau_D}\right)\right] \times \cos\left(\frac{m\pi y'}{a}\right) \quad (5.35)$$

$$\overline{D}^e(t|y') = D^{\text{ens}}(t|y') - \frac{\sigma^2 l}{2a}t - \frac{2\sigma^2 l}{a}\tau_D \sum_{n=1}^{\infty} \frac{1}{(n\pi)^2} \times \left[\exp\left(-\frac{(n\pi)^2}{4}\frac{t}{\tau_D}\right) - \exp\left(-\frac{(n\pi)^2}{2}\frac{t}{\tau_D}\right)\right] \times \left[1 + (-1)^n \cos\left(\frac{n\pi y'}{a}\right)\right] \quad (5.36)$$

Explicit expressions for the instantaneous line source are obtained by integration of (5.35) and (5.36) over the vertical cross-section of the two-dimensional medium. This yields,

$$D^{\text{ens}}(t) = D_L + \frac{\sigma^2 l}{2a}t + \frac{2\sigma^2 l}{a}\tau_D \sum_{n=1}^{\infty} \frac{1}{(n\pi)^2}\left[1 - \exp\left(-\frac{(n\pi)^2}{4}\frac{t}{\tau_D}\right)\right] \quad (5.37)$$

$$\overline{D}^e(t) = D_L + \frac{2\sigma^2 l}{a}\tau_D \sum_{n=1}^{\infty} \frac{1}{(n\pi)^2}\left[1 - \exp\left(-\frac{(n\pi)^2}{4}\frac{t}{\tau_D}\right)\right]^2 \quad (5.38)$$

for the ensemble and average global effective dispersion coefficients, respectively. For the average apparent dispersion coefficients we obtain by inserting (5.15) into (5.28),

$$\overline{D}^a(t) = D_L + \frac{2\sigma^2 l}{a}\tau_D \sum_{n=1}^{\infty} \frac{1}{(n\pi)^2}\left[1 - \exp\left(-\frac{(n\pi)^2}{4}\frac{t}{\tau_D}\right)\right]. \quad (5.39)$$

The average Taylor dispersion-type coefficient (5.29) can be obtained as the asymptotic long time value of the average effective dispersion coefficient,

$$\overline{D}^* = D_L + \frac{\sigma^2 l \tau_D}{3a}. \quad (5.40)$$

The transverse dimension clearly determines the asymptotic long time behavior of the dispersion coefficients. In the limit of $a \to \infty$, we obtain from (5.35) and (5.36) (see Appendix A),

$$\lim_{a\to\infty} D^{\text{ens}}(t|y') \equiv D_L + \frac{\sigma^2\sqrt{\tau_D^m}}{\sqrt{\pi}}\sqrt{t}, \tag{5.41}$$

$$\lim_{a\to\infty} \overline{D}^{\text{e}}(t|y') \equiv D_L + \frac{\sigma^2\sqrt{\tau_D^m}}{\sqrt{\pi}}\left(2-\sqrt{2}\right)\sqrt{t}, \tag{5.42}$$

where the microscopic dispersion scale, τ_D^m, is defined as follows,

$$\tau_D^m = \frac{l^2}{D_T}, \tag{5.43}$$

and quantifies the time for the vertical solute spreading over a stratum.

Note that neither the average local effective nor the ensemble dispersion coefficients depend on the source location anymore. As a consequence, the global effective dispersion coefficient does not depend on the source and is identical to the local effective dispersion coefficient. Furthermore, in this limit the average apparent dispersion coefficient (5.39) for the line source (now infinitely extended) is identical to the ensemble dispersion coefficient,

$$\lim_{a\to\infty} D^{\text{ens}}(t) \equiv \lim_{a\to\infty} \overline{D}^{a}(t). \tag{5.44}$$

Note that in contrast to the behavior observed in a confined medium where in the the limit of $t \to \infty$, or strictly speaking when the solute has sampled the hole medium by local transverse dispersion for times $t \gg \tau_D$, $\overline{D}^{a}(t)$ and $\overline{D}^{\text{e}}(t)$ converge to the same asymptotic Taylor dispersion coefficient, (5.22), here for a infinitely extended initial plume the apparent and the global effective dispersion coefficients do not converge at large times because $\tau_D \to \infty$. This means first that the limits $a \to \infty$, and $t \to \infty$, are not commutative. Furthermore, as $\tau_D \to \infty$ the complete transverse mixing is never reached for a infinite medium, which in turns leads to the Non-Fickian behavior of the effective dispersion coefficients.

5.4 Effective Mixing and Spreading

We study effective mixing and spreading using explicit analytical expressions for the transport coefficients presented in the previous section, and numerical random walk simulations described in the following.

5.4.1 Numerical Random Walk Simulations

The numerical solution of the transport problem using random walk simulations is described in section 2.7.3. In the scenario under consideration here the random flow field is given by,

$$\mathbf{u}'\left(\mathbf{x}^{(i,r)}(t|\mathbf{x}')\right) = \left[1 - k^{(r)}\left(\mathbf{y}^{(i,r)}(t|\mathbf{y}')\right)\right], \tag{5.45}$$

with $k^{(r)}(y)$ the r-th realization of $k(\mathbf{y})$. Here, the impermeable horizontal walls are modeled as reflecting boundaries. The random fluctuations of the conductivity field are modeled by (5.13).

The $d = 2$ dimensional medium under consideration here, see Section 5.2.4, consists of 100 strata of equal thickness $l = 1$, the halfwidth of the medium is given by $a = 50$. The time discretization for the random walk simulations is $\Delta t = 10^{-1}$, the transverse and longitudinal local dispersion coefficients are given by $D_T = D_L = 1$. The line source consists of $M = 200$ points that are uniformly distributed over the medium cross-section, the number of injected particles at each point is 50. The ensemble average is taken over $R = 10^3$ realizations of the random conductivity field.

5.4.2 Point-Like Initial Distribution

We investigate the temporal behavior of the dispersion coefficients $\overline{D}^e(t|y')$ and $D^{\text{ens}}(t|y')$, for different dispersion time scales τ_D, and for different vertical initial positions y'.

Figure 5.2 illustrates a particle distribution evolving from an instantaneous injection at $y' = 0$ in one given realization of the stratified medium. The snap shots of the spatial distribution are taken after $t = 10^{-3}\tau_D$, $t = 10^{-2}\tau_D$, $t = 10^{-1}\tau_D$, and $t = \tau_D$.

We distinguish two relevant dispersion time scales; the dispersion scale τ_D, (5.34), which quantifies solute mixing over a vertical medium, and the microscopic dispersion scale τ_D^m, (5.43), which quantifies the time for the vertical solute spreading over a stratum. Thus, τ_D^m sets the relevant scale for the activation of the transverse conductivity contrast as a macroscopic spreading mechanism. For the parameter values chosen here, $\tau_D^m = 10^{-3}\tau_D$. This is illustrated in Figure 5.2a. With increasing time the concentration distribution becomes more spread out in horizontal direction, see Figure 5.2b. As soon as the solute samples a larger part of the vertical conductivity contrast, the particle distribution starts homogenizing, Figure 5.2c, until it becomes uniform for times larger than τ_D, Figure 5.2d.

This behavior is reflected in the temporal evolution of the average dispersion coefficients. Figure 5.4 shows the temporal evolution of $\overline{D}^e(t|0)$ and $D^{\text{ens}}(t|0)$ for $\tau_D = 2500$ and $\tau_D = 625$ given by (5.35) and (5.36) and derived from numerical random walk simulations. For times smaller than τ_D^m, $t < \tau_D^m$, the solute has only seen one single strata with constant conductivity and spreading is due to local dispersion only. At times of the order of the microscopic dispersion time scale τ_D^m the solute starts sampling the vertical conductivity contrast, which leads to an increase of longitudinal spreading; the effective dispersion coefficients increases. In the time regime $\tau_D^m \ll t \ll \tau_D$, the dispersion coefficients display the characteristic $\sqrt{t}$ behavior. In this regime, conductivity contrasts are activated as a macroscopic spreading mechanism ($t > \tau_D^m$) and the medium looks infinite for the so-

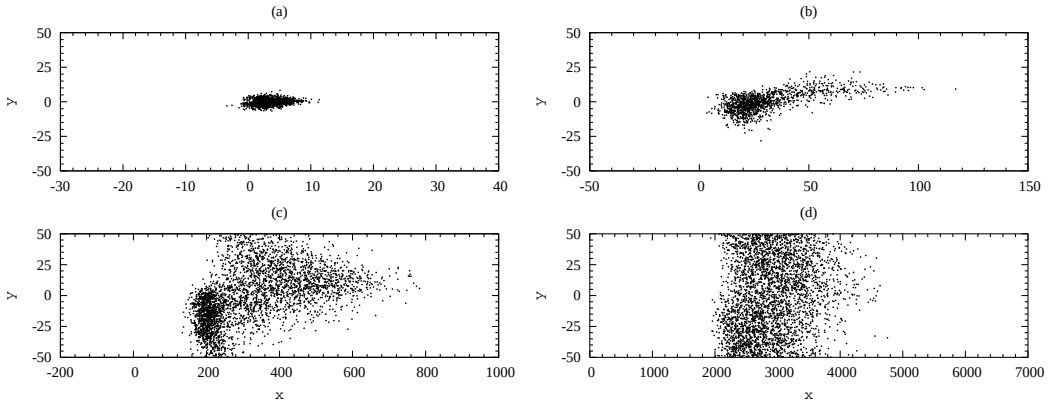

Figure 5.2: Distribution of solute particles evolving from a point source located at $y' = 0$ for one given realization of a vertically stratified random medium with a halfwidth $a = 50$, equal strata thickness $l = 1$, and $D_L = D_T = 1$, after (a) $t = 10^{-3}\tau_D$, (b) $t = 10^{-2}\tau_D$, (c) $t = 10^{-1}\tau_D$, and (d) $t = \tau_D$.

lute as it has spread out vertically over a distance much smaller than the transverse extent of the medium ($t << \tau_D$). Thus, in this regime, the dispersion coefficient shows the same behavior as for an infinite stratified medium, given by (5.42). In the asymptotic long time limit of times $t \gg \tau_D$, when the solute has sampled the whole vertical conductivity contrast, the effective dispersion coefficient converges to its constant long time value given by the Taylor dispersion coefficient (5.40).

The ensemble dispersion coefficient $D^{\text{ens}}(t|0)$ is consistently larger than the effective coefficients. The ensemble dispersion coefficient, takes into account an artificial spreading effect due to the variability of the center of mass position of the concentration distribution in different realizations of the stratified medium. In the intermediate regime $\tau_D^m \ll t \ll \tau_D$, $D^{\text{ens}}(t|0)$ increases with the square root of time as given by (5.41). In the asymptotic long time limit of $t \gg \tau_D$, the ensemble dispersion coefficient increases linearly with time

$$D^{\text{ens}}(t|y')|_{t\to\infty} = D_L + \frac{\sigma^2 l \tau_D}{3a} + \frac{\sigma^2 l}{2a} t. \tag{5.46}$$

This linear increase is due to persistent center of mass fluctuations, which increase quadratically with time. This can be seen as follows: The center of mass position in a given realization is given by (2.68). Thus, the center of mass fluctuation is given by,

$$\begin{aligned} \delta\mu^{(1)}(t|\mathbf{y}') &= \overline{\mu^{(1)}(t|\mathbf{y}')} - \mu^{(1)}(t|\mathbf{y}') \\ &= \int_{-a}^{a} \mathrm{d}\mathbf{y}'' \int_{0}^{t} \mathrm{d}t' k(\mathbf{y}'') c_0(y'', t'|\mathbf{y}'). \end{aligned} \tag{5.47}$$

In the limit $t \gg \tau_D$, the Green function $c_0(\mathbf{y}'', t'|\mathbf{y}')$ tends to $1/(2a)$, as in this limit the solute is uniformly distributed over the medium cross-section.

Thus, $\delta\mu^{(1)}(t|\mathbf{y}')$ is given by,

$$\delta\mu^{(1)}(t|\mathbf{y}') = \langle k(\mathbf{y}')\rangle t \tag{5.48}$$

where the angular brackets denote the spatial average over the medium cross-section, see Section 5.2.4. Thus, the variance of the center of mass position is given in terms of the variance (5.17) of the spatial average conductivity as,

$$\overline{\delta\mu^{(1)}(t|\mathbf{y}')^2} = \frac{\sigma^2 l}{2a} t^2. \tag{5.49}$$

Half the temporal rate of change of the latter is the difference between the effective and ensemble coefficients, see (2.44), and explains the linear increase of $D^{\mathrm{ens}}(t|y')$ for $t \gg \tau_D$. Note that the center of mass fluctuations decrease with increasing vertical extent, or vertical sampling volume. This mechanism is illustrated in Figure 5.3. The difference between the global ensemble and the apparent dispersion coefficients obtained by numerical random-walk simulations for three different vertical extended sources $10\,l$, $100\,l$ and a line source that extends over the whole medium cross-section of $1000\,l$ are shown. For an extended source distribution, the difference between the global ensemble and apparent dispersion coefficients quantifies the fluctuations of the center of mass position. Hence, at preasymptotic times, Figure 5.3 demonstrates that there is a bigger contrast between the center of mass position for small extended sources, this contrast decreases with increasing the source size or vertical extent of the medium.

Note that for finite a, the difference between $\overline{D}^a(t)$ and $D^{\mathrm{ens}}(t)$ always increases linearly for times $t \gg \tau_D$. Particularly, equation (5.49) is based on the assumption of complete transverse mixing, i.e., implicitly we assume that the medium is finite. Thus, in the limit of $a \to \infty$ (5.49) is not valid because $\tau_D \to \infty$, and the transverse mixing condition is never fulfilled. This

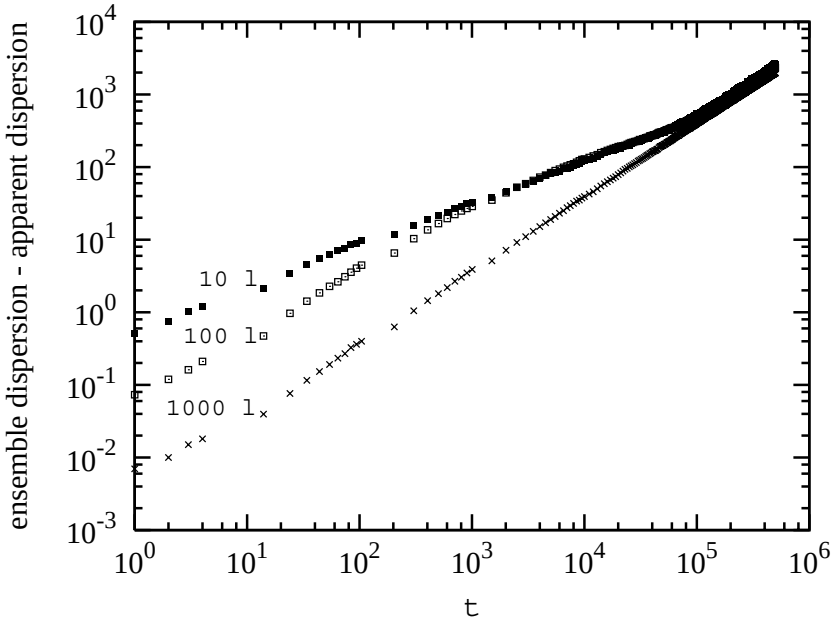

Figure 5.3: Numerical results of the differences between the global ensemble and apparent dispersion coefficients for three extended sources of $10\,l$, $100\,l$, and a line source that extends over the whole medium cross-section of $1000\,l$.

is manifested in the difference between $\overline{D}^{\mathrm{ens}}(t)$ and $\overline{D}^{\mathrm{e}}(t)$ for the infinite medium given in (5.41) and (5.42), respectively, for which,

$$\lim_{a\to\infty} \overline{\delta\mu^{(1)}(t)^2} = \frac{2}{3}\frac{\sigma^2\sqrt{\tau_D^m}}{\sqrt{\pi}}\left(1-\sqrt{2}\right)t^{3/2}. \tag{5.50}$$

Figure 5.5 illustrates the temporal behavior of a distribution of solute particles evolving from a point source located at $y' = 0.9a$ for a given realization of the stratified medium. In order to study the effect of the initial position point source on solute transport, the stratified medium analyzed here, is the same as in Figure 5.2. For point sources starting in the vicinity of the horizontal boundaries, at early times, $t \geq \tau_D^m$, the solute particles experience the layer to layer permeability variations by transverse local dispersion in a non

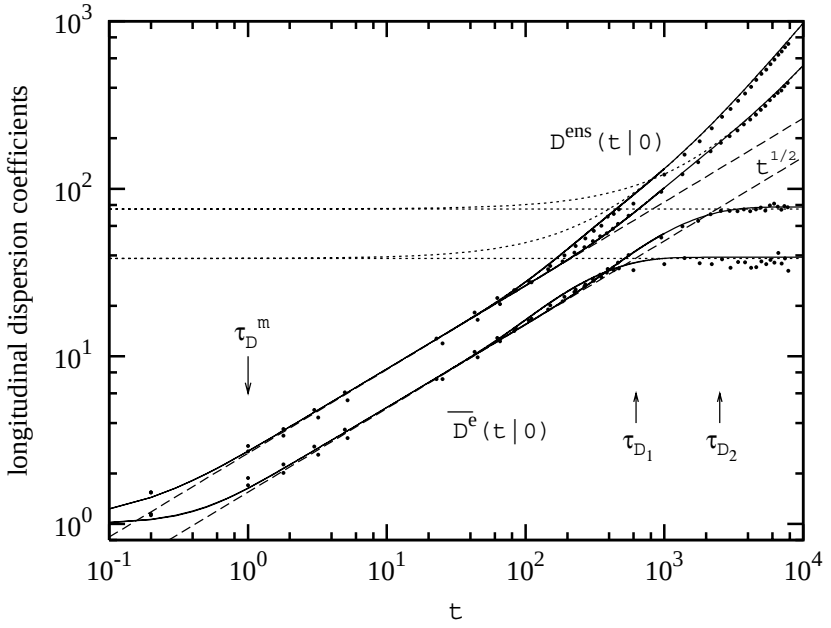

Figure 5.4: Temporal behavior of the local effective and ensemble dispersion coefficients evolving from a point source at $y' = 0$, for two different dispersion time scales, $\tau_{D_1} = 625$, and $\tau_{D_2} = 2500$ in a vertically stratified random media with $a = 25$, $a = 50$, respectively, $l = 1$, and $D_L = D_T = 1$. The solid lines describe the $D^{\text{ens}}(t, y')$ and $\overline{D}^e(t, y')$ behavior given by (5.35) and (5.36), respectively. For the intermediate time regime $\tau_D^m \ll t \ll \tau_D$, the $\sqrt{t}$ behavior given by (5.41) and (5.42) is showed in dashed lines. The doted lines describe the long time behavior, given by (5.46) and (5.40). Numerical random walk simulation in dots.

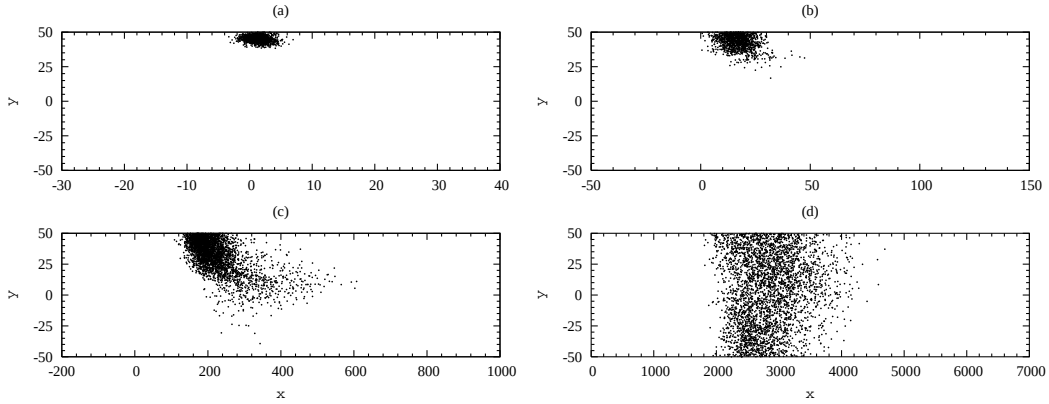

Figure 5.5: Distribution of solute particles evolving from a point source located at $y' = 0.9a$ for one given realization of a vertically stratified random medium with a halfwidth $a = 50$, equal strata thickness $l = 1$, and $D_L = D_T = 1$, after (a) $t = 10^{-3}\tau_D$, (b) $t = 10^{-2}\tau_D$, (c) $t = 10^{-1}\tau_D$, and (d) $t = \tau_D$.

symmetrical way due to reflection at the medium boundaries. Hence, the time needed for a solute particle to sample the transverse variability of the velocity field is larger than when starting at $y' = 0$. This difference for the distribution starting at different vertical locations is clearly shown in Figures 5.2(c) and 5.5(c), for $t = 10^{-1}\tau_D$. The particle distribution for $y' = 0$, is more uniform than for $y' = 0.9a$, and it occupies almost the entire medium cross section. For times of the order or larger than the dispersion time scale $t \geq \tau_D$, the solute particles are distributed uniformly over the medium cross section in both cases; the memory of the initial distribution is wiped out.

This behavior is again reflected in the temporal evolution of the effective dispersion coefficients shown in Figure 5.6. The effective diffusion coefficient $\overline{D}^{\mathrm{e}}(t|y')$ evolves slower for $y' = 0.9a$, than for $y' = 0$, and for times large

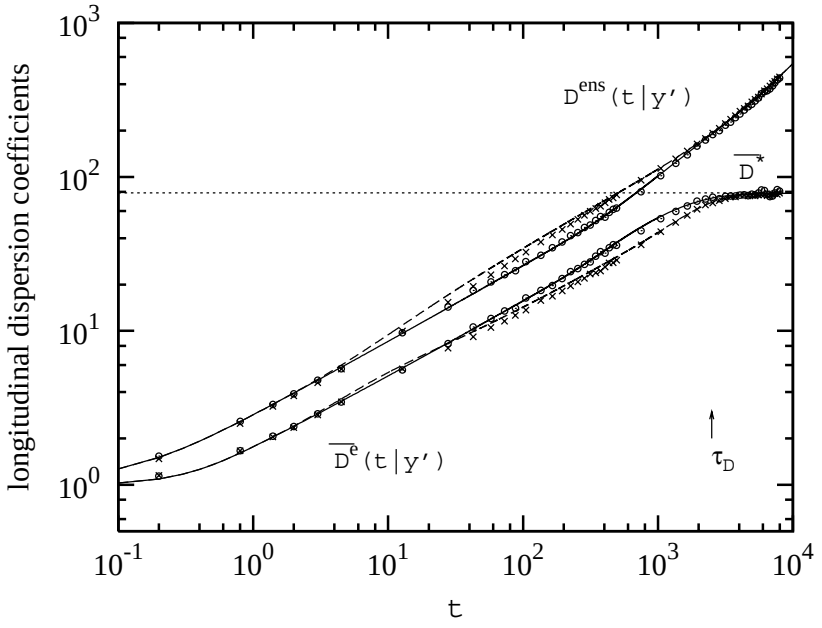

Figure 5.6: Time behavior of the local effective and ensemble dispersion coefficients evolving from two point sources located at $y' = 0$, in solid lines, and $y' = 0.9a$, in dashed lines, in a vertically stratified random media with $a = 50$, $l = 1$, and $D_L = D_T = 1$. The doted line describe the average asymptotic long time Taylor dispersion $\overline{D}^*$ given by (5.40). Numerical random walk simulations in dots.

compared to τ_D, the local effective dispersion coefficients converge to the same asymptotic long time value.

The slower sampling of the conductivity contrast by particles close to the boundaries compared to solute particles originating from $y' = 0$ is also reflected by the ensemble dispersion coefficient. Due to the slower sampling for $y' = 0.9$, there is a bigger contrast between the mean flow velocity in each realization and the ensemble mean velocity for $t < \tau_D$, which in turn causes a faster increase of $D^{\text{ens}}(t|y')$, see Figure 5.6. For $t > \tau_D$ both ensemble dispersion coefficients evolve linearly to (5.46), independently of the source location.

5.4.3 Vertical Line Source

Here, we investigate mixing and spreading for a solute that evolves from the instantaneous uniform line source (5.32).

Figure 5.7 shows a distribution of solute particles at at $t = 10^{-3}\tau_D$, $t = 10^{-2}\tau_D$, $t = 10^{-1}\tau_D$, and $t = \tau_D$ in a single realization of the stratified random medium. At small times compared to the dispersion time scale $t \ll \tau_D$, the distribution reflects the conductivity profile as shown in Figure 5.7a. For increasing time, Figures 5.7b and c, local transverse dispersion leads to vertical mass exchange and the profile disperses, the concentration distribution becomes more uniform and concentration contrasts are smoothed out. For times large compared to τ_D, the solute distribution has been homogenized, Figure 5.7d.

For one given realization of the stratified medium, solute spreading and mixing are quantified by the effective and apparent dispersion coefficients (2.33) and (2.37), respectively. The time behavior of $D^e(t)$ and $D^a(t)$ is evaluated numerically using random walk simulations. Figure 5.8 shows $D^e(t)$ and

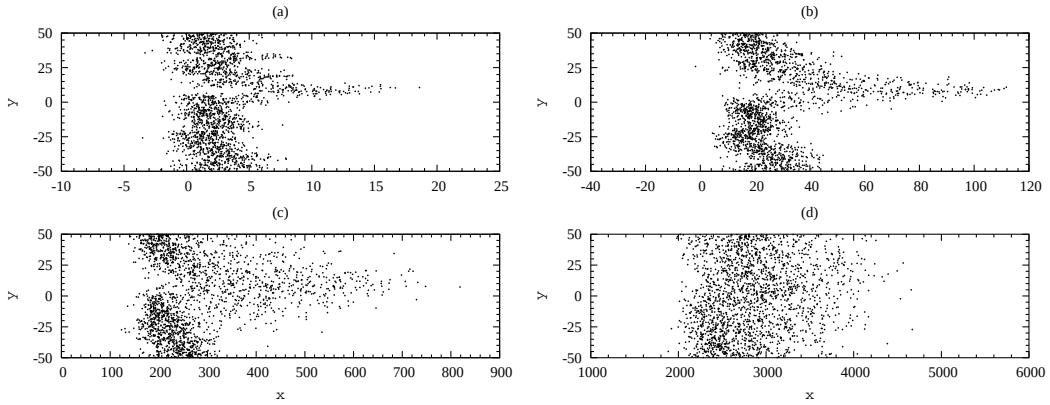

Figure 5.7: Distribution of solute particles evolving from a uniform line source in a single realization of a vertically stratified random medium with a halfwidth $a = 50$, constant strata thickness $l = 1$, local dispersion $D_L = D_T = 1$, after (a) $t = 10^{-3}\tau_D$, (b) $t = 10^{-2}\tau_D$, (c) $t = 10^{-1}\tau_D$, and (d) $t = \tau_D$.

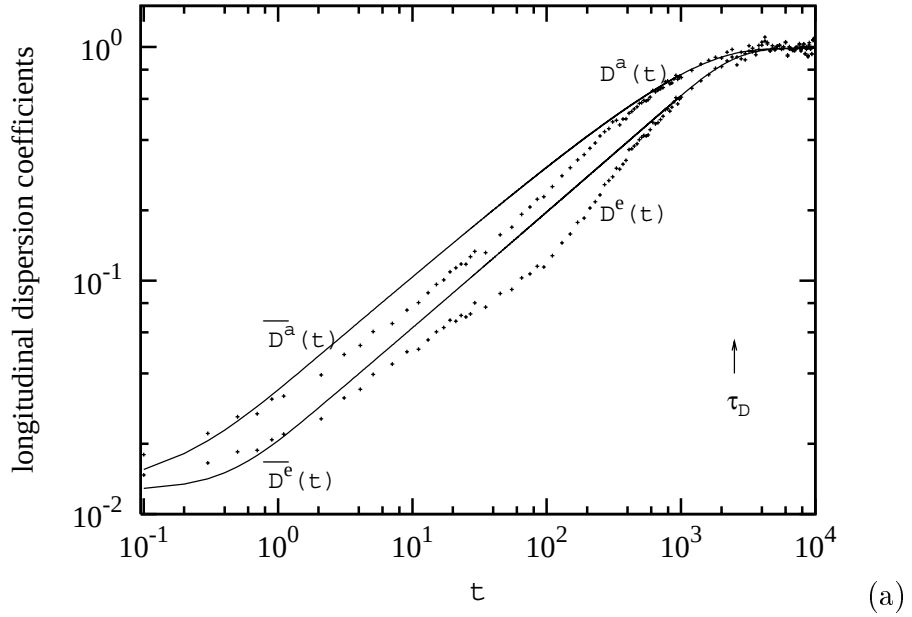

(a)

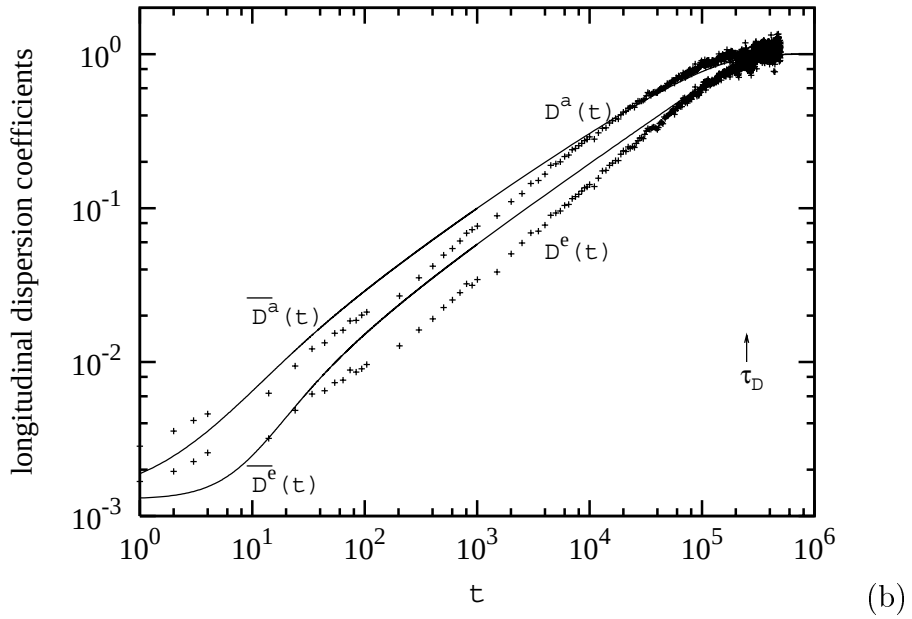

(b)

Figure 5.8: Comparison between the normalized average effective $\overline{D}^e(t)/\overline{D}^*$, and apparent $\overline{D}^a(t)/\overline{D}^*$, dispersion coefficients, with their single realization normalized counterparts, $D^e(t)/D^*$ and $D^a(t)/D^*$, respectively, for (a) vertical line source of $100l$, and (b) vertical line source of $1000l$. Temporal behavior of $\overline{D}^e(t)$, and $\overline{D}^a(t)$ given by (5.38) and (5.39), is presented in solid lines. Numerical random walk simulations of $D^e(t)$ and $D^a(t)$ in dots.

$D^a(t)$ normalized by their asymptotic long time value. The apparent and effective coefficients evolve in a qualitatively and quantitatively different way. As outlined in Section 2.6.3, the apparent dispersion coefficient quantifies the center of mass fluctuations within the extended source, which are suppressed by the definition of the effective dispersion coefficient, see (2.38). Hence, for $t < \tau_D$, the conductivity contrast along the extended source leads to a faster increase of $D^a(t)$. The effective dispersion coefficient measures the average mixing along the source distribution caused by the interaction of transverse local dispersion and the vertical conductivity contrast. At times $t \geq \tau_D$ both $D^a(t)$ and $D^e(t)$ evolve towards their common asymptotic long time value given by D^*, (5.23).

The behavior of the average coefficients $\overline{D}^e(t)$ and $\overline{D}^a(t)$, given by (5.38) and (5.39), respectively, reflects very well the behavior observed in a single realization. Figure 5.8 shows $\overline{D}^e(t)$ and $\overline{D}^a(t)$ normalized by their asymptotic long time value compared to their single realization counterparts for (a) vertical line source of $100l$, and (b) vertical line source of $1000l$. Due to the finiteness of the medium, the asymptotic Taylor dispersion-type coefficient D^*, (5.23), varies from realization to realization of the stratified medium. The quantification of uncertainty due to sample to sample fluctuations as well as the self-averaging behavior of the effective dispersion coefficient is work in progress.

5.4.4 Small Extended Source

Here we investigate by numerical random-walk simulations the effective mixing and spreading behavior for solute distributions starting from small extended source distributions, i.e., small compared to the domain size.

The $d = 2$ dimensional model under consideration here consist of 1000

strata of equal thickness $l = 1$. The time discretization here is $\Delta t = 1$, the transverse and longitudinal local dispersion are given by $D_T = D_L = 1$. We investigate in the following three different vertical extended sources $10l$, $100l$ and for comparison porpoises, a line source that extends over the whole medium cross section of $1000l$. The total number of injected particles in each case was 10000. The ensemble average was taken over $R = 10^2$ realizations of the random conductivity field.

Memory of the Initial Source Size

Here we investigate the impact of the initial source size on the temporal behavior of $D^{\text{ens}}(t)$, $\overline{D}^{\text{e}}(t)$ and $\overline{D}^{a}(t)$.

For one given realization of the stratified medium the temporal evolution of solute particles starting from the sources of $10l$ and $100l$ are illustrated in Figures 5.9, 5.10 respectively. In order to study the effect of the initial source size on solute transport, the stratified medium is the same for the two sources under investigation. The extended sources were instantaneously and symmetrically injected starting from $y' = 0$. The snap shots of the spatial distribution are taken after $t = 10^{-4}\tau_D$, $t = 10^{-2}\tau_D$, $t = 10^{-1}\tau_D$ and $t = \tau_D$.

At times of the order of the microscopic dispersion scale τ_D^m, the small vertical extended sources experience the conductivity contrast along its vertical sampling extension. It is clear that the conductivity contrast experienced by the initial extended source of $100l$ is greater than the one experienced by the $10l$ source. This is illustrated in Figures 5.9a and 5.10a. Whit increasing time the concentration distributions becomes more spread out in the horizontal direction, see Figures 5.9b and 5.10b. The solute distribution for the line source of $100l$ is slightly greater than the one observed for $10l$. Note however,

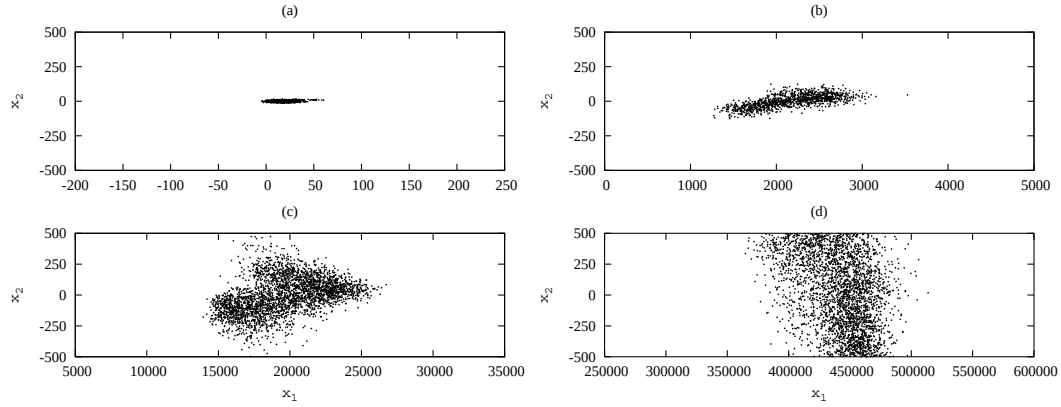

Figure 5.9: Distribution of solute particles evolving from a line source of $10l$ in a single realization of a vertically stratified random medium with a halfwidth $a = 500$, constant strata thickness $l = 1$, local dispersion $D_L = D_T = 1$, after (a) $t = 10^{-4}\tau_D$, (b) $t = 10^{-2}\tau_D$, (c) $t = 10^{-1}\tau_D$, and (d) $t = \tau_D$.

that the memory of the initial source size is wiped out with increasing time, even for times smaller than the time for complete vertical mixing, the solute distributions are practically identical for both sources, see 5.9c and 5.10c for $t = 10^{-1}\tau_D$. For times of the order or larger than τ_D, the solute particles are distributed uniformly over the medium cross section in both cases, Figures 5.9d and 5.10d.

The memory of the source size is reflected by the apparent dispersion coefficient. By definition, $\overline{D}^a(t)$ quantifies for preasymptotic times, purely advective spreading of the solute due to the velocity contrast within the initial source. The apparent dispersion for the extended sources of $10l$ and $100l$ are shown in Figure 5.11, we also included for comparison porpoises the global apparent dispersion coefficient for a line source that extends over the whole medium cross section. With increasing vertical extension of the initial

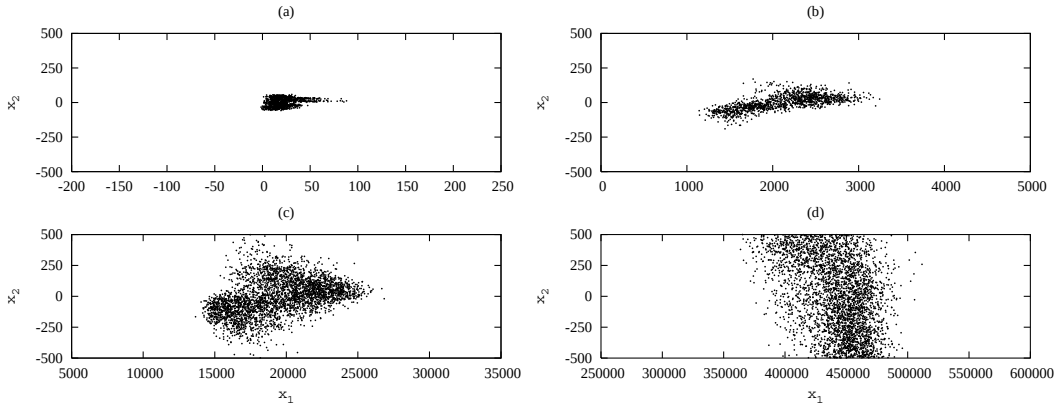

Figure 5.10: Distribution of solute particles evolving from a line source of $100l$ in a single realization of a vertically stratified random medium with a halfwidth $a = 500$, constant strata thickness $l = 1$, local dispersion $D_L = D_T = 1$, after (a) $t = 10^{-4}\tau_D$, (b) $t = 10^{-2}\tau_D$, (c) $t = 10^{-1}\tau_D$, and (d) $t = \tau_D$.

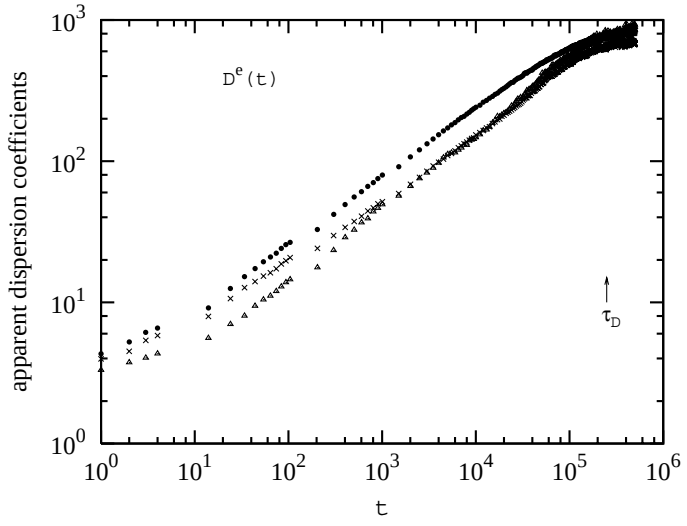

Figure 5.11: Numerical results of the global apparent dispersion coefficients for extended sources of $10\,l$ in triangles, $100\,l$ in small crossed lines, and $1000l$ in filled dots.

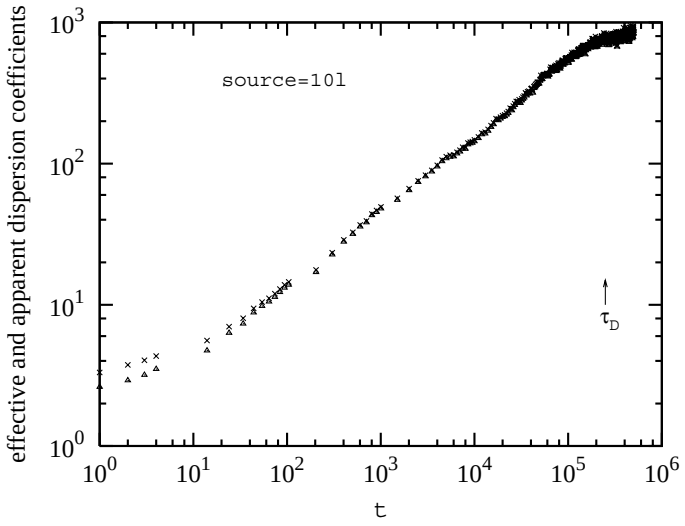

Figure 5.12: Numerical results of the global effective and apparent dispersion coefficients for an extended source of $10\,l$.

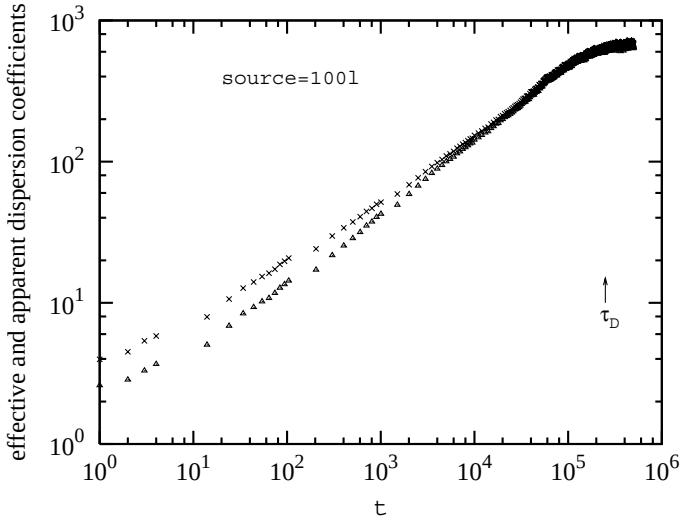

Figure 5.13: Numerical results of the global effective and apparent dispersion coefficients for an extended source of $100\,l$.

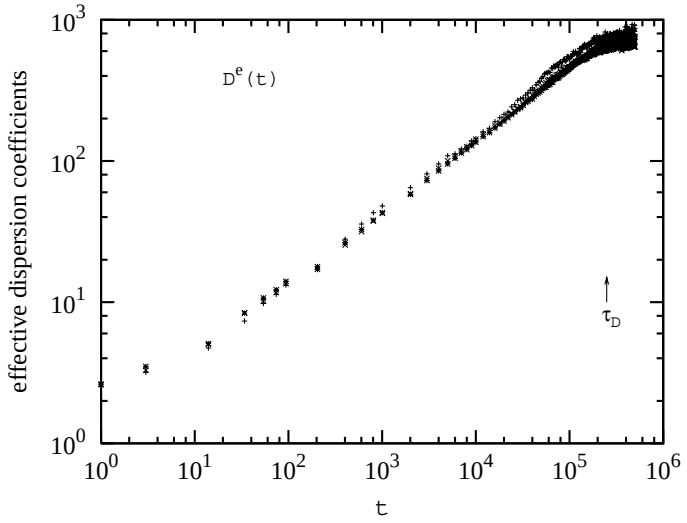

Figure 5.14: Numerical results of the global effective dispersion coefficients for three extended sources of $10\,l$, $100\,l$, and a line source that extends over the whole medium cross-section of $1000\,l$.

source, $\overline{D}^a(t)$ evolves faster to the common asymptotic long time value. As observed in one given realization, the memory of the initial source size is lost for times smaller than the dispersion time scale, here $t \approx 10^{-2}\tau_D$, and the apparent dispersion coefficients of the small extended sources are identical.

Note that as shown in Figures 5.12 and 5.13, when the memory of the initial source size is wiped out, the apparent and the global effective dispersion coefficients show the same temporal behavior.

As shown in Figures 5.14 and 5.15 the global effective and the ensemble dispersion coefficients are not impacted in a sensible manner by the source size. For the three initial sources under consideration, $D^{\mathrm{ens}}(t)$ and $\overline{D}^{\mathrm{e}}(t)$ show a similar behavior which is controlled at long times by the dispersion time scale τ_D.

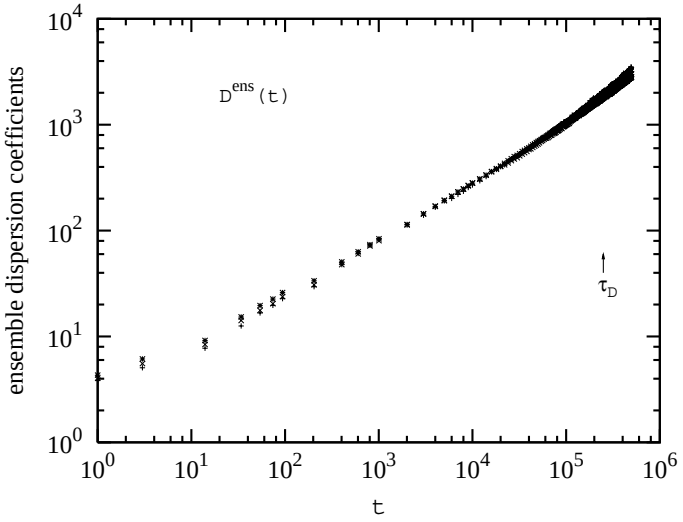

Figure 5.15: Numerical results of the ensemble dispersion coefficients for three extended sources of $10\,l$, $100\,l$, and a line source that extends over the whole medium cross-section of $1000\,l$.

Memory of the initial position

As solute particles evolving from a point source, small extended sources are also impacted by its position within the medium boundaries. Here we investigate the initial position memory effects for two extended sources of $10l$ and $100l$. Figures 5.16 and 5.17 illustrate the temporal behavior of solute distributions starting from the extended sources of $10l$ and $100l$ with its upper part situated at $y' = 0.9a$. As the temporal behavior observed for initial point sources, here, for small extended sources starting in the vicinity of the medium boundaries the solute particles experience the permeability variations by transverse local dispersion in a non symmetrical way, hence, the solute particles evolution towards the uniform occupation of the medium cross section is slower than when starting at $y' = 0$. This behavior is again reflected in the temporal evolution of the effective dispersion coefficient and

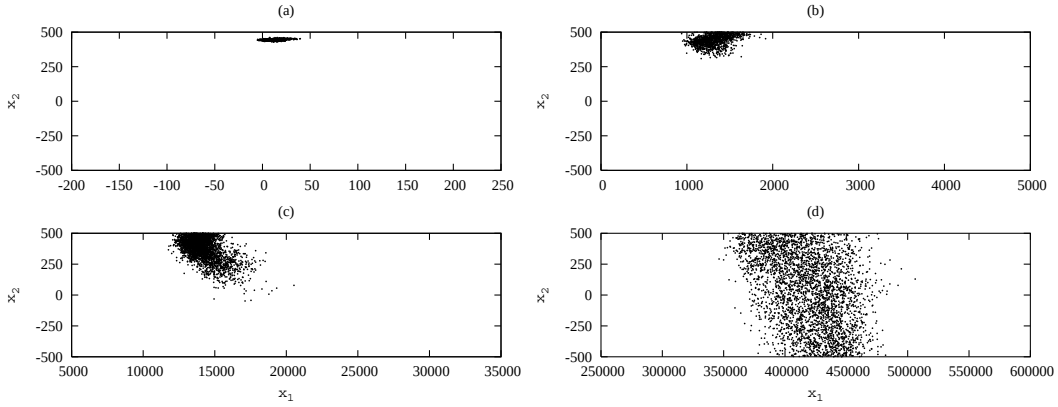

Figure 5.16: Distribution of solute particles evolving from a line source of $10l$ in a single realization of a vertically stratified random medium with a halfwidth $a = 500$, constant strata thickness $l = 1$, local dispersion $D_L = D_T = 1$, after (a) $t = 10^{-4}\tau_D$, (b) $t = 10^{-2}\tau_D$, (c) $t = 10^{-1}\tau_D$, and (d) $t = \tau_D$.

is very similar to the behavior observed for a point-like injection in section 5.4.2.

5.5 Summary

We studied here effective solute spreading and mixing in confined stratified random media as an idealized model for layered geological media. For point-like initial distributions, the second centered moment of the concentration distribution (identical to the transport Green function), quantifies the interaction of vertical conductivity variations and local dispersion on the effective spreading and mixing properties of a solute. For an extended source this is different. For times smaller than the dispersion time for complete vertical solute mixing $\tau_D = a^2/D_T$, the width of the solute distribution reflects

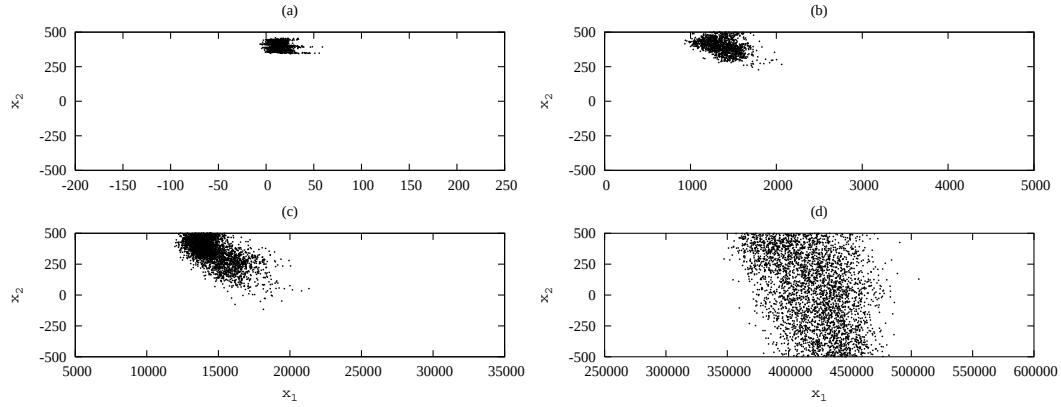

Figure 5.17: Distribution of solute particles evolving from a line source of $10l$ in a single realization of a vertically stratified random medium with a halfwidth $a = 500$, constant strata thickness $l = 1$, local dispersion $D_L = D_T = 1$, after (a) $t = 10^{-4}\tau_D$, (b) $t = 10^{-2}\tau_D$, (c) $t = 10^{-1}\tau_D$, and (d) $t = \tau_D$.

purely advective spreading effects due to velocity fluctuations within the initial plume.

The two dimensional model medium under consideration consists of strata of the constant thickness l. Within each stratum the conductivity is constant, but varies randomly from stratum to stratum. Thus, for a vertical extent that is much larger than l, the correlation of the conductivity fluctuations can be approximated by a delta-distribution. The conductivity distribution is arbitrary but with a positive support. Here it is chosen to be log-normal. The transport problem is solved numerically using random walk simulations and analytically using axial moment equations. We derive explicit analytical expressions for the effective, apparent and ensemble dispersion coefficients.

The preasymptotic mixing and spreading behavior is studied for transport in the two-dimensional model medium for point-like initial distributions as

well as for a line source that extends over the whole medium cross-section.

The early time regime is defined by the microscopic dispersion scale $\tau_D^m = l^2/D_T$, which measures the time for vertical solute spreading over one stratum by local dispersion. Thus, for a point-like injection, heterogeneity is activated as a macroscopic spreading mechanisms for $t > \tau_D^m$. The asymptotic long time regime, in which solute transport homogenizes vertically, is given by the dispersion scale τ_D. In the intermediate regime $\tau_D^m \ll t \ll \tau_D$, the interaction of spreading due to vertical velocity contrast and transverse local dispersion leads to effective macroscale mixing as quantified by the Taylor dispersion coefficient. At preasymptotic times, spreading and mixing behavior is superdiffusive; the effective dispersion coefficients increase with the square root of time, like for an infinitely extended stratified random medium. Then as soon as the solute is completely mixed over the vertical it crosses over to its constant asymptotic value.

The evolution of the effective dispersion coefficient depends on the initial position. As the medium is confined by impermeable horizontal boundaries (in the random walk picture the impermeable boundaries are modeled as reflecting walls), the vertical position of the initial injection affects the temporal behavior of the effective dispersion coefficients. For point and small sources located in the vicinity of the medium boundaries, at early times, the time needed for the solute to sample the entire medium cross section is longer than for a solute that originates from an initial plume in the center of the medium. Thus, the effective dispersion coefficient evolves slower for y' close to the boundaries than for y' located in the vicinity of the medium axis. On the other hand, as the concentration distribution remains longer near the boundaries, we have a bigger contrast between the center of mass velocities in different realizations and the ensemble mean center of mass velocity, which

causes a faster increase of the ensemble dispersion coefficient. Due to the finite vertical extent of the medium, sample to sample fluctuations of the center of mass velocity persist and lead to a linear increase of the ensemble dispersion coefficient for $t > \tau_D$.

We also observed memory of the initial source size. This memory is reflected by the apparent dispersion coefficient which by definition quantifies for preasymptotic times, purely advective spreading of the solute due to the velocity contrast within the initial source. When increasing time, this size memory is wiped out even for times smaller than the dispersion time scale, and the apparent dispersion coefficient converges to the local effective dispersion coefficient obtained for a point-like injection, independently of the initial source size. Only for an extended source which extends over the all medium cross section, the apparent and the global effective dispersion coefficient converge to the same asymptotic Taylor dispersion for times of the order of the dispersion time scale.

In the limit of infinite vertical extent (and thus also infinitely extended source distribution), the apparent and ensemble dispersion coefficients converge; the vertical (spatial) average and the ensemble average are equivalent in this limit.

The dependence of the spreading and mixing behavior on the initial plume position and size clearly demonstrates that the effective transport dynamics at pre-asymptotic times, i.e., $t < \tau_D$, have memory and are impacted by the transport history. As soon as the solute samples the velocity contrast across the entire medium cross section for $t > \tau_D$, the memory of the initial position vanishes, the solute distribution homogenizes and the effective and ensemble dispersion coefficients are independent of the initial position. This is clearly demonstrated for transport in a single medium realization as well as in aver-

age for the confined medium. In the limit of an infinite stratified medium, the memory of the initial position is wiped out by the ensemble average, which leads to vertical homogenization and makes the average medium isotropic. This symmetry is broken for the confined medium so that even in average, the memory of the initial position is preserved in the behavior of the effective and ensemble dispersion coefficients.

For single realizations, the center of mass velocity varies with time, while in average it is constant and identical to the mean flow velocity. Thus, the ensemble average wipes out memory effects of the center of mass velocity even for confined media.

For an initial plume that is spread over the whole medium cross-section, the global effective dispersion coefficient quantifies the average spreading and mixing behavior. It evolves slower than the apparent dispersion coefficient, which, at early times, reflects purely advective spreading due to local center of mass fluctuations within the extended initial distribution. At asymptotic times both coefficients converge to the Taylor dispersion-type coefficient.

In the limit of an infinite medium, the memory of the initial position is wiped out by the ensemble average, which leads to vertical homogenization and makes the average medium isotropic. This symmetry is broken for the confined medium so that even in average, the memory of the initial position is preserved in the behavior of the effective and ensemble dispersion coefficients.

Chapter 6

Summary and Conclusions

The general aim of this thesis was the systematic investigation of mixing and spreading in heterogeneous media in terms of adequately defined effective dispersion coefficients. We were specially interested in the identification of the principal mixing and spreading mechanisms as well as the characteristic spatial and temporal scales which lead not only an increase of mixing and spreading increase, but also to the transition from the non-Fickian to the Fickian transport behavior regime.

Following the method suggested by Dentz and Carrera [29] to characterize mixing and spreading for a single medium, in the first part of the thesis we proposed a generalization of these measures for transport in heterogeneous media within a stochastic modeling approach.

For a point-like injection in a single medium realization the local effective dispersion coefficient is defined as the second centered moment of the concentration distribution. This effective coefficient quantifies the interaction of the medium (spatial, chemical) heterogeneities, temporal flow fluctuations and local dispersion. For extended initial conditions solute spreading and mixing is quantified in terms of local distributions which originate from the

point-sources that constitute the extended source. We thus define global effective dispersion coefficient as the weighted average over the local effective dispersion coefficients. This observable characterize spreading and mixing for the solute distributions that evolve from the point sources that form the extended initial plume. It thus represents a global measure for the heterogeneity impact on mixing and spreading. Furthermore, we define the apparent dispersion coefficient as the half rate of change of the width of a distribution evolving from an extended initial plume. For early times, it reflects the purely advective spreading effects due to velocity variations in the extended initial distribution.

For a randomly heterogeneous medium, the impact of spatially/chemically heterogeneities as well as temporal flow fluctuations on effective transport is quantified within a stochastic modeling framework. Effective and apparent dispersion coefficients are defined as ensemble averages of their single realization counterparts. In addition, we define a local ensemble dispersion coefficient, which is derived from the averaged transport Green function. The global ensemble dispersion coefficient then is given by the average of the local counterpart over the initial distribution. While the apparent dispersion coefficient quantifies center of mass fluctuations within the initial plume for a given realization, the ensemble dispersion coefficient quantifies the artificial spreading effect of center of mass fluctuations from realization to realization of the heterogeneous random medium.

The defined local effective dispersion coefficient was used to characterize mixing and spreading in a chemically heterogeneous medium subjected to temporal flow fluctuations. Within a stochastic modeling approach we derived analytical solutions for the longitudinal and transverse effective dispersion coefficients. The interaction of transverse temporal flow fluctuations,

chemical heterogeneities and local dispersion was identified as the mixing mechanism that leads to a transverse dispersion coefficient enhancement. We observed a self-organization of the system given by the simultaneous transverse dispersion coefficient increase and the longitudinal effective dispersion coefficient decrease. The transition from the non-Fickian to Fickian behavior is determined by the dispersion time scale which characterize the time for dispersive transport over one correlation length, here assumed to be short. For times larger than the dispersion time scale, the effective dispersion coefficients can be modeled by a constant macroscopic value, since Fickian transport model can be assumed.

Fickian transport model cannot be assumed for infinite stratified media models in the absence of a constant velocity component transverse to the stratification. We have proved that even when considering transverse temporal flow fluctuations or spatially flow variations, the superdiffusive behavior of the effective and ensemble dispersion coefficients remains at large times. This is because the full heterogeneity spectrum in the transverse direction is never sampled, since the dispersion time scale which determines the transition to a Fickian asymptotic behavior becomes infinite and the transverse mixing condition is never fulfilled.

In contrast, when considering a bounded stratified medium, a finite dispersion time scale controls the process of the solute sampling the whole vertical velocity distribution. Then for times large compared to the dispersion time scale, the Taylor dispersion coefficient quantifies both large scale mixing and spreading. However, here the dispersion time scale characterize the time for transverse dispersive transport over all the vertical extent of the flow domain. Hence, in hydrological applications this dispersion time scale can be large and must be taken into account that the asymptotic macrodispersion

coefficient does not provide a measure of mixing and spreading.

The correct definition of the ensemble average of the dispersion coefficients allow us identifying and understanding the main mixing and spreading mechanisms as well as the characteristic times that control transport in heterogeneous media. This is important not only for the dynamics approaches, but also for reactive transport modeling, risk assessment studies and remediation strategy design.

The derived analytical solutions can be used to improve the efficiency of numerical transport simulations and to correctly take into account the temporal behavior of the effective dispersion coefficients.

As the aim of the effective dispersion coefficients derived here is to characterize transport behavior in a "real" medium, we are also interested in solute transport in individual realizations. We study the agreement between the effective parameters and the ones observed for one typical realization as a test of the applicability of our effective results.

As the effective dispersion coefficients proposed here were constructed as stochastic averages, they are subject to uncertainties, i.e., there are fluctuations about these average. These uncertainties must be studied due to its importance to geohydrological purposes and risk assessment exercises. Furthermore, the self-averaging of the effective dispersion coefficients must be investigated in order to verify if the effective parameters derived would be able to correctly represent a typical medium realization.

Appendix A

Chemically Heterogeneous Media under Temporally Fluctuating Flow. Integral expressions

Here we present the explicit integral expressions for the contributions to the effective transport velocity and the effective dispersion coefficients due to the interaction between temporal fluctuations of the flow conditions and chemical heterogeneity.

We derive approximate expressions for small inverse Peclet numbers. In order to keep the derivations as transparent as possible, the derived expressions are approximated successively, which means that, in the course of the derivations, we successively disregard subleading terms until we arrive at the consistent final result that represents the leading behavior in the limit of small inverse Peclet numbers.

Inserting expansion (2.54) for $\widetilde{c}(\mathbf{k},t)$ into $\overline{\ln[\widetilde{c}(\mathbf{k},t)]}$ and expanding the

resulting expression up to first order in $\sigma^2_{\mu\mu}$, we obtain

$$\overline{\ln[\widetilde{c}(\mathbf{k},t)]} = \widetilde{c}_0(\mathbf{k},t) + \sigma^2_{\mu\mu}\left[I_1(\mathbf{k},t) + I_2(\mathbf{k},t)\right] \tag{A.1}$$

and thus for the effective center of mass velocity (3.3) and the effective dispersion coefficients (3.4),

$$\overline{v}^{\mathrm{e}}_i(t) = u\delta_{i1} - \sigma^2_{\mu\mu}\frac{\mathrm{d}}{\mathrm{dt}}\mathrm{i}\frac{\partial}{\partial k_i}\left[\langle I_1(\mathbf{k},t)\rangle - \frac{1}{2}\langle I_2(\mathbf{k},t)\rangle\right]_{\mathbf{k}=\mathbf{0}} \tag{A.2}$$

$$\overline{D}^{\mathrm{e}}_{ij}(t) = D_{ij} - \sigma^2_{\mu\mu}\frac{1}{2}\frac{\mathrm{d}}{\mathrm{dt}}\frac{\partial^2}{\partial k_i \partial k_j}\left[\langle I_1(\mathbf{k},t)\rangle - \frac{1}{2}\langle I_2(\mathbf{k},t)\rangle\right]_{\mathbf{k}=\mathbf{0}} \tag{A.3}$$

The auxiliary functions $I_1(\mathbf{k},t)$ and $I_2(\mathbf{k},t)$ are defined by

$$I_1(\mathbf{k},t) = \frac{1}{\widetilde{c}_0(\mathbf{k},t,0)}\int_{k'}\int_{-\infty}^{\infty} dt' \int_{-\infty}^{\infty} dt'' C^{\mu\mu}(\mathbf{k}')\widetilde{c}_0(\mathbf{k},t,t') \frac{\partial}{\partial t'}\widetilde{c}_0(\mathbf{k}-\mathbf{k}',t',t'')\frac{\partial}{\partial t''}\widetilde{c}_0(\mathbf{k},t'',0) \tag{A.4}$$

$$I_2(\mathbf{k},t) = \frac{1}{\widetilde{c}_0(\mathbf{k},t,0)^2}\int_{k'}\int_{-\infty}^{\infty} dt' \int_{-\infty}^{\infty} dt'' C^{\mu\mu}(\mathbf{k}')\widetilde{c}_0(\mathbf{k},t,t') \frac{\partial}{\partial t'}\widetilde{c}_0(\mathbf{k}-\mathbf{k}',t',0)\widetilde{c}_0(\mathbf{k},t,t'')\frac{\partial}{\partial t''}\widetilde{c}_0(\mathbf{k}+\mathbf{k}',t'',0) \tag{A.5}$$

respectively. By partially integrating with respect to t' and t'', the internal time derivatives are shifted to the propagators that contain only external wave vectors $\mathbf{k}$. Evaluating the resulting time derivatives, we obtain for $I_1(\mathbf{k},t)$ and $I_2(\mathbf{k},t)$

$$I_1(\mathbf{k},t) = I_{11}(\mathbf{k},t) + I_{12}(\mathbf{k},t) + I_{13}(\mathbf{k},t) + \ldots$$

$$I_2(\mathbf{k},t) = I_{21}(\mathbf{k},t) + 2I_{22}(\mathbf{k},t) + \ldots \tag{A.6}$$

where the dots denote contributions which are small for small inverse Peclet numbers and contributions that are independent of $\mathbf{k}$. The auxiliary func-

tions contributing to $I_1(\mathbf{k},t)$ are defined by,

$$I_{11}(\mathbf{k},t) = -\int_{k'}\int_0^t \mathrm{d}t' \int_0^{t'} \mathrm{d}t'' \mathbf{k}\cdot\mathbf{u}(t')\mathbf{k}\cdot\mathbf{u}(t'')B_1(\mathbf{k}',t',t'') \quad (A.7)$$

$$I_{12}(\mathbf{k},t) = \int_{k'}\int_0^t \mathrm{d}t' \mathrm{i}\mathbf{k}\cdot\mathbf{u}(t')B_1(\mathbf{k}',t',0) \quad (A.8)$$

$$I_{13}(\mathbf{k},t) = \int_{k'}\int_0^t \mathrm{d}t' \mathrm{i}\mathbf{k}\cdot\mathbf{u}(t')B_1(\mathbf{k}',t,t'), \quad (A.9)$$

where we defined

$$B_1(\mathbf{k}',t_1,t_2) = \widetilde{C}^{\mu\mu}(\mathbf{k}')\widetilde{g}_0(-\mathbf{k}',t_1-t_2)[h(\mathbf{k}',t_1,t_2)+1] \quad (A.10)$$

with

$$h(\mathbf{k}',t_1,t_2) = \exp\Big[-\mathrm{i}u\mathbf{k}'\int_{t_2}^{t_1}\mathrm{d}y\boldsymbol{v}(y)\Big]-1. \quad (A.11)$$

The auxiliary functions contributing to $I_2(\mathbf{k},t)$ are given by,

$$I_{21}(\mathbf{k},t) = -\int_{k'}\int_0^t \mathrm{d}t' \int_0^{t} \mathrm{d}t'' \mathbf{k}\cdot\mathbf{u}(t')\mathbf{k}\cdot\mathbf{u}(t'')B_2(\mathbf{k}',t',t'') \quad (A.12)$$

$$I_{22}(\mathbf{k},t) = \int_{k'}\int_0^t \mathrm{d}t' \mathrm{i}\mathbf{k}\cdot\mathbf{u}(t')B_2(\mathbf{k}',t,t'), \quad (A.13)$$

where we defined

$$B_2(\mathbf{k}',t_1,t_2) = \widetilde{C}^{\mu\mu}(\mathbf{k}')\widetilde{g}_0(-\mathbf{k}',t_1)\widetilde{g}_0(\mathbf{k}',t_2)[h(\mathbf{k}',t_1,t_2)+1] \quad (A.14)$$

Note that the contributions $I_{11}(\mathbf{k},t)$ and $I_{21}(\mathbf{k},t)$ are of second order in $\mathbf{k}$ and contribute only to the effective dispersion coefficients, while $I_{12}(\mathbf{k},t)$ and $I_{22}(\mathbf{k},t)$ are linear in $\mathbf{k}$ and thus contribute only to the effective center of mass velocity.

The determination of the effective center of mass velocity and dispersion coefficients involves the following averages,

$$\langle h(t_1,t_2)\rangle = \sigma_{\nu\nu}^2 A(\mathbf{k}',t_1-t_2)+\ldots \tag{A.15}$$

$$\langle \nu_l(t_3)h(t_1,t_2)\rangle = \sigma_{\nu\nu}^2 A_l(\mathbf{k}',t_1-t_2,t_3-t_2)+\ldots \tag{A.16}$$

$$\langle \nu_l(t_3)\nu_m(t_4)h(t_1,t_2)\rangle = \sigma_{\nu\nu}^2 C_{lm}^{\nu\nu}(t_3-t_4)+\ldots, \tag{A.17}$$

where the dots denote contributions of the order of $\sigma_{\nu\nu}^4$. We defined the auxiliary functions

$$A(\mathbf{k}',t) = -\frac{u^2}{2}\int_0^t \mathrm{d}y \int_0^t \mathrm{d}y' k_l' C_{lm}^{\nu\nu}(y-y')k_m' \tag{A.18}$$

$$A_l(\mathbf{k}',t_1,t_2) = -\mathrm{i}u\int_0^{t_1} \mathrm{d}y C_{lm}^{\nu\nu}(t_2-y)k_m' \tag{A.19}$$

Note that the average over $h(t_1,t_2)$ can be performed exactly for a Gaussian distributed $\boldsymbol{\nu}(t)$, see Appendix B. This yields,

$$\langle h(t_1,t_2)\rangle = \exp\Big[-\sigma_{\nu\nu}^2\frac{u^2}{2}\int_{t_2}^{t_1}\mathrm{d}y\int_{t_2}^{t_1}\mathrm{d}y' k_l' C_{lm}^{\nu\nu}(y-y')k_m'\Big]-1. \tag{A.20}$$

Note that (A.20) is always positive, while the first order approximation of this expression can be negative.

Inserting (A.8), (A.9) and (A.13) into (A.2), expansion up to second order in the temporal fluctuations and subsequent average over the temporal random fields, we obtain for the effective center of mass velocity,

$$\overline{\nu}_i^{\mathrm{e}}(t) = u\delta_{i1} + \delta^{\mu\mu}\overline{\nu}_i^{\mathrm{e}}(t) + \delta^{\mu\nu}\overline{\nu}_i^{\mathrm{e}}(t) \tag{A.21}$$

with the contributions,

$$\delta^{\mu\mu}\overline{\nu}_i^{\mathrm{e}}(t) = u\delta_{i1}\sigma_{\mu\mu}^2 \int_{k'} \widetilde{C}^{\mu\mu}(\mathbf{k}')\widetilde{g}_0(-\mathbf{k}',t) + \ldots \tag{A.22}$$

$$\begin{aligned}\delta^{\mu\nu}\overline{\nu}_i^{\mathrm{e}}(t) &= u\sigma_{\mu\mu}^2\sigma_{\nu\nu}^2 \int_{k'} \widetilde{C}^{\mu\mu}(\mathbf{k}')\left[\delta_{i1}A(\mathbf{k}',t)\right. \\ &\qquad \left. + A_i(\mathbf{k}',t,0)\right]\widetilde{g}_0(-\mathbf{k}',t) + \ldots,\end{aligned} \tag{A.23}$$

where again the dots denote contributions that are small for small inverse Peclet numbers.

Correspondingly, we obtain for the effective dispersion coefficients by inserting (A.7) and (A.12) into (A.3),

$$\overline{D}_{ij}^{\mathrm{e}}(t) = D_{ij} + \delta^{\mu\mu}\overline{D}_{ij}^{\mathrm{e}}(t) + \delta^{\mu\nu}\overline{D}_{ij}^{\mathrm{e}}(t), \tag{A.24}$$

where we defined,

$$\delta^{\mu\mu}\overline{D}_{ij}^{\mathrm{e}}(t) = u^2\sigma_{\mu\mu}^2\delta_{i1}\delta_{j1} \int_{k'} \int_0^t \mathrm{d}t' \widetilde{C}^{\mu\mu}(\mathbf{k}')\widetilde{g}_0(-\mathbf{k}',t')\left[1 - \widetilde{g}_0(\mathbf{k}',t)\right] \tag{A.25}$$

$$\begin{aligned}\delta^{\mu\nu}\overline{D}_{ij}^{\mathrm{e}}(t) &= u^2\sigma_{\mu\mu}^2\sigma_{\nu\nu}^2 \int_{k'} \int_0^t \mathrm{d}t' \widetilde{C}^{\mu\mu}(\mathbf{k}')\left[\delta_{i1}\delta_{j1}A(\mathbf{k}',t')\right. \\ &\quad \left. + \delta_{j1}A_i(\mathbf{k}',t',0) + \delta_{i1}A_j(\mathbf{k}',t',0) + C_{ij}^{\nu\nu}(t')\right] \\ &\quad \times \left[\widetilde{g}_0(-\mathbf{k}',t') - \widetilde{g}_0(-\mathbf{k}',t)\widetilde{g}_0(\mathbf{k}',t-t')\right]\end{aligned} \tag{A.26}$$

We obtain the leading behavior of $\delta^{\mu\nu}\overline{\nu}_i^{\mathrm{e}}(t)$ and $\delta^{\mu\nu}\overline{D}_{ij}^{\mathrm{e}}(t)$ for small inverse Peclet numbers, (3.10) and (3.11) by inserting the expansions

$$\begin{aligned}\widetilde{g}_0(-\mathbf{k}',t') &= \exp\left(-{k_j'}^2 l_j^2 \epsilon_j t'/\tau_u - \mathrm{i}k_1' l_1 t'/\tau_u\right) \\ &= \exp\left(-\mathrm{i}k_1' l_1 t'/\tau_u\right) + \ldots\end{aligned} \tag{A.27}$$

and

$$\begin{aligned}\widetilde{g}_0(-\mathbf{k}',t)\widetilde{g}_0(\mathbf{k}',t-t') &= \exp\left(-2{k_j'}^2 l_j^2 t/\tau_{D_j}\right)\widetilde{g}_0(\mathbf{k}',-t') \\ &= \exp\left(-2{k_j'}^2 l_j^2 t/\tau_{D_j} - \mathrm{i}k_1' l_1 t'/\tau_u\right) + \ldots\end{aligned} \tag{A.28}$$

into (A.23) and (A.26). The dots denote subleading contributions of the order of the inverse Peclet numbers.

Appendix B

Average Over a Gaussian Random Field

The time fluctuations $v(t)$ have a multivariate Gaussian distribution defined in discrete form as follows,

$$P\Big\{v(t)\Big\} = \lim_{N\to\infty}(2\pi)^{-N/2}(det\mathbf{C})^{-1/2} \times \exp\Big(-\frac{1}{2}\sum_{i=0}^{N}\sum_{j=0}^{N}v_i(t))C_{ij}^{-1}v_j(t)\Big) \tag{B.1}$$

where $N = t/\Delta t$. The correlation matrix $\mathbf{C}$ is defined by the correlation coefficients C_{ij}. The coefficients of the inverse correlation matrix are denoted by C_{ij}^{-1}.

The characteristic function of the random flow field is defined as,

$$\Big\langle f\Big\{v(t)\Big\}\Big\rangle = \int_{-\infty}^{\infty} D\Big\{v(t)\Big\}f\Big\{v(t)\Big\}P\Big\{v(t)\Big\} \tag{B.2}$$

where, $D\Big\{u'(t)\Big\} = \lim_{N\to\infty}\mathrm{d}\,v_i(t)...\mathrm{d}\,v_N(t)$.

The corresponding characteristic function then reads,

$$\begin{aligned}\Big\langle f\Big\{\Big\}\Big\rangle \;=\; & \lim_{N\to\infty}(2\pi)^{-N/2}(det\mathbf{C})^{-1/2}\int_{-\infty}^{\infty}\mathrm{d}v_i(t)\ldots\int_{-\infty}^{\infty}\mathrm{d}v_N(t)\\ & \times\exp\Big(-\frac{1}{2}\sum_{i=N'}^{N}\sum_{j=N'}^{N}v_i(t)C_{ij}^{-1}v_j(t)\Big)\\ & \exp\Big(-\mathrm{i}\mathbf{k}\sum_{i=N'}^{N}\Delta t v_i(t')\Big)\\ & \exp\Big(-\frac{1}{2}\sum_{i=0}^{N'}\sum_{j=0}^{N'}v_i(t)C_{ij}^{-1}v_j(t)\Big)\end{aligned}\tag{B.3}$$

where,

$$\exp\Big(-\frac{1}{2}\sum_{i=0}^{N'}\sum_{j=0}^{N'}u_i'(t)C_{ij}^{-1}u_j'(t)\Big)=1\tag{B.4}$$

Finally, based on properties of the correlation matrix, i.e., symmetric and positive definite, the average over the multivariate Gaussian distribution becomes,

$$\Big\langle f\Big\{v(t)\Big\}\Big\rangle=\exp\Big(-\frac{1}{2}\mathbf{k}^2\sum_{i=N'}^{N}\sum_{j=N'}^{N}C_{ij}\Big)\tag{B.5}$$

Expressed in continuous form:

$$\Big\langle f\Big\{v(t)\Big\}\Big\rangle=\exp\Big(-\frac{1}{2}\mathbf{k}^2\int_{t'}^{t}\mathrm{d}t''\int_{t'}^{t}dt'''C_{ij}(t''-t''')\Big)\tag{B.6}$$

Appendix C

First and Second Moments in the Transverse Direction to the Stratification

The first and second moments in the transverse direction to the stratification of the concentration distribution of solute transported through a perfectly stratified media are derived here.

By applying (2.30) to the transport equation in (2.25) we obtain for the first moment,

$$\frac{\partial m_T^{(1)}(t)}{\partial t} + uv_T(t) + \int_{-\infty}^{\infty} \mathrm{d}x \int_{-\infty}^{\infty} \mathrm{d}\mathbf{y}\,[u'(\mathbf{y}) + u'(\mathbf{y},t)]\,\frac{\partial c(\mathbf{x},t)}{\partial x} = 0, \qquad \text{(C.1)}$$

after executing the integral over x the third term in (C.1) is zero because we assume vanishing concentration at infinity as a boundary condition, thus we can write,

$$m_T^{(1)}(t) = -u \int_0^t \mathrm{d}t' \boldsymbol{v}_T(t'). \tag{C.2}$$

Following the same procedure for the second moment (2.31) we obtain,

$$m_T^{(2)}(t) = 2D_T t + 2u^2 \int_0^t \mathrm{d}t' \int_0^{t'} \mathrm{d}t'' \boldsymbol{v}_T(t') \boldsymbol{v}_T(t''). \tag{C.3}$$

For the center of mass velocity in the transverse direction we obtain after inserting (C.2) in (2.39) and taking the ensemble average over all realizations of the stratified media and over the temporal random process,

$$\overline{\nu}_T = 0. \tag{C.4}$$

The effective and ensemble dispersion coefficients in the transverse direction are derived after inserting (C.2) and (C.3) into (2.40) and (2.43).

$$\overline{D}_T^{\mathrm{e}}(t) = D_T, \tag{C.5}$$

$$D_T^{\mathrm{ens}}(t) = D_T. \tag{C.6}$$

Appendix D

Confined Stratified Media. Correlation Function

We determine the conductivity correlation function for the confined stratified medium by taking the ensemble average $\overline{k(y)k(y')}$, where $k(y)$ is given by representation (5.13). As k_n and $k_{n'}$ are independent for $n \neq n'$ and have mean zero and variance σ^2, we obtain,

$$\begin{aligned}\overline{k(y)k(y')} &= \frac{\sigma^2}{2l}\int_{-l}^{l} \mathrm{d}b \sum_{n=-a/l}^{a/l} \Theta\left[y - nl + b\right]\left\{1 - \Theta\left[y + b - (n+1)l\right]\right\} \\ &\quad \times \Theta\left[y' - nl + b\right]\left\{1 - \Theta\left[y' + b - (n+1)l\right]\right\} \qquad \text{(D.1)}\end{aligned}$$

Setting $y = y' + \Delta y$, and defining $y' = nl + \delta$, where $0 \leq \delta < l$. Thus, we obtain,

$$\begin{aligned}\overline{k(y)k(y')} &= \frac{\sigma^2}{2l}\int_{-l}^{l} \mathrm{d}b \Theta\left[\Delta y + \delta + b\right]\left\{1 - \Theta\left[\Delta y + b - l\right]\right\} \\ &\quad \times \Theta\left[\delta + b\right]\left\{1 - \Theta\left[\delta + b - l\right]\right\}. \qquad \text{(D.2)}\end{aligned}$$

Executing the remaining integrations, we obtain expression (5.14). The translation invariance indicated in (D.2) holds across the whole medium ex-

cept in $0 < a - |y'| < l/2$.

Appendix E

Confined Stratified Media. Limiting case. Average Dispersion Coefficients for the Infinite Stratified Media

Here we detail the development of the expressions for the local and global dispersion coefficients for the hypothetical case of an infinite stratified medium. Expressions (5.35) and (5.36) can be rewritten as,

$$D^{\text{ens}}(t|y') = D_L + \frac{1}{2}\Delta\kappa\sigma^2 lt + \frac{2}{D_T\pi^2}\sigma^2 l\sum_{n=1}^{\infty}\frac{\Delta\kappa}{(n\Delta\kappa)^2}\times$$
$$\left[1-\exp\left(-\frac{D_T\pi^2(n\Delta\kappa)^2}{4}t\right)\right] + \frac{2}{3D_T\pi^2}\sigma^2 l\sum_{n=1}^{\infty}(-1)^n\frac{\Delta\kappa}{(n\Delta\kappa)^2}\times$$
$$\left[\exp\left(-\frac{D_T\pi^2(n\Delta\kappa)^2}{4}t\right)-\exp\left(-D_T\pi^2(n\Delta\kappa)^2 t\right)\right]\cos\left(\pi y' n\Delta\kappa\right) \quad \text{(E.1)}$$

and

$$\begin{aligned}\overline{D}^{e}(t|y') &= D^{\mathrm{ens}}(t|y') - \frac{2}{D_T\pi^2}\sigma^2 l \sum_{n=1}^{\infty} \frac{\Delta\kappa}{(n\Delta\kappa)^2} \times \\ &\left[\exp\left(-\frac{D_T\pi^2(n\Delta\kappa)^2}{4}t\right) - \exp\left(-\frac{D_T\pi^2(n\Delta\kappa)^2}{2}t\right)\right] \\ &-\frac{2}{D_T\pi^2}\sigma^2 l \sum_{n=1}^{\infty}(-1)^n \frac{\Delta\kappa}{(n\Delta\kappa)^2}\left[\exp\left(-\frac{D_T\pi^2(n\Delta\kappa)^2}{4}t\right)\right. \\ &\left.-\exp\left(-\frac{D_T\pi^2(n\Delta\kappa)^2}{2}t\right)\right]\cos(\pi y' n\Delta\kappa), \qquad \text{(E.2)}\end{aligned}$$

where we set $\tau_D = a^2/D_t$ and defined $\Delta\kappa \equiv 1/a$. For $a \to \infty$, i.e., $\Delta\kappa \to 0$ we take the continuum limit. We define $n\Delta\kappa \equiv \kappa$ and substitute the summations in (E.1) and (E.2) by integrations over κ. This yields,

$$D^{\mathrm{ens}}(t|y') \equiv D^{\mathrm{ens}}(t) = D_L + \frac{2\sigma^2 l}{D_T\pi}\int_0^{\infty}\frac{\mathrm{d}\kappa}{\kappa^2}\left[1-\exp\left(-\frac{D_T\kappa^2}{4}t\right)\right] \qquad \text{(E.3)}$$

$$\begin{aligned}\overline{D}^{e}(t|y') &\equiv \overline{D}^{e}(t) = D^{\mathrm{ens}}(t) - \\ &\frac{2\sigma^2 l}{D_T\pi}\int_0^{\infty}\frac{\mathrm{d}\kappa}{\kappa^2}\left[\exp\left(-\frac{D_T\kappa^2}{4}t\right) - \exp\left(-\frac{D_T\kappa^2}{2}t\right)\right]. \qquad \text{(E.4)}\end{aligned}$$

Note that the linear term in (E.1) as well as the terms containing the initial position y' in (E.1) and (E.2) cancel out in this limit. The integrals in (E.3) and (E.4) can be performed straightforwardly and give (5.41) and (5.42), respectively.

Bibliography

[1] L. Smith, F. W. Schwartz, Mass transport, 1. A stochastic analysis of macroscopic dispersion, Water Resour. Res. 17 (1980) 351–369.

[2] M. Levy, B. Berkowitz, Measurement and analysis of non-Fickian dispersion in heterogeneous porous media, J. Contam. Hydrol. 64 (2003) 203–226.

[3] S. E. Silliman, E. S. Simpson, Laboratory evidence of the scale effect in dispersion of solutes in porous media, Water Resour.Res. 23 (1987) 1667–1673.

[4] A. Cortis, B. Berkowitz, Anomalous transport in "classical" soil and sand columns, Soil Science Society of America Journal 68 (2004) 1539–1548.

[5] S. P. K. Sternberg, Dispersion measurements in highly heterogeneous laboratory scale porous media, Trans. Porous Media 54 (2004) 107–124.

[6] E. A. Sudicky, C. J. A., Field observations of tracer dispersion under natural flow conditions in a unconfined sandy aquifer, Water Pollut. Res. Can. 14 (1979) 1–17.

[7] D. L. Freyberg, A natural gradient experiment on solute transport in a sandy aquifer, 2, Spatial moments and the advection and dispersion of nonreactive tracer, Water Resour. Res. 22 (1986) 2031–2046.

[8] L. W. Gelhar, C. Welty, K. R. Rehfeldt, A critical review of data on field-scale dispersion in aquifers, Water Resour. Res. 28 (7) (1992) 1955–1974.

[9] B. Berkowitz, A. Cortis, M. Dentz, H. Scher, Modeling transport in geological formations as a continuous time random walk, Rev. Geophys. 44 (RG2003) (2006) doi:10.1029/2005RG000178.

[10] M. Dentz, B. Berkowitz, Transport behavior of a passive solute in continuos time random walks and multirate mass transfer, Water Resour. Res. 39 (5) (2003) 1111, doi:10.1029/2001WR001163.

[11] M. Dentz, A. Cortis, H. Scher, B. Berkowitz, Time behavior of solute transport in heterogeneous media: transition from anomalous to normal transport, Adv. Water Resour. 27 (2004) 155–173.

[12] S. M. Haggerty, R. ann Gorelick, Multiple-Rate Mass Transfer for Modeling Diffusion and Surface Reactions in Media with Pore-Scale Heterogeneity, Water Resour. Res. 31 (10) (1995) 2383–2400.

[13] J. Carrera, X. Sanchez-Vila, I. Benet, A. Medina, G. Galarza, J. Guimera, On matrix diffusion: formulations, solution methods and qualitative effects, Hydrology Journal 6 (1998) 178–190.

[14] D. A. Benson, W. Wheatcraft, M. M. M., The fractional-order governing equation of Levy motion, Water Resour. Res. 36 (2000) 1413–1423.

[15] L. Gelhar, C. Axness, Three dimensional stochastic analysis of macrodispersion in aquifers, Water Resour. Res. 19 (1) (1983) 161–180.

[16] W. Kinzelbach, P. Ackerer, Modlisation du transport de contaminant dans un champ d'coulement non-permanent, Hydrolgologie 2 (1986) 197–205.

[17] G. Dagan, Time-dependent macrodispersion for solute transport in anisotropic heterogeneous aquifers, Water Resour. Res. 24 (9) (1988) 1491–1500.

[18] K. Rehfeldt, L. Gelhar, Stochastic analysis of dispersion in usteady flow in heterogeneous aquifers, Water Resour.Res. 28 (8) (1992) 2085–2099.

[19] D. Burr, A. Sudicky, R. Naff, Nonreactive and reactive solute transport in three-dimensional heterogeneous porous media: Mean displacement, plume spreading, and uncertainty, Water Resour. Res. 30 (3) (1994) 791–815.

[20] M. Dentz, J. Carrera, Effective dispersion in temporally fluctuating flow through a heterogeneous medium, Phys. Rev. E. 68 (2003) 036310.

[21] M. Matheron, G. de Marsily, Is the transport in porous media always diffusive? A counter-example, Water Resour. Res. 16 (1980) 901–917.

[22] F. Miralles-Wilhelm, L. W. Gelhar, Stochastic analysis of sorption macrokinetics in heterogeneous aquifers, Water Resour.Res. 32 (6) (1996) 1541–1549.

[23] H. Rajaram, Time and scale dependent effective retardation factors in heterogeneous aquifers, Adv. Water Resour. 20 (4) (1997) 217–230.

[24] R. Reichle, W. Kinzelbach, H. Kinzelbach, Effective parameters in heterogeneous and homogeneous transport models with kinetic sorption, Water Resour.Res. 34 (4) (1998) 583–594.

[25] S. Attinger, M. Dentz, H. Kinzelbach, W. Kinzelbach, Temporal behaviour of a solute cloud in a chemically heterogeneous porous medium, J. Fluid Mech. 386 (1999) 77–104.

[26] M. Dentz, H. Kinzelbach, S. Attinger, W. Kinzelbach, Temporal behavior of a solute cloud in a heterogeneous porous medium: 1. Point-like injection, Water Resour. Res. 36 (12) (2000a) 3591–3604.

[27] M. Dentz, H. Kinzelbach, S. Attinger, W. Kinzelbach, Temporal behavior of a solute cloud in a heterogeneous porous medium: 2. Spatially extended injection, Water Resour. Res. 36 (12) (2000b) 3605–3614.

[28] P. K. Kitanidis, The concept of the dilution index, Water Resour. Res. 30 (1994) 2011–1026.

[29] M. Dentz, J. Carrera, Mixing and spreading in stratified flow, Phys. of Fluids 19 (1) (2007) 017107.

[30] V. Zavala-Sanchez, M. Dentz, X. Sanchez-Vila, Effective Dispersion in a Chemical Heterogeneous Medium under Temporally Fluctuating Flow Conditions, Adv. Water Res. 30 (5) (2007) 1342–1354.

[31] M. Clincy, H. Kinzelbach, Stratified disordered media: exact solutions for transport parameters and their self-averaging properties, J. Phys. A: Math. Gen. 34 (2001) 7141–7152.

[32] T. Toftegaard, N. J. Wigard, Performance Enhancements in a Frequency Hopping GSM Network, Springer, 2000.

[33] M. Avellaneda, A. J. Majda, Superdiffusion in Nearly Stratified Flows, J. Stat. Phys. 69 (3/4) (1992) 689–729.

[34] G. I. Taylor, Dispersion of soluble matter in solvent flowing through a tube, Proc. Roy. Soc. A 219 (1953) 186–203.

[35] V. Zavala-Sanchez, M. Dentz, X. Sanchez-Vila, Characterization of Mixing and Spreading in a bounded stratified medium, accepted for publication in Adv. Water Resour. (june 2008).

[36] J. Bear, Dynamics of fluids in porous media, American Elsevier, 1972.

[37] O. A. Cirpka, S. Attinger, Effective dispersion in heterogeneous media under random transient flow conditions, Water Resour. Res. 39 (9) (2003) 1257.

[38] M. Dentz, J. Carrera, Effective solute transport in temporally fluctuating flow through heterogeneous media, Water Resour. Res. 41 (2005) W08414.

[39] G. Dagan, Flow and Transport in Porous Formations, Springer, 1989.

[40] L. W. Gelhar, Stochastic Subsurface Hydrology, Prentice-Hall, 1993.

[41] A. Fiori, G. Dagan, Transport of a Pasive Scalar in a Stratified Porous Medium, Transport in Porous Media 47 (2002) 81–98.

[42] P. K. Kitanidis, Prediction by the method of moments of transport in a heterogeneous formation, J. Hydrology 102 (1988) 453–473.

[43] G. Dagan, Dispersion of passive solutes in non ergodic transport by steady velocity fields in heterogenous formations, J. of Fluid Mech. 233 (1991) 197–210.

[44] H. Rajaram, L. W. Gelhar, Three-dimensional spatial moments analysis of the borden tracer test, Water Resour. Res. 27 (1991) 1239–1251.

[45] C. Chrysikopoulos, K. P.K., P. Roberts, Analysis of one dimensional solute transport through porous media with spatially variable retardation factor, Water Resour. Res. 26 (1990) 437–446.

[46] A. Bellin, A. Rinaldo, W. J. P. Bosma, S. E. A. T. M. V. d. Zee, Y. Rubin, Linear equilibrium adsorbing solute transport in physically and chemically heterogeneous posous formations 1. Analytical solutions, Water Resour. Res. 29 (12) (1993) 4019–4030.

[47] D. Metzger, H. Kinzelbach, W. Kinzelbach, Asymptotic trasnport parameters in a heterogeneous porous medium: Comparison of two ensemble-averaging procedures, Stochastic Env. Res. and Risk Assessment. 13 (1999) 396–415.

[48] D. Metzger, H. Kinzelbach, W. Kinzelbach, Effective dispersion of a solute cloud in a chemically heterogeneous porous medium: comparison of two ensemble-averaging procedures, Water Resour. Res. 32 (11) (1996) 3311–3319.

[49] D. Fernndez-Garcia, T. H. Illangasekare, R. H., Differences in the scale dependence of dispersivity and retardation factors estimated from forcedgradient and uniform flow tracer tests in three-dimensional physically and chemically heterogeneous porous media, Water Resour. Res. 41 (2005) W03012.

[50] D. Fernandez-Garcia, H. Rajaram, T. H. Illangasekare, Differences in the scale dependence of dispersivity and retardation factors estimated from forced-gradient and uniform flow tracer tests in three-dimensional physically and chemically heterogeneous porous media, Water Resour. Res. 41 (2005) W04002.

[51] P. C. Linchtner, D. Tartakovsky, Upscaled effective rate constant for heterogeneous reactions, Stochastic Environ. Res. and Risk Assessment (SERRA) 17 (6) (2003) 419–492.

[52] A. M. Aucour, F. X. Tao, P. Moreira-Turcq, P. Seyler, S. Sheppard, M. F. Benedetti, The Amazon River: behaviour of metals (Fe, Al, Mn) and dissolved organic matter in the initial mixing at the Rio Negro/Solimoes confluence, Chem. Geol. 197 (1-4) (2003) 271–285.

[53] J. Tonkin, L. Balistrieri, J. Murray, Modeling metal removal onto natural particles formed during mixing of acid rock drainage with ambient surface water, Env. Science & Tech. 36 (3) (2002) 484 –492.

[54] W. Sanford, L. Konikow, Simulation of calcite dissolution and porosity changes in saltwater mixing zones in coastal aquifers, Water Resour.Res. 25 (1989) 655–667.

[55] E. Abarca, J. Carrera, X. Sanchez-Vila, M. Dentz, Anisotropic dispersive henry problem, Adv. Water Resour. 30 (2007) 913–926.

[56] M. Chu, P. K. Kitanidis, P. L. McCarty, Modeling microbial reactions at the plume fringe subject to transverse mixing in porous media: When can the rates of microbial reaction be assumed to be instantaneous?, Water Resour. Res. 41 (2005) WR003495.

[57] C. E. Knutson, C. J. Werth, A. J. Valocchi, Pore-scale simulation of biomass growth along the transverse mixing zone of a model two-dimensional porous medium, Water Resour. Res. 41 (2005) W07007.

[58] M. De Simoni, J. Carrera, X. Sanchez-Vila, A. Guadagnini, A procedure for the solution of multicomponent reactive transport problems, Water Resour. Res. 41 (2005) WR004056.

[59] Z. Kabala, G. Sposito, A stochastic model of reactive solute transport with time-varying velocity in a heterogeneous aquifer, Water Resour. Res. 27 (3) (1991) 341–350.

[60] D. Zhang, S. P. Neuman, Effect of local dispersion on solute transport in randomly heterogeneous media, Water Resour. Res. 32 (1996) 2715–2723.

[61] G. Dagan, A. Bellin, Y. Rubin, Lagrangian analysis of transport in heterogeneous formations under transient flow conditions, Water Resour.Res. 32 (4) (1996) 899–900.

[62] O. A. Cirpka, Effects of sorption on transverse mixing in transient flows, J. Cont. Hydrol. 78 (2005) 207–229.

[63] O. A. Cirpka, Choice of dispersion coefficients in reactive transport calculations on smoothed fields, J. Cont. Hydrol. 58 (2002) 261–282.

[64] O. A. Cirpka, E. Frind, R. Helming, Numerical simulation of biodegradiaton controlled by transverse mixing, J. Cont. Hydrol. 40 (2) (1999) 159–182.

[65] D. M. Tartakovsky, P. C. Lichtner, R. J. Pawar, PDF methods for reactive transport in porous media, in: Z. C. o. C. Eds. K. Kovar, Reliability in Groundwater Modelling (ModelCARE (Eds.), IAHS-AISH Publication, no. No. 277, Prague, Czech Republic, 2003, pp. 162–167.

[66] O. Güven, F. J. Molz, J. G. Melville, An analysis of macrodispersion in a stratified aquifer, Water Resour. Res. 20 (10) (1984) 1337–1353.

[67] O. Güven, F. J. Molz, Deterministic and Stochastic Analyses of Dispersion in an Unbounded Stratified Porous Medium, Water Resour. Res. 22 (11) (1986) 1556–1574.

[68] V. K. Gupta, R. N. Bhattacharya, Solute Dispersion in Multidimensional Periodic Saturated Porous Media, Water Resour. Res. 22 (2) (1986) 156–164.

[69] G. Dagan, Transport in Heterogeneous Porous Formations: Spatial Moments, Ergodicity, and Effective Dispersion, Water Resour. Res. 26 (6) (1990) 1281–1290.

[70] P. Salandin, A. Rinaldo, G. Dagan, A note on transport in stratified formations by flow tilted with respect to the beding, Water Resour. Res. 27 (1991) 3009–3017.

[71] H. Rajaram, L. Gelhar, Plume Scale Dependent Dispersion in Heterogeneous Aquifers 1. Lagrangian Analisis in Stratified Aquifer, Water Resour. Res. 29 (1993) 3249–3260.

[72] G. Sposito, S. W. Weeks, Tracer advection by steady groundwater flow in a stratified aquifer, Water Resour. Res. 34 (1998) 1051–1059.

[73] J. Bouchaud, A. Georges, Anomalous diffusion in disordered media: Statistical mechanisms, models and physical applications, Physics Rep. 195 (1990) 127–293.

[74] J. Bouchaud, A. Georges, J. Koplik, A. Provata, S. Redner, Superdiffusion in random velocity fields, Phys. Rev. Lett. 64 (1990) 2503–2506.

[75] A. Compte, M. Caceres, Fractional dynamics in random velocity fields, Phys. Rev. Lett. 81 (1998) 3140–3143.

[76] S. Weeks, G. Sposito, Mixing and streching efficiency in steady and unsteady groundwater flows, Water Resour. Res. 34 (1998) 3315–3322.

[77] G. Sposito, Chaotic solute advection by unsteady groundwater flow, Water Resour. Res. 42 (2006) W06D03.

[78] G. Károlyi, T. Tél, Chemical Transients in Closed Chaotic Flows: The Role of Effective Dimensions, Phys. Rev. Lett. 95 (2005) 264501.

[79] P. E. Arratia, J. P. Gollub, Predicting the Progress of Diffusively Limited Chemical Reactions in the Presence of Chaotic Advection, Phys. Rev. Lett. 96 (2006) 024501.

[80] R. H. Kraichnan, Diffusion by Random Velocity Field, Phys. Fluids 13 (1970) 22–31.

[81] R. H. Kraichnan, Diffusion of a passive-scalar and magnetic fields by helical turbulence, J. Fluid Mech. 77 (1976) 753–768.

[82] C. Marle, P. Simandoux, J. Pacsirsky, C. Gaulier, Etude du deplacement de fludes miscibles en milieu poreux stratifie, 22, 272 294., Rev. Inst. Fr. Pet. 22 (1967) 272–294.

[83] T. Le Borgne, J. R. de Dreuzy, O. Davy, Bour, Characterization of the velocity field organization in heterogeneous media by conditional correlation, Water Resour. Res. 43 (2007) W02419.

[84] M. Dentz, T. Le Borgne, J. Carrera, Correlated random walks in random flows, submitted to Phys. Rev. Lett.

[85] S. N. Majumdar, Persistence of a particle in the Matheron-de Marsily velocity field., Phys. Rev. E. 68 (2003) 050101(R).

[86] W. R. Young, S. Jones, Shear dispersion, Phys. Fluids A 3 (5) (1991) 1087–1101.

[87] J. Camacho, Purely global model for Taylor dispersion, Phys. Rev. E 48 (1) (1993) 310–320.

[88] C. W. J. Berensten, M. L. Verlaan, C. P. J. W. van Kruijsdijk, Upscaling and reversibility of Taylor dispersion in heterogeneous porous media, Phys. Rev. E 71 (2005) 046308.

[89] C. W. J. Berensten, M. L. Verlaan, C. P. J. W. van Kruijsdijk, Upscaling, relaxation and reversibility of dispersive flow in stratified porous media, Transp. Porous Media 68 (2) (2006) 187–218.

[90] M. Dentz, B. Berkowitz, Exact effective transport dynamics in a one-dimensional random environment, Phys. Rev. E 72 (3) (2005) 031110.

[91] M. Abramowitz, I. A. Stegun, Handbook of Mathematical Functions, Dover Publications, 1972.